

Light Scattering by Fractal Aggregates: A Review

C. M. Sorensen

Department of Physics and Program for Complex Fluid Flows, Kansas State University, Manhattan, Kansas

This paper presents a review of scattering and absorption of light by fractal aggregates. The aggregates are typically diffusion limited cluster aggregates (DLCA) with fractal dimensions of $D \approx 1.75$, which occur frequently in aerosols and colloids, but other types of aggregates are discussed as well. The results of the review are quite general. A scaling description of the scattering of waves forms the basis of our understanding. This description yields the optical structure factor $S(q)$ of the aggregate, where q is the scattering wavevector, a key quantity. The rigorous approach to the structure factor, the Fourier transform of the density correlation function, is also given and various forms provided in the literature are compared and the best selected. Light scattering is directly related to the structure factor under the assumption of no internal multiple scattering. This so-called Rayleigh-Debye-Gans (RDG) approximation is compared to more rigorous electromagnetic approaches and found to be quite accurate for fractal aggregates. This results despite the presence of internal multiple scattering, which leads to depolarization, and which is also extensively described. For ensembles of aggregates, the effects of aggregate polydispersity on scattering experiments are described and methods for proper analysis are given. A description of optical particle sizing and morphology analysis is given for a complete in situ characterization of the aggregate system. The review relies strongly on straightforward physical reasoning and experimental examples, largely from aerosols, especially those of carbonaceous soot. This paper not only reviews and consolidates, but also presents new results including a scaling analysis of multiple scattering, which leads to depolarization, with a successful comparison to available data and an understanding of structural subtleties; demonstration of the significance of a phase shift parameter for evaluating the range of validity of the RDG theory; a Maxwell-Garnet analysis of fractal aggregate scattering; calculations of the albedo and successful comparison to available simulation data; and speculations on multiple scattering and the interior field.

Received 1 September 1999; accepted 20 March 2000.

I am pleased to acknowledge the pleasant collaborations with my students and post-docs who have worked with me in this area over the past several years. They are Jian Cai, G. Feke, Dave Fischbach, S. Gangopadhyay, Will Hageman, H. Huang, N. Lu, C. Oh, Rajiv Pande, G. Roberts, Dan Shi, and G. M. Wang. This work has been supported by the NSF.

Address correspondence to Christopher M. Sorensen, Department of Physics and Program for Complex Fluid Flows, Kansas State University, Manhattan, KS 66506-2601. E-mail: sor@phys.ksu.edu

INTRODUCTION

The purpose of this review is to unify our knowledge of how fractal aggregates scatter (and absorb) light. This is of value for light scattering diagnostics of aerosols and colloids and for understanding the optics of these systems in the environment. The subject has seen able and useful reviews before by Teixeira (1986), Martin and Hurd (1987), Charalampopoulos (1992), and a brief overview by myself (Sorensen 1997). Very recently Fuller and Mackowski (2000) have given an excellent review of the superposition theory of scattering from aggregates. My desire here is to provide an up-to-date and comprehensive review useful for the experimentalist. Any theory that does appear will be based on simple physical arguments rather than detailed mathematical analysis. Many of the general results to be described here apply to nonfractal aggregates as well, although such aggregates are usually in some manner contrived and not the result of “natural” processes. Light scattering is the central theme of this review, but it is set in the context of the scattering of waves in general. This is done not only because many of the results to be described were derived from and/or can be applied to other scattering processes such as x-rays and neutrons, but also because it sets a simple, lowest-order approximation for light scattering which proves to be very useful.

Colloids and aerosols are common in nature and important for our technology, and since the process of aggregation is integral to how these systems evolve, we have motive to understand the properties of the resulting clusters. This can be a difficult task because random aggregates are just that, random, and, because they are aggregates, not simple. For current science the first step in describing, hence progressing to understanding, is a mathematical description; a process much like naming. Two decades ago this naming and descriptive process for aggregates took a major step forward when Forrest and Witten (1979) used the fractal concept (Mandelbrot 1977, 1982) to describe aggregates of metal smokes. Fractal aggregates are scale invariant, that is, within limits they appear the same when viewed over a range of scales. This concept is of value because it includes a mathematical description and a quantifiable parameter, the Hausdorff or fractal dimension D (Hausdorff 1919). Moreover, the mathematical description is simple and can be

expressed as

$$N = k_o(R_g/a)^D. \quad [1]$$

In Equation (1), N is the number of primary particles or monomers in the aggregate (proportional to the mass), R_g is a measure of the overall aggregate radius (specifically, the radius of gyration), a is the monomer radius, and k_o is a proportionality constant of order unity. We say that for a fractal aggregate the mass scales with the overall size to the D power.

In the intervening years, subsequent work has found the fractal description of aggregates to be nearly universal (Weitz and Oliveria 1984; Schaefer et al. 1984; Family and Landau 1984; Martin et al. 1986; Meakin 1988; Sampson et al. 1987; Dobbins and Megaridis 1987; Viscek 1992; Sorensen and Feke 1996). Figures 1 and 2 give examples of fractal aggregates and, in Figure 1, a demonstration of the scale invariance. In colloids and aerosols, clusters meet other clusters through random motion. If they stick together with near unity probability, the process is called diffusion limited cluster aggregation, (DLCA) because the rate limiting step is the diffusive motion of the clusters (Meakin 1983, 1988; Kolb et al. 1983). This is a common situation and leads to fractal dimensions on the order of $D \simeq 1.75$ to 1.8. The aggregates in both Figures 1 and 2 are DLCA with $D \simeq 1.8$. It is possible in aerosols for the cluster motion between collisions to be a straight line (ballistic) rather than a random walk and then $D \simeq 1.9$ (Meakin 1984; Mulholland et al. 1988). In colloids, solute modification of the double layer surrounding the particles can drastically reduce the sticking probability and then the reaction limited cluster aggregation (RLCA) regime is entered with $D \simeq 2.1$ to 2.2 (Weitz et al. 1985; Lin et al. 1990b). These two situations represent the great majority of aggregates, although application of external fields during aggregation or modification of the clusters after aggregation can modify the morphology to other fractal dimensions or nonfractal morphologies.

Returning now to scattering, we recognize that the scattering of radiation, viz. light, x-rays, neutrons, etc., is foremost the scattering of waves. This wave nature is the foundation of the scattering process in each case, and it is the common bond that allows much of the mutual mathematical analysis and terminology. Differences occur in the way the various radiations interact with matter. In particular, light and x-rays are both electromagnetic radiation and hence interact with the electrons of the system, but because of some three orders of magnitude difference in frequency the interactions are significantly different. At optical frequencies, the electrons of many materials readily respond, hence the refractive index (the square root of the optical frequency dielectric constant) is greater than unity. Because of this, scattering of light involves phase changes due to different wave velocities in the medium and boundary conditions at interfaces. On the other hand, x-ray frequencies are too fast for most electronic responses and this makes the refractive index for x-rays very nearly unity. Consequently, without the complications of differing wave velocities and boundary conditions,

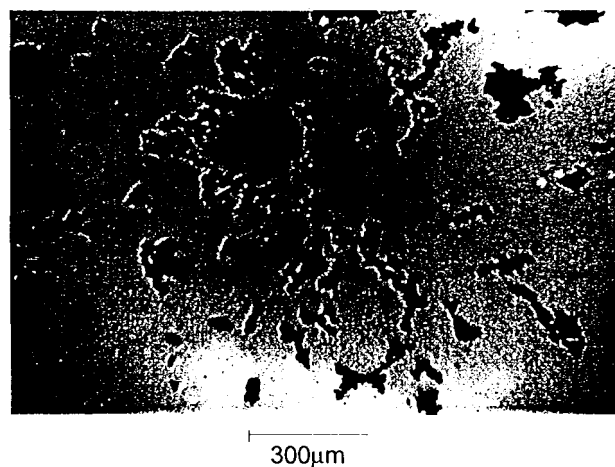
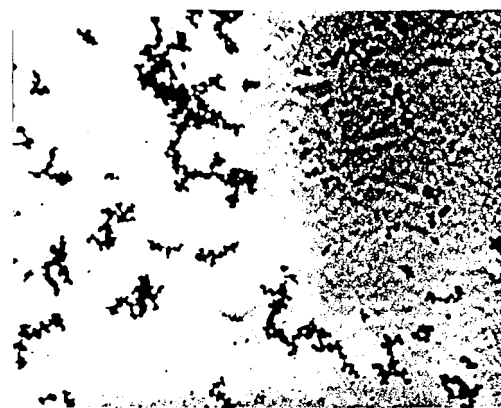


Figure 1. Soot fractal aggregates from an acetylene diffusion flame. The upper picture was taken with a TEM and individual monomers (primary particles) can be seen. The lower picture was taken with an optical microscope at a scale two and one half orders of magnitude larger than the upper picture. Despite this difference in scale, the aggregates in each picture look the same, demonstrating scale invariance. The fractal dimensions are $D \simeq 1.8$.

x-ray scattering is, too a good approximation, simply a wave problem.

Our task here, however, is to understand and describe the scattering of light. But light's relationship to x-rays can be useful in that endeavor. We shall view light scattering as involving two separable aspects. First, like x-rays, it is a wave. As we shall see, the mathematical embodiment of wave scattering is the Fourier transform, which is both powerful and well understood. Second, light scattering involves its nontrivial electromagnetic nature, which in the classic electromagnetic approach requires use of appropriate boundary conditions and wave velocities.

Our approach to understanding and describing light scattering will thus be twofold. First, we will scatter waves. This will be

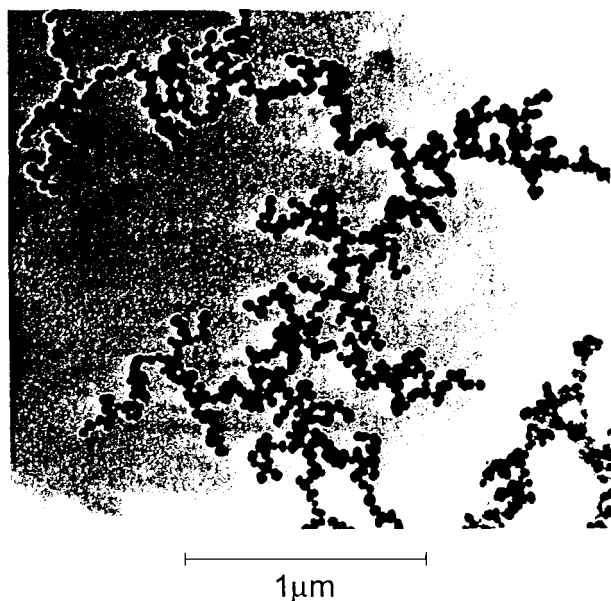


Figure 2. TEM picture of titania (TiO_2) fractal aggregates with $D \simeq 1.8$ produced by pyrolysis of Titanium Isopropoxide.

either by Fourier transforms or more simply by keeping track of whether waves scattered by the parts of the aggregate are in phase or not. Then if necessary, we will “add the optics,” but not by accounting for additional phase changes incurred by the velocities or boundary conditions as one would for a uniform sphere. Instead, putting in the optics for aggregates will involve accounting for multiple scattering. I suspect these two methods are equivalent, but this has yet to be worked out. As it turns out, for aggregates, especially those with $D < 2$, the second step, adding the optics, is largely unnecessary.

THE STRUCTURE FACTOR

The structure factor is so named because it carries information regarding the structure of the object or system scattering the waves. Thus it is of prime importance. As we will see, it is both the Fourier transform of the density autocorrelation function of the scattering system and the square of the Fourier transform of the density distribution of the scattering system; thus it is the q -space (reciprocal space with units of inverse length) description of the structure. Experimentally it describes scattered intensity as a function of scattering angle. The independent variable of the structure factor is the scattering wave vector.

The Scattering Wave Vector

Consider a scalar electromagnetic field with incident wave vector \vec{k}_i incident upon a scattering element at \vec{r} as in Figure 3. The incident field at \vec{r} is

$$E_i(\vec{r}) \propto e^{i\vec{k}_i \cdot \vec{r}}, \quad [2]$$

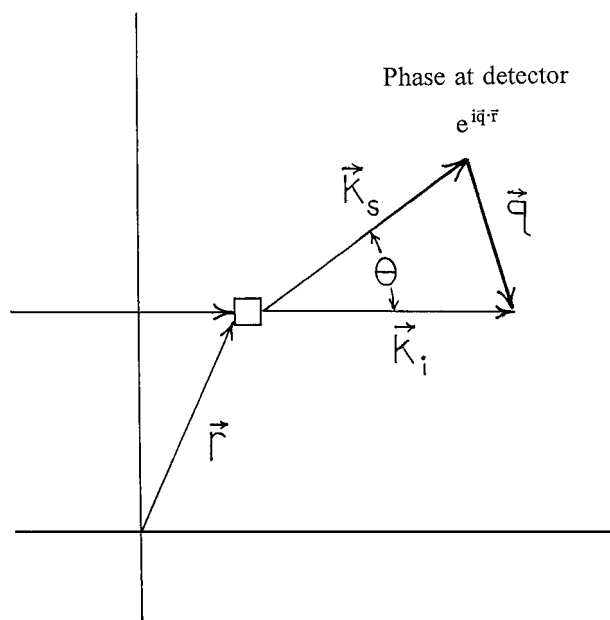


Figure 3. Diagram of light incident from the left with wave vector \vec{k}_i scattering from a scattering element at \vec{r} toward the detector with scattering wave vector \vec{k}_s at a scattering angle θ . The difference $\vec{k}_i - \vec{k}_s$ is \vec{q} , the scattering wave vector.

where complex notation is used, $i = \sqrt{-1}$, and we keep track of phase information only. Phase is the argument of the sinusoidally varying wave and as such is the essence of the wave’s “wave nature.” Thus two waves add constructively when their phases are equal (or differ by an even integer times π), a condition well known as constructive interference, and they add destructively when their phases differ by π (or an odd integer times π), a condition known as destructive interference. The field scatters toward the detector in the direction \vec{k}_s , the scattered wave vector. Under the assumption of elastic scattering, i.e.,

$$|\vec{k}_i| = |\vec{k}_s| = \frac{2\pi}{\lambda}, \quad [3]$$

the field at the detector, which is at \vec{R} , is

$$E(\vec{R}) \propto E(\vec{r}) e^{i\vec{k}_s \cdot (\vec{R} - \vec{r})}. \quad [4]$$

Substitution of Equation (2) into Equation (4) yields

$$E(\vec{R}) \propto e^{i\vec{k}_s \cdot \vec{R}} e^{i(\vec{k}_i - \vec{k}_s) \cdot \vec{r}}. \quad [5]$$

The second term of Equation (5) shows that the phase at the detector is a function of the position of the scattering element and the vector

$$\vec{q} = \vec{k}_i - \vec{k}_s. \quad [6]$$

This vector \vec{q} is called the *scattering wave vector*. Its direction is in the scattering plane from \vec{k}_s to \vec{k}_i , as shown in Figure 3.

From Figure 3 and the elasticity condition Equation (3), simple trigonometry yields the magnitude of \vec{q} to be

$$q = 2k_i \sin(\theta/2) \tag{7a}$$

$$= 4\pi\lambda^{-1} \sin(\theta/2), \tag{7b}$$

where θ is the scattering angle.

The importance of q is that its inverse, q^{-1} , represents the length scale, or the probe length, of the scattering experiment. This follows from the second term in Equation (5), which can now be written as

$$E_{sca} \propto e^{i\vec{q}\cdot\vec{r}}, \tag{8}$$

where E_{sca} is the amplitude of the scattered wave. Equation (8) shows that if the variation of r is small compared to q^{-1} , the scattered field will not significantly change; whereas if r varies greatly relative to q^{-1} , the scattered field will change significantly. Thus q^{-1} represent a length scale to be compared to length scales of the scatterer; this comparison determines the scattered field.

Fundamental Equation for The Structure Factor

The structure factor quickly follows from Equation (8) with normalization to unity incident wave and cross section for scattering by the element (whatever that might be) at \vec{r} . In this regard it is useful to conceive of a “system of scatterers” as a system of N identical points. The structure factor is proportional to the scattered intensity $I(q)$, hence the square of the scattered amplitude. Then by Equation (8) we write

$$I(q) = \left| \sum_{i=1}^N e^{i\vec{q}\cdot\vec{r}_i} \right|^2. \tag{9}$$

Since we must often deal with ensembles of scatterers with random orientations, we have dropped the vector notation on the left-hand side of Equation (9). The structure factor is defined with the normalization $N^{-2}I(q)$; thus

$$S(q) = N^{-2} \left| \sum_{i=1}^N e^{i\vec{q}\cdot\vec{r}_i} \right|^2. \tag{10}$$

This normalization ensures $S(0) = 1$. Equation (10) has its use; an equally useful form is to rewrite it as

$$S(q) = N^{-2} \sum_i^N \sum_j^N e^{i\vec{q}\cdot(\vec{r}_i - \vec{r}_j)}, \tag{11}$$

where \vec{r}_i and \vec{r}_j represent the positions of i and j th scatterers.

The Scaling Approach for the Structure Factor

We now present a simple and physically appealing method for determining the scattering, hence the structure factor, from an arbitrary system of scatterers, a method we call the scaling approach (Oh and Sorensen 1999). The scaling approach is based on comparing the inherent length scale of the scattering, q^{-1} , and length scales in the system of scatterers. The magnitude of the wave vector q is an experimental parameter because it is

controlled by the scattering angle via Equations (7). Comparison of length scales determines whether the waves combine in phase (constructively) or randomly at the detector. For a system of N scatterers there are two limiting situations:

1. If the N scatterers are within q^{-1} of each other, the phase of the N scattered waves will be essentially the same, hence the waves will be in phase and thus add constructively. Then the total scattered amplitude will be proportional to N , thus the total scattered intensity will be proportional to N^2 . From the point of view of Equation (11), this is when $\vec{q} \cdot (\vec{r}_i - \vec{r}_j) < 1$, hence the double sum equals N^2 .
2. If the N scatterers have all pairs separated by distances $> q^{-1}$, the phases of the N scattered waves will be random, hence the waves will add randomly. Then the total scattered amplitude will be proportional to \sqrt{N} , thus the total scattered intensity will be proportional to N . From the point of view of Equation (11), this is when $\vec{q} \cdot (\vec{r}_i - \vec{r}_j) > 1$, then the N^2 terms in the double sum can be represented as a random walk of N^2 unit steps with an average sum proportional to the square root of the number of steps, i.e., N .

In addition, we remember that

3. Only when there are fluctuations in the density of the scatterers is there a nonzero contribution to the total scattering at nonzero scattering angles. This is a consequence of the Ewald-Oseen extinction theorem (Born and Wolf 1975; Hecht 1998).

Some discussion is warranted on the remarkable Ewald-Oseen extinction theorem. A single point scatterer, an electron, for example, will scatter isotropically in all directions perpendicular to the incident polarization. Two point scatterers will create an interference pattern (Young’s fringes) and $N \gg 1$ uniformly spaced scatterers will interfere so that scattering will occur only in certain special directions (similar to Bragg scattering or a diffraction grating). Finally, an infinite system of regularly and closely spaced (distance $< \lambda$) scatterers will not scatter at all at finite θ , according to Ewald-Oseen. Scattering does occur in the exact forward ($\theta = 0$) direction to cancel the incident wave and create a new wave traveling at c/n , where n is the refractive index of the system. The bottom line of all this is that uniform systems do not scatter light. From where does the scattering come? From fluctuations in the density of the scatterers. Thus when asked why the sky is blue, one should respond with two reasons: blue light scatters more than red and there are fluctuations in the density of the air.

Fluctuations can occur either internally due to a variation in the density of the scatterers within the system (e.g., a variation of the mass density of a gas occur due to thermodynamics) or on the surface since there the density changes discontinuously. Here we will only consider this surface scattering. See Oh and Sorensen (1999) for a discussion on the general effects of internal scattering.

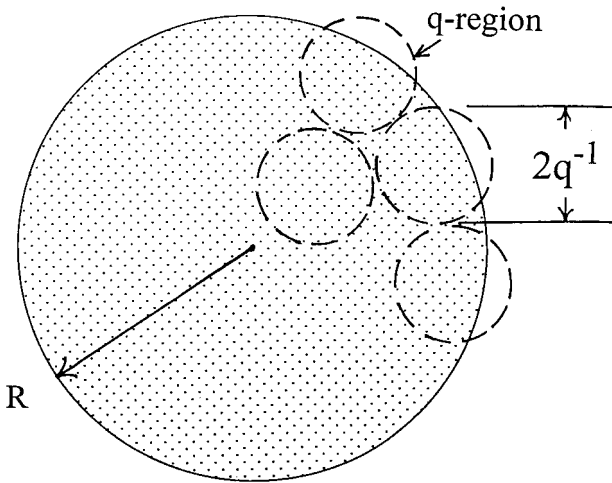


Figure 4. Drawing of a system of point scatterers in a region of size R . Also drawn are q -regions of size q^{-1} .

Application of the Scaling Approach. Consider a system of scatterers in a d -dimensional, spherical region of radius R . Let the density of the scatterers be uniform by placing them on a regular lattice with $2a$ the nearest neighbor separation, as drawn in Figure 4. Then the only fluctuation in density of the scatterers is on the surface of the system in the form of a discontinuity. The scaling approach allows us to understand how waves are scattered by the system. To do this envision a situation where the system is covered throughout its volume by smaller imaginary “ q -regions” of size q^{-1} , as drawn in Figure 4. For all the scatterers in the same q -region, the phase factor in Equation (11) is $\vec{q} \cdot (\vec{r}_1 - \vec{r}_j) \lesssim 1$. Then the scattered waves are in phase at the detector (situation 1 above) so that

$$I(q) \propto N_q^2, \quad [12]$$

where N_q is the number of scatterers in the q -region. There are many such q -regions in the system of radius R , but only those on the surface of the system contribute to the scattering because it is only on the surface of this uniform system that there is a fluctuation in density (condition 3 above). Let n_q be the number of q -regions of size q^{-1} needed to cover the surface of the system. Because of their size, they must all be separated by distances $> q^{-1}$, thus their scattered waves add randomly (situation 2 above) to yield

$$I(q) \propto n_q. \quad [13]$$

Combining Equations (12) and (13), we have

$$I(q) \propto n_q N_q^2. \quad [14]$$

Now consider Equation (14) for arbitrary q .

(i) $q < R^{-1}$. In this case $n_q = 1$ and $N_q = N$, then Equation (14) yields

$$I(q) \propto N^2. \quad [15]$$

This result is also obtained from the argument that when $q^{-1} > R$, all N scatterers of the system yield waves that are in phase at the detector. Notice how q^{-1} represents the resolution of the scattering; that is, the scattering can't see features smaller than q^{-1} . From this perspective all N scatterers in the volume of the system of scatterers are on the surface of the system.

(ii) $R^{-1} < q < a^{-1}$. The most general approach allows for arbitrary mass and surface dimensions, D_m and D_s , respectively, of the system of scatterers. (Note in Equation (1) that we used D as the fractal dimension of the aggregate. For an aggregate, however, $D = D_m = D_s$.) Then we can compare the length scales of the system of scatterers and the q -regions. The number of scatterers in a q -region is proportional to the total N and the ratio of the length scale of the q -region, q^{-1} , and the length scale of the system of scatterers, R , raised to the mass dimension power, i.e., $N_q = N(q^{-1}/R)^{D_m}$. A similar argument finds the number of q -regions on the surface of the system to be proportional to a ratio of the two characteristic lengths raised to the surface dimension power, i.e., $n_q \sim (R/q^{-1})^{D_s}$. When applied to Equation (14), these yield

$$I(q) \propto N^2 (qR)^{-2D_m + D_s}. \quad [16]$$

The size of the system is represented by both N and R . To eliminate one for the other in Equation (16) define

$$N = k_m (R/a)^{D_m}, \quad [17]$$

$$N_s = k_s (R/a)^{D_s}, \quad [18]$$

where N_s is the number of scatterers on the surface and k_m and k_s are constants of order unity dependent upon the monomer lattice. Then one obtains

$$I(q) \propto k_o N_s (qa)^{-2D_m + D_s}, \quad [19]$$

where $k_o = k_m^2/k_s$. This is the same k_o as in Equation (1).

(iii) $q > a^{-1}$. In this regime all scatterers scatter waves that have random phases at the detector, but only those on the surface contribute to the scattering. Thus $I(q) \propto N_s$. Continuity with Equation (19) at $q = a^{-1}$ implies

$$I(q) \propto k_o N_s. \quad [20]$$

In summary

$$I(q) \propto \begin{cases} N^2 & \text{for } q < R^{-1}, \\ k_o N_s (qa)^{-2D_m + D_s} & \text{for } R^{-1} < q < a^{-1}, \\ k_o N_s & \text{for } q > a^{-1}. \end{cases} \quad [21a], [21b], [21c]$$

It is useful to rewrite these equations because k_o is dependent on the lattice geometry of the point scatterers and N_s is an unusual parameter. (Note that the product $k_o N_s$ is not lattice dependent.) Use of Equations (17) and (18) yields

$$I(q) \propto \begin{cases} N^2 & \text{for } q < R^{-1}, \\ N^2 (qR)^{-2D_m + D_s} & \text{for } R^{-1} < q < a^{-1}, \\ N^2 (R/a)^{-2D_m + D_s} & \text{for } q > a^{-1}. \end{cases} \quad [22a], [22b], [22c]$$

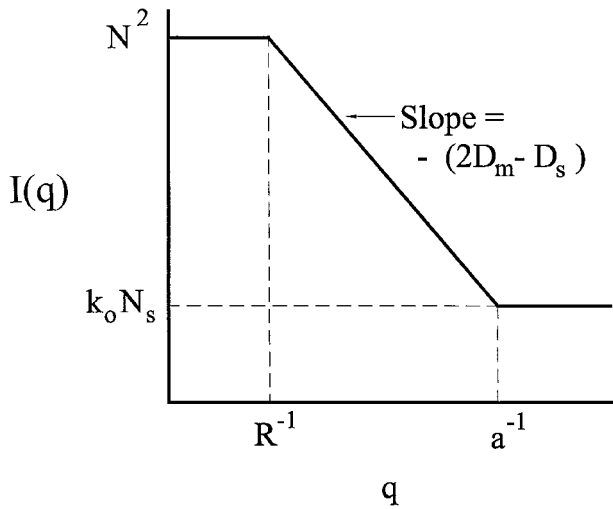


Figure 5. Log-log plot of the scattered intensity versus q , Equations (21), for a system of N point scatterers separated by $2a$ in a region of size R with mass and surface fractal dimensions D_m and D_s , respectively. There are N_s scatterers on the surface of the region. The constant k_o is defined in Equation (1).

Figure 5 shows the generic behavior of Equation (21). Equation (22) shows that a graph of $N^{-2}I(q) = S(q)$ versus qR is universal for all sizes R when $q < a^{-1}$. This fact and the simplicity of Equations (22) are an advantage over Equations (21). However, Equations (21) explicitly show the volume and surface regimes and are more facile for considering complex examples.

The scaling result is general and can be applied to a number of physical situations. We give two examples:

a. *A Solid Sphere.* Let $a \rightarrow 0$ and $D_m = d$, $D_s = d - 1$, where d is the spatial dimension. Then by Equation (21b), when $R^{-1} < q < a^{-1}$, $S(q) \sim I(q) \sim N_s q^{-(d+1)} \sim q^{-4}$ for $d = 3$, a result known as Porod’s Law (Porod 1951; Guinier et al. 1955). Figure 6 shows the Rayleigh–Debye–Gans (RDG) result of electromagnetic theory for light scattering from a sphere (Kerker

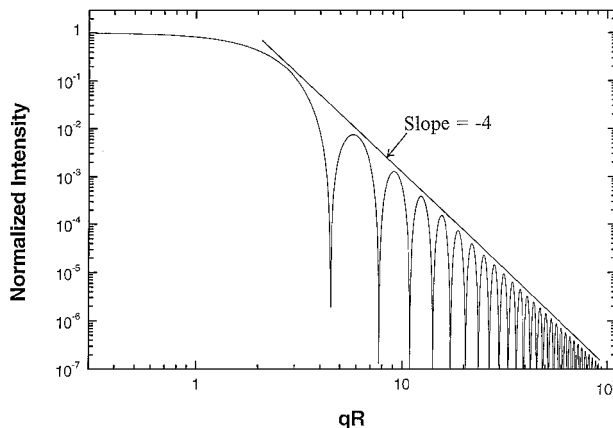


Figure 6. RDG scattering for a sphere $I(u) = [3(\sin u - u \cos u)u^{-3}]^2$, where $u = qR$.

1969). This applies when $\rho = 2kR|m - 1| \ll 1$, where m is the sphere’s refractive index relative to the medium. For $qR < 1$, this theory predicts scattering proportional to R^6 , consistent with Equations (21a) or (22a) since $N \sim R^3$. For $qR > 1$, the envelop of the $I(q)$ versus q functionality is equal to $9(qR)^{-4}$, again consistent with the scaling approach prediction of Porod’s law, Equations (21b) or (22b). Note, however, that the scaling approach cannot predict the shape of the crossover at $qR \sim 1$, the interference ripples when $qR > 1$, nor the factor of 9 proceeding the Porod law. If the solid sphere has a fractally rough surface, $d > D_s > d - 1$ and $S(q) \sim q^{-6+D_s}$ for $d = 3$, a well-known result (Martin and Hurd 1987).

b. *A Fractal Aggregate.* In a fractal, essentially all the monomeric particles are on the surface. Thus we will use for the fractal dimension $D = D_m = D_s < d$. (Hereafter in this review we will simply use D for the fractal dimension of an aggregate.) Then by Equations (21), $S(q) \propto q^{-D}$ for $q > R^{-1}$, another well-known result (Martin and Hurd 1987; Sorensen 1997). Since the structure factor of the fractal aggregate is of prime importance in this review, we now quantify the results of the scaling approach as much as possible. The small $q < R^{-1}$ limit in Equation (22) for $I(q)$ is exact because no approximations are made to obtain this result. We can eliminate the proportionality in the intermediate q -regime, $R^{-1} < q < a^{-1}$, with a constant. Thus, using Equations (9), (10), and (22), we have for a fractal aggregate

$$S(q) = 1, \quad qR_g < 1 \tag{23a}$$

$$= C(qR_g)^{-D}, \quad qR_g > 1. \tag{23b}$$

Scaling cannot address the crossover region $qR_g \sim 1$. In Equations (23) we now use the radius of gyration R_g of the aggregate. The radius of gyration is the root mean square of the monomer distances from the center of mass of the aggregate. We do this because R_g comes naturally out of the rigorous derivation of the structure factor, as we will see below, and because R is ill defined for an aggregate given its indefinite perimeter. This replacement is also allowable because any R is proportional to R_g and hence any difference can be absorbed in the proportionality constant C . Below we will find empirically that $C \simeq 1.0$.

Equations (23) do not include the possibility of the monomer being observable with q , which can be achieved when $q > a^{-1}$. To include N dense spherical monomers with smooth surfaces, we apply Equations (21) twice, once for the fractal and once for the sphere, to yield a total structure factor which is the product

$$S_{TOT}(q) = S_{FA}(q)S_{sphere}(q), \tag{24}$$

where FA means “fractal aggregate.” This product is depicted in Figure 7 and is consistent with experiment. The crossover at $qa \sim 1$ was well described by Hasmy et al. (1993).

The scaling approach is based entirely on wave physics, which includes linear superposition, the energy proportional to the amplitude squared, and the Ewald–Oseen extinction theorem. It applies to all waves. It and the concept of a system of scatterers are quite powerful in accurately describing the general

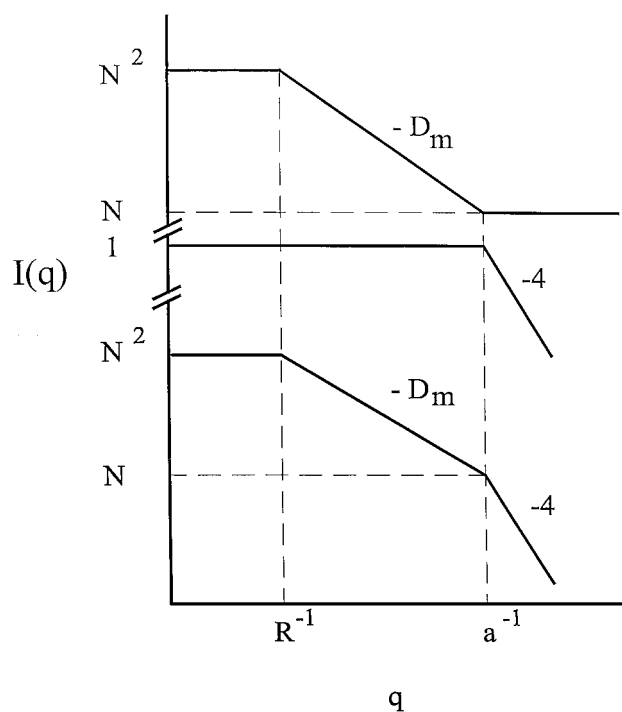


Figure 7. Generic depiction of scattering from a mass fractal aggregate of radius R with a of fractal dimension D_m made up of spherical, smooth surfaced monomers of radius a . Upper curve is for a fractal of point particles, second curve is for spherical particles, lowest curve is the product of these, a representation of Equation (24).

features of wave scattering from a variety of systems, and the reader is encouraged to see Sorensen et al. (1998) and Oh and Sorensen (1999) for other examples. It also enhances physical intuition for the scattering process. However, its simplicity makes it powerless for describing crossover regions as q^{-1} passes through a characteristic length scale of the system, hence Figures 5 and 7 show unphysical sharp turns at the crossovers. The scaling approach also does not predict details such as the interference ripples present in scattering from objects with sharp surfaces such as spheres nor the coefficients of the functionalities as discussed above in reference to RDG theory for spheres.

Scattering and Absorption by a Fractal Aggregate

The scaling approach allows the scattering and absorption of light by an aggregate to be calculated to lowest order. To put in the optics to lowest order let each point-like scatterer in the system of scatterers become a spherical monomer (or primary particle) of radius a . Assume that the monomers are Rayleigh scatterers which are met by the conditions

$$ka \ll 1, \quad [25a]$$

$$|m|ka \ll 1. \quad [25b]$$

In Equation (25b) $m = n + ik$ is the complex refractive index of the monomer. This Rayleigh condition ensures a uniform field

across the monomer. Then the Rayleigh differential scattering cross section for the monomer is (Kerker 1969)

$$\frac{d\sigma}{d\Omega} = k^4 a^6 F(m), \quad [26]$$

where

$$F(m) = \left| \frac{m^2 - 1}{m^2 + 2} \right|^2. \quad [27]$$

The scaling approach becomes applicable when we assume that the monomers scatter (and absorb) independently. Then they see only the incident light wave and none of the waves scattered by their neighbors; that is, there is no intracluster multiple scattering. With this and the concepts of the scaling approach, it then follows that the differential scattering cross section for the aggregate is

$$\frac{d\sigma^{agg}}{d\Omega} = N^2 \frac{d\sigma^m}{d\Omega} S(q). \quad [28]$$

For absorption the particle independence and nonmultiple scattering conditions imply the simple result

$$\sigma_{abs}^{agg} = N\sigma_{abs}^m, \quad [29]$$

where for a Rayleigh monomer

$$\sigma_{abs}^m = 4\pi k a^3 E(m), \quad [30]$$

$$E(m) = Im \left(\frac{m^2 - 1}{m^2 + 2} \right). \quad [31]$$

The total scattering cross section is related formally to the differential cross section by $\sigma = \int (d\sigma/d\Omega) d\Omega$, where $d\Omega = d(\cos \phi) d\theta$ is the solid angle differential. This form, however, ignores polarization. For the common experimental situation of light vertically polarized relative to the scattering plane which contains θ , the polarization causes an additional factor of $\sin^2 \phi$ (Sorensen 1997). Thus

$$\sigma = \int_0^{2\pi} \int_{-1}^1 \frac{d\sigma}{d\Omega} \sin^2 \phi d(\cos \phi) d\theta. \quad [32]$$

Substitution of the expression for the differential cross section of a fractal aggregate, Equation (28), leads to an integral over the structure factor, which leads to algebraically elaborate results with any of the forms currently used and discussed below. Therefore we follow Dobbins and Megaridis (1991), who used the small qR_g , Guinier form (see Equation (48) below) universal to all structure factors and which can be integrated to yield $\sigma_{sca} \sim (1 - (2/3)k^2 R_g^2)$, where $k = 2\pi/\lambda$. To turn this into an expression good for all qR_g (not just the Guinier regime), they wrote the generalization $(1 - 2/3k^2 R_g^2) \simeq (1 + (4/3D)k^2 R_g^2)^{-D/2}$. This strategy, although not mathematically rigorous, was based on analogy to the Fisher-Burford (1967) (see below) structure factor and its small qR_g expansion. The final expression for the total scattering cross section is

$$\sigma_{sca}^{agg} = N^2 \sigma_{sca}^m G(kR_g), \quad [33]$$

where the single particle total Rayleigh scattering cross section is simply

$$\sigma_{sca}^m = \frac{8\pi}{3} k^4 a^6 F \quad [34]$$

and where

$$G(kR_g) = \left(1 + \frac{4}{3D} k^2 R_g^2\right)^{-D/2}. \quad [35]$$

Dobbins and Megaridis (1991) compared Equations (33)–(35) to both simulation data for total scattering of Mountain and Mulholland (1988) and their own porous sphere model with success.

Koylu and Faeth (1994a), Kazakov and Frenklach (1998), and Mulholland and Choi (1998) have all considered the problem of the total scattering cross section for an aggregate. Koylu and Faeth (1994a) and Kazakov and Frenklach (1998) integrated, via Equation (32), the Dobbins and Megaridis (1991) structure factor (see Table 2 below) for unpolarized incident light. Rather complex equations were obtained and used successfully by both. However, their results have a singularity at $D = 2$ and hence are rapidly varying at $D = 1.8$, which is problematic. Our attempt to perform the integral in Equation (32) for polarized incident light (the more common laser laboratory situation) led to similar singularities at $D = 2$ when D was assumed not equal to 2 and a logarithmic divergence when it was assumed $D = 2$. Both groups noted that the Dobbins and Megaridis result, Equation (35), is in error at large kR_g . Figure A1 of Kazakov and Frenklach shows good agreement for $kR_g \leq 3$, but for $kR_g \geq 10$ Equation (35) is 20% too small. Mulholland and Choi (1998) performed the integral in Equation (32) for unpolarized incident light and the Fisher–Burford structure factor, Equation (52) below. Again a complex equation was obtained, but the result does not have a singularity at $D = 2$. One possible drawback to this result is that we have shown (Sorensen et al. 1992a; and see below) that the Fisher–Burford form does a poor job of describing the q -dependent structure factor of real aggregates over predicting the scattering when $q > R_g^{-1}$. Comparison of the Mulholland and Choi total scattering to the results above is good for $kR_g \leq 1$, but for $kR_g \geq 10$ it is 25% bigger than that predicted by Koylu and Faeth and Kazakov and Frenklach, hence 45% bigger than the prediction of Equation (35), all for $D \simeq 1.8$. Below, when we discuss the albedo, we will see that Equation (35) is successful even when $kR_g \simeq 25$. The straightforward simplicity of Equation (35), lack of singularities, and validity of $S(q)$ make it a good choice, but consideration of the integrated forms is advised at large kR_g .

The structure factor is a consequence of the scattering of a uniform wave of any sort from a weakly scattering cluster. Being a Fourier transform of the real space structure it is a mathematical idealization. By “putting in the optics” to lowest order we give reality to the problem by identifying the wave as electromagnetic, more precisely light. The complete description must account for the facts that the wave may scatter more than once

within the aggregate, multiple scattering, and the fields across the individual monomers may not be uniform, i.e., the so-called Rayleigh approximation breaks down.

This first description of fractal aggregate scattering and absorption, presented above, represents a first-order approximation to the true situation. The weak, single scattering approximation is essentially the first Born approximation of quantum mechanical wave theory. However, since we are dealing with light, this term seems inappropriate. Although the Rayleigh approximation has been taken for the monomers, the scattering from the aggregates, unlike Rayleigh scattering, will have a scattering angle dependency. Because of this weak scattering yet scattering angle dependent situation, it is appropriate to call this first-order approximation the RDG approximation, as coined by Koylu and Faeth (1994a), in analogy to the theory of the same name that describes weakly scattering yet finite-sized spheres. As we will see, it is a most viable description for $D < 2$. Table 1 compiles the results above for the RDG theory for scattering and absorption by an aggregate.

Rigorous Derivation of the Structure Factor

Both Equations (10) and (11) are viable for calculating the structure factor of a scattering object. They yield equivalent results and each has its regime of facility. To gain more understanding of their relationship, we convert the sums to integrals by introducing the density function (number per unit volume) of a system of scatterers as

$$n(\vec{r}) = N^{-1} \sum_i^N \delta(\vec{r} - \vec{r}_i), \quad [37]$$

where δ is the Dirac delta function. Then

$$\sum_i^N e^{i\vec{q}\cdot\vec{r}_i} = N \int e^{i\vec{q}\cdot\vec{r}} n(\vec{r}) d\vec{r}. \quad [38]$$

Comparing Equations (8) and (38) shows that the amplitude of the wave scattered from a system of N scatterers is proportional to the Fourier transform of the density function. The structure factor is the N^{-2} normalized square of this amplitude, as written in Equation (10).

Now we recall the convolution theorem of Fourier analysis (e.g., Hecht 1998) that states that the product of Fourier transforms is the Fourier transform of the convolution of the nontransformed functions. That implies that the structure factor, which is the square of the Fourier transform of the density function, is also the Fourier transform of the convolution of the density function with itself. The self-convoluted density function is

$$g(\vec{r}) = \int n(\vec{r} - \vec{r}') n(\vec{r}') d\vec{r}'. \quad [39]$$

Then the convolution theorem implies

$$S(\vec{q}) = \int e^{i\vec{q}\cdot\vec{r}} g(\vec{r}) d\vec{r}. \quad [40]$$

Table 1

RDG cross sections for scattering and absorption by an aggregate of N monomers of radius a and refractive index m

Absorption:

$$\sigma_{abs}^m = -4\pi k a^3 E(m), \quad (30)$$

$$\sigma_{abs}^{agg} = N \sigma_{abs}^m. \quad (29)$$

Differential scattering:

$$\frac{d\sigma^m}{d\Omega} = k^4 a^6 F(m), \quad (26)$$

$$\frac{d\sigma^{agg}}{d\Omega} = N^2 \frac{d\sigma^m}{d\Omega} S(q), \quad (28)$$

where

$$E(m) = \text{Im} \left[\frac{m^2 - 1}{m^2 + 2} \right], \quad (31)$$

$$F(m) = \left| \frac{m^2 - 1}{m^2 + 2} \right|^2. \quad (27)$$

The structure factor (see also Table 2):

$$S(q) = 1 \quad q R_g \ll 1 \quad (36a)$$

$$= 1 - q^2 R_g^2 / 3, \quad q R_g \lesssim 1 \quad (36b)$$

$$= C(q R_g)^{-D}, \quad q R_g > 1. \quad (36c)$$

Total scattering:

$$\sigma_{sca}^m = \frac{8}{3} \pi k^4 a^6 F(m), \quad (34)$$

$$\sigma_{sca}^{agg} = N^2 \sigma_{sca}^m G(k R_g), \quad (33)$$

where, for a fractal aggregate,

$$G(k R_g) = \left(1 + \frac{4}{3D} k^2 R_g^2 \right)^{-D/2}. \quad (35)$$

Now we show that Equation (40) is equivalent to Equation (10). Use of Equation (37) for the double sum in Equation (11) implies

$$S(\vec{q}) = N^{-2} \sum_i^N \sum_j^N e^{i\vec{q} \cdot (\vec{r}_i - \vec{r}_j)} = \iint n(\vec{r}) n(\vec{r}') e^{i\vec{q} \cdot (\vec{r} - \vec{r}')} d\vec{r} d\vec{r}'. \quad (41)$$

Changing variables of the right-hand side (RHS) of Equation (41) to \vec{r} and $\vec{u} = \vec{r} - \vec{u}'$, we obtain

$$S(\vec{q}) = \iint n(\vec{r}) n(\vec{r} - \vec{u}) e^{i\vec{q} \cdot \vec{u}} d\vec{r} d\vec{u}. \quad (42)$$

Now apply Equation (39) to Equation (42) to obtain

$$S(\vec{q}) = \int g(\vec{u}) e^{i\vec{q} \cdot \vec{u}} d\vec{u}, \quad (43)$$

which is equivalent to Equation (40).

The function $g(\vec{u})$ of Equation (43) is well known in the scattering literature and beyond, not so much as the self-convolution but as the density autocorrelation function. Its importance transcends scattering theory and for condensed matter includes the

thermodynamics of the system. The standard description of the structure factor is that it is the Fourier transform of the all important density autocorrelation function, i.e., $S(\vec{q})$ and $g(\vec{u})$ are Fourier transform pairs. This is the description of Equations (11) and (40). However, there is an equally valid but less used view given by Equation (10) combined with Equation (38), namely,

$$S(\vec{q}) = \left| \int n(\vec{r}) e^{i\vec{q} \cdot \vec{r}} d\vec{r} \right|^2. \quad (44)$$

Equation (44) shows that the structure factor is the square of the Fourier transform of the density. As we have seen, these two points of view are connected by the convolution theorem.

Under the assumption of isotropy, $S(\vec{q}) = S(q)$ and $g(\vec{u}) = g(u)$ and the solid angle integration can be performed on Equation (43) to yield

$$S(q) = 4\pi \int g(u) \frac{\sin qu}{qu} u^2 du. \quad (45)$$

Before we proceed with Equation (45) for various explicit physical realizations of the density autocorrelation function, it is valuable to study both the small and large q behavior of the structure factor.

$qR_g < 1$ Behavior of the Structure Factor. The Guinier-Regime

We expand the integrand of Equation (45) for small qu . To do this, first pull the factor of 4π into Equation (45) to create a volume integral, $4\pi u^2 du = d\bar{u}$. Next expand $x^{-1} \sin x \simeq 1 - x^2/3!$. Then Equation (45) becomes two integrals, the first of which is unity by the normalization of $g(u)$ so that we obtain

$$S(q) \simeq 1 - \frac{q^2}{6} \int u^2 g(u) d\bar{u}. \quad [46]$$

We show in Appendix A that

$$R_g^2 = \frac{1}{2} \int u^2 g(u) d\bar{u}, \quad [47]$$

where R_g is the radius of gyration of the aggregate. Hence at small q we obtain

$$S(q) \simeq 1 - \frac{1}{3} q^2 R_g^2. \quad [48]$$

This result is often called the Guinier equation (Guinier 1939; Guinier et al. 1955; Teixeira 1986). It is sometimes written as $S(q) \simeq \exp[-q^2 R_g^2/3]$ and is valid for $qR_g < 1$. (Note that this defines what is meant by “small q .”) Its form is independent of the form of $g(u)$. Its great utility is that it allows for measurement of the aggregate size regardless of the refractive index of the aggregate.

$qR_g > 1$ Behavior of the Structure Factor and the Fractal Cluster Density Autocorrelation Function

In order to consider the large qR_g behavior of the structure factor with Equation (43), an explicit form for the density autocorrelation function must be used. The general form is expected to be (Teixeira 1986)

$$g(r) = Ar^{D-d} h(r/\xi), \quad [49]$$

where A is an appropriate constant, d is the spatial and D is the fractal dimension, $h(r/\xi)$ is a cutoff function faster than any power law, and ξ is a characteristic length representing the size of the cluster. The r^{D-d} term is the fractal part, and when Fourier transformed yields $S(q) \propto q^{-D}$, the well-known characteristic behavior for fractal scattering at large q , and a result obtained above from scaling arguments. The perimeter of the aggregate is described by the cutoff function $h(r/\xi)$, which is independent of the fractal nature.

Before we describe the current best expressions for $h(r/\xi)$, we discuss the generic behavior of $S(q)$ as a function of D and the cutoff function. To do this we write the cutoff function as

$$h(r/\xi) = e^{-(r/\xi)^\beta}, \quad [50]$$

where the larger the value of β , the sharper the cutoff. Jullien (1992) and, in particular, Nicolai et al. (1994) have studied the behavior of $S(q)$ as a function of D and β for $d = 3$.

Figure 8 shows the effect of β for a fractal dimension of $D = 2$. As β increases, the real space cutoff becomes sharp. In q -space, Figure 8 shows that as β increases a distinct hump develops just beyond the Guinier regime near $qR_g \sim 2$. After the

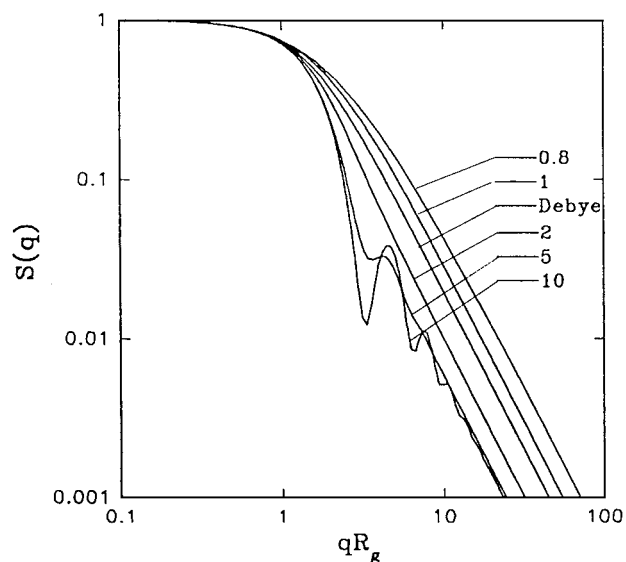


Figure 8. Structure factor versus qR_g for fractal aggregates all with $D = 2$, but with different values of the cut-off exponent β . The Debye function is for a random chain.

hump, the characteristic power law q^{-D} ensues but at different levels depending on β . To describe these levels we write the asymptotic structure factor as

$$S(qR_g \gg 1) = C(qR_g)^{-D}, \quad [51]$$

where C is a constant quantifying the level. Figure 8 shows that the values of C decrease as β increases. Also notice that for very large β , “ripples” occur due to the sharp cutoff. The minima in these ripples occur at $qR_g \simeq 3.2$ and 6.7 . These can be compared to the first minima in the RDG equation for a $d = 3$ sphere, which has the sharpest possible physical cutoff, which are at $qR_g = 3.5$ and 6.0 (see Figure 6 and recall $R_g = \sqrt{3/5}R$ for a solid sphere).

Figures 9 and 10 show the effect of D on $S(q)$ for $\beta = 1$ (exponential) and $\beta = 2$ (Gaussian) cutoffs. In each case the asymptotic slope on these log-log plots is $-D$ for all $D < d = 3$. For $\beta = 1$ and D just less than 3, $S(q)$ comes out of the Guinier regime with a slope of -4 , the Porod result for a smooth surfaced sphere of $D = d = 3$. This Porod law crosses to slope $-D$ at larger qR_g . However, this crossover extends beyond the Guinier regime, and hence becomes noticeable, only for $D \gtrsim 2.9$. For $\beta = 2$ the hump near $qR_g \sim 3$ is part of the functionality $S(q) = \exp[-(qR_g)^2/3]$ which results at $D = 3$. $S(q) \sim q^{-D}$ again for all $D < 3$ asymptotically beyond this hump. For $D = 2.9$ the crossover to power law begins near $qR_g \simeq 5$. Thus we conclude that for these two, as we shall see, common cutoffs, the asymptotic $S(q) \sim q^{-D}$ behavior begins immediately after the Guinier regime for all $D \lesssim 2.9$.

Explicit Forms for the Structure Factor

As seen above, the fractal aggregate structure factor is dependent on both the fractal dimension D and the sharpness of the

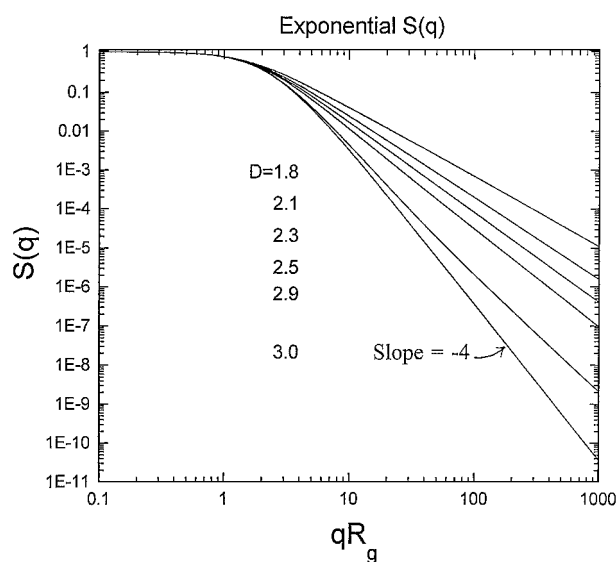


Figure 9. Structure factor for exponential cut-offs ($\beta = 1$) and a variety of fractal dimensions D . Large qR_g slopes are $-D$, except when $D = 3.0$, and then the slope is -4 .

cutoff as determined by β . Explicit calculation of the structure factor as the Fourier transform of the density autocorrelation function shows that the functional form of the structure factor is determined by β , and once the form is set D becomes a parameter in that functional form. Use of the Fourier transform of $g(u)$ has been limited to two values of β : $\beta = 1$, the exponential cutoff, and $\beta = 2$, the Gaussian cutoff. The exponential cutoff has the longest history, having been used in some of the earliest studies of fractal aggregate scattering by Freltoft et al. (1986), Berry

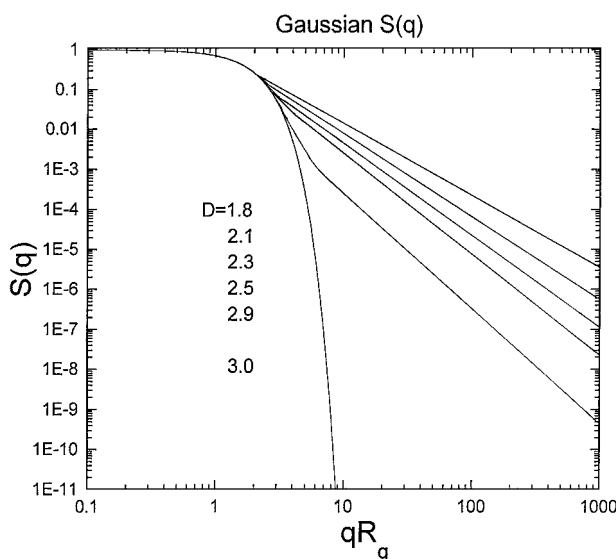


Figure 10. Structure factor for Gaussian cut-offs ($\beta = 2$) and a variety of fractal dimensions D . Large qR_g slopes are $-D$, except when $D = 3.0$, and then the functionality is $S(q) = \exp[-(qR_g)^2]$.

and Percival (1986), and Teixeira (1986). The resulting structure factor and the relation of ξ to the cluster radius of gyration R_g are listed in Table 2. The sharper Gaussian cutoff was first proposed in our work (Sorensen et al. 1992a). Again the resulting structure factor and relation to R_g are given in Table 2. Two forms are given; they are related by the Kumar Transformation (Abramowitz and Stegun 1965). Both represent infinite series, but the second form, with the negative argument converges faster. Unfortunately, neither form converges very fast and therefore high speed computing is necessary for fitting to data.

A number of other structure factors have been proposed, only one of which is related to a correlation function with a generalized exponential cutoff, Equation (50). Based on the real space analysis of simulated DLCA clusters, Mountain and Mulholland (1988) found a best fit to Equation (50) with $\beta = 2.5 \pm 0.5$. This is within error consistent with the Gaussian cutoff, but not the exponential. The resulting equation for the structure factor does not appear to be analytically solvable, but Mountain and Mulholland calculated it numerically. Hurd and Flower (1988) proposed that the fractal aggregates had sharp spherical perimeters, hence the cutoff is described by the autocorrelation function of a sphere. Because we have shown that the density autocorrelation function is equivalent to a self convolution, this cutoff may be called the “overlapping spheres” cutoff because the convolution integral essentially overlaps the real space density function. Its form can be calculated analytically and is given in Table 2, but the resulting structure factor must be calculated numerically.

Another popular expression for the structure factor is the so-called Fisher–Burford or modified Ornstein–Zernike (Fisher and Burford 1967; Martin et al. 1986; Teixeira 1986) form

$$S(q) = \left(1 + \frac{2}{3D}q^2R_g^2\right)^{-D/2}. \quad [52]$$

This formula came to us from the way fluids near a critical point scatter waves, although there need not be any connection between fractal aggregates and critical fluids. The Fisher–Burford form is equal to the exponential structure factor at $D = 2$ and is a good approximation near $D = 2$. Its great advantage is its simplicity.

Dobbins and Megaridis (1991) proposed a straightforward structure factor not based on any density correlation function. Its form, also given in Table 2, is based on use of the Guinier formula at small qR_g and the expected power law $C(qR_g)^{-D}$ at large qR_g with a condition of continuity in the function and its slope where they meet. This puts a condition on the constant C , which is also given in Table 2.

Lin et al. (1990b) gave polynomial expansions for the structure factor based on fitting the polynomial to the structure factor of computer-generated aggregates created via both diffusion-limited and reaction-limited (DLCA and RLCA, respectively) algorithms. The polynomials were built with the correct low qR_g (Guinier) and large qR_g (power law) limits. Again, these forms are given in Table 2.

Table 2
Structure factors and cut-off functions for fractal aggregates

Name	$h(r/\xi)$	$\xi^2 =$	$S(q)$	C
Exponential	$e^{-r/\xi}$	$\frac{2R_g^2}{D(D+1)}$	$\frac{\sin[(D-1)\tan^{-1}(q\xi)]}{(D-1)q\xi(1+q^2\xi^2)^{(D-1)/2}}$	$\frac{\sin[(D-1)\pi/2]\left[\frac{D(D+1)}{2}\right]^{D/2}}{D-1}$
Gaussian	$e^{-(r/\xi)^2}$	$\frac{4}{D}R_g^2$	$e^{-(qR_g)^2/D} {}_1F_1\left(\frac{3-D}{2}, \frac{3}{2}; \frac{(qR_g)^2}{D}\right)$ $= {}_1F_1\left[\frac{D}{2}, \frac{3}{2}; -\frac{(qR_g)^2}{D}\right]$	$D^{D/2} \frac{\Gamma(3/2)}{\Gamma(\frac{3-D}{2})}$
Mountain and Mullholland	$e^{(-r/\xi)^{3.5}}$		${}_1F_1$ is the Kummer or hypergeometric function	ca. 0.77 for $D = 1.8$
Overlapping spheres	$= \left(\frac{4}{3}\pi\xi^3\right)(1+r/4\xi)$ $(1-r/2\xi)^2, r < 2\xi$ $= 0, r > 2\xi$	$\frac{(D+2)(D+5)}{2D(D+1)}R_g^2$	Numerical	ca. 1.07 for $D = 1.75$
Fisher-Burford	ca. $C^{-r/\xi}$	$\frac{R_g^2}{3}$	$\left(1 + \frac{2}{3D}q^2R_g^2\right)^{-D/2}$	$(3D/2)^{D/2}$
Dobbins and Megaridis	—	—	$\exp[-(qR_g)^2/3]$, small qR_g $C(qR_g)^{-D}$, large qR_g join with continuous slope	$(3D/2e)^{D/2}$
Lin et al.	—	—	$\sum \left[1 + \sum_{s=1}^4 C_s(qR_g)^{2s}\right]^{-D/8}$	$1 - D/400$
				$C_1 = 8/3D, C_2 = 2.5$ $C_3 = -1.52, C_4 = 1.02$

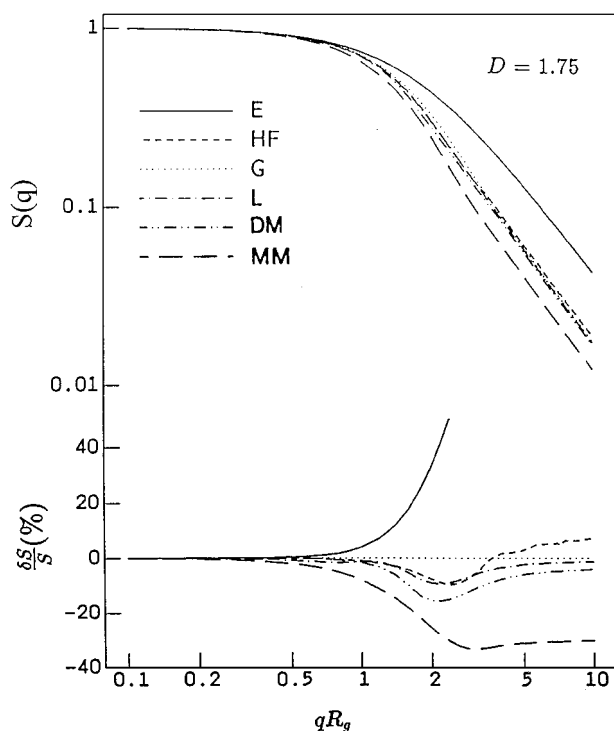


Figure 11. Comparison of various theoretical forms for the structure factor $S(q)$: upper section shows the structure factors, lower section shows the normalized deviation from the Gaussian structure factor ($\delta S = S - S_G$). Key: E = exponential; HF = Hurd and Flower; G = Gaussian; L = Lin et al.; DM = Dobbins and Megaridis; MM = Mountain and Mulholland.

All these structure factors are compared in Figure 11 (Sorensen et al. 1992a). The Gaussian, Dobbins and Megaridis, overlapping sphere, and Lin et al. DLCA structure factors are all consistent to within 10%. The exponential structure factor is much too high at large qR_g , and the Mountain and Mulholland structure factor is 20–30% lower than the agreeing group at large qR_g .

Figure 11 shows that the various structure factors differ in the coefficient of the power law C in Equation (51). This coefficient can be calculated from the various forms in Table 2, and the results as a function of D are displayed in Figure 12.

Figure 12 shows that in the DLCA aggregate regime near $D \simeq 1.8$, the Gaussian, Dobbins and Megaridis, and Lin et al. forms all yield a coefficient C within a few percent of unity. This is consistent with the comparison in Figure 11, and this comparison also implies that the overlapping sphere structure factor would also yield ($C \simeq 1$) for $D \simeq 1.8$ had we calculated it. In contrast, the exponential and Fisher–Burford forms yield large values of C , $C = 2.73$ and 2.44 , respectively, for $D = 1.7$. Both of these are rapidly varying functions of D in this regime as well, in contrast to the other structure factors.

The relevant question now is what cutoff, hence what structure factor, best describes fractal aggregates? Previous work

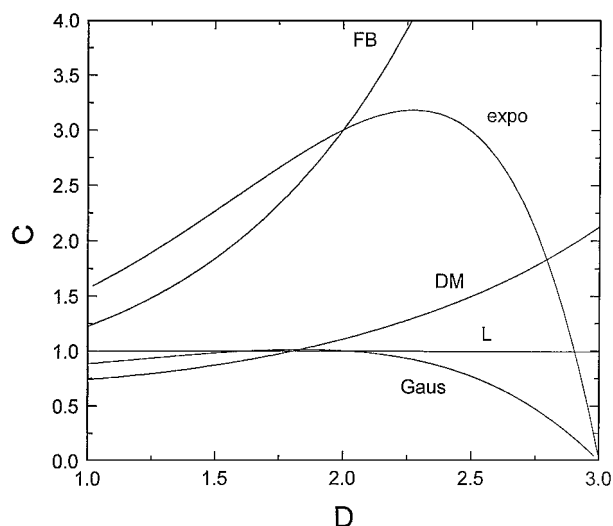


Figure 12. Coefficient C of the power law $S(q) = C(qR_g)^{-D}$ for the structure factor of a single fractal aggregate when $qR_g \gg 1$ as a function of the fractal dimension D for various structure factors: FB = Fisher–Burford; $expo$ = exponential cut off; DM = Dobbins and Megaridis; L = Lin et al.; $Gaus$ = Gaussian cut off.

from this laboratory (Sorensen et al. 1992a) considered light scattering from soot fractal aggregates in flames. It was found that structure factors derived from autocorrelation functions with roughly Gaussian, $\beta = 2$, cutoffs gave the best fits to the data when the effect of the aggregate polydispersity was included. The structure factor derived from the exponential, $\beta = 1$, cutoff did a poor job of fitting the data, as did the Fisher–Burford form, which approximates the exponential structure factor. We also found that if the effects of polydispersity were not included, i.e., if the experimental data were fit with the single cluster structure factors, the best fits were obtained with the exponential and Fisher–Burford forms. Of course, such a fit cannot be correct because real systems are polydisperse. Below we will see that polydispersity increases the effective value of C so that the exponential and Fisher–Burford forms with their too large C values can fit the data, thus demonstrating why these two forms work so well for fitting data when the analysis overlooks polydispersity. Subsequently we used TEM images of soot aggregates thermophoretically captured from a flame to compute $g(u)$ directly (Cai et al. 1993). Again cutoffs much sharper than exponential, and well described by a Gaussian, were found. Lin et al. (1990a) created both DLCA and RLCA aggregates with computer simulation. These were Fourier transformed to $S(q)$ and then an average $S(q)$ was fit to a polynomial in qR_g . These are given in Table 2. Nicolai et al. (1994) fit both these DLCA and RLCA structure factors to structure factors derived from Equations (45), (49), and (50) with arbitrary β and found that $\beta = 2$ fit best. Recently, Haw et al. (1995) have also concluded that a cutoff significantly faster than exponential is necessary to describe scattering data.

Given the experimental evidence in favor of a structure factor derived from a Gaussian cutoff and the agreement of the coefficient C in the relevant range of fractal dimensions with other empirically based structure factors, we shall take $C = 1.0 \pm 0.05$ as the best value to describe the power law regime of the structure factor of a single aggregate with D in the range 1.7–2.2.

This major variation in the C values of the asymptotic regime is important. But as yet we have only a partial story with regard to fitting real scattering data. Nearly any real system will be polydisperse in cluster size, and that affects the overall appearance of the structure factor, especially in the large qR_g regime, and hence the value of the power law's coefficient.

The Structure Factor of an Ensemble of Polydisperse Aggregates

Any real experiment detecting scattered radiation from an ensemble of fractal aggregates will involve a polydisperse (in cluster size) ensemble. Aggregates are a result of aggregation, which always gives a finite width to the cluster size distribution. This polydispersity causes the shape of the observed structure factor to be different than that of the structure factor of any single cluster in the distribution (Nicolai et al. 1994; Sorensen and Wang 1999). The single cluster structure factor, dependent on the cutoff and D , was described above. Now we consider how the shape is modified by a distribution in cluster sizes. The modifications will occur in both the Guinier and power law regimes.

One could argue that only an individual aggregate has a structure factor, not an ensemble of aggregates. However, an ensemble of aggregates will scatter light and the scattered intensity when plotted versus q gives an effective structure factor for the ensemble. To consider the optical structure factor for an ensemble of aggregates, we will use the RDG approximation in Table 1 for our analysis of the effect of polydispersity on the ensemble structure factor.

In general, the effective structure factor for an ensemble of aggregates can be written as

$$S_{\text{eff}}(q) = \int N^2 n(N) S[qR_g(N)] dN / \int N^2 n(N) dN, \quad [53]$$

where $n(N)$ is the size distribution, i.e., the number of clusters per unit volume with N monomers per cluster. The number of monomers per cluster and the cluster radius of gyration are related by Equation (1). Certainly one procedure to fit data is to select a single cluster structure factor and an appropriate size distribution and then fit the data numerically to Equation (53) with fit variables such as D and the size distribution parameters of most probable size, distribution width, etc. Such a procedure, while viable, can be easily abused because the fitter can lose sight of the physical meaning of the fit parameters. How often has reliance on a goodness of fit parameter been substituted for physical sense of the fit? Here we attempt to create an analysis that relies on physical sense and simplicity.

Useful analytical solutions to the polydispersity problem in the power law regime can be obtained if we ignore the Guinier

regime and represent the single aggregate structure factor by its Rayleigh and power law limits:

$$S(q) = 1, \quad qR_g \ll 1 \quad [23a]$$

$$= C(qR_g)^{-D}, \quad qR_g \gg 1. \quad [23b]$$

To compute the results of Equation (53) applied to Equations (23), we define the i th moment of the size distribution as (Equation (B4))

$$M_i = \int N^i n(N) dN. \quad [B4]$$

Note that the moment is an average and could also be written as \bar{N}^i or $\langle N^i \rangle$. With Equation (1), we find

$$S_{\text{eff}}(q) = 1, \quad qR_g \ll 1 \quad [54a]$$

$$= \frac{M_1}{M_2} k_o C (qa)^{-D}, \quad qR_g \gg 1. \quad [54b]$$

The functionality on monomer radius a in Equation (54b) can be useful when a is known, as we will see. Here, however, we continue to consider the experimental situation. Since an experiment deals with an ensemble of different-sized aggregates, we require $S(q)$ as a function of $q\langle R_g \rangle$, where $\langle R_g \rangle$ is the "average" R_g measured by the experiment. Since the experiment is scattering, the average is determined by the scattering. The average R_g is best determined from analysis of scattering in the Guinier regime. Below (Equation (88)) we will show that this is the z -average radius of gyration

$$R_{g,z}^2 = a^2 k_o^{-2/D} \frac{M_{2+2/D}}{M_2}. \quad [55]$$

Recalling once again the laboratory, the experimentalist will measure an uncalibrated $I(q)$ and normalize it with the Rayleigh regime scattering, $I(0)$, to obtain Equations (54). He or she will then use the Guinier regime to determine $R_{g,z}$, Equation (55). Then plot $I(q)/I(0)$ versus $qR_{g,z}$ to obtain the structure factor of the ensemble. Thus we use Equations (54) and (55) and substitute on $k_o a^{-D}$ to obtain

$$S_{\text{eff}}(q) = 1, \quad qR_g \ll 1 \quad [56a]$$

$$= C \frac{M_1}{M_2} \left(\frac{M_{2+2/D}}{M_2} \right)^{D/2} (qR_{g,z})^{-D}, \quad qR_g \gg 1. \quad [56b]$$

The most notable result in Equations (56) is that the coefficient of the power law is modified by the polydispersity of the ensemble. Thus a strong warning is that if this modifying factor is significantly different than unity, then use of single cluster structure factors on scattering data could yield erroneous results. The result also opens an opportunity to measure, to some degree, the polydispersity of the ensemble.

We next evaluate the polydispersity factor in Equation (56b), which we shall call C_p :

$$C_p = \frac{M_1}{M_2} \left(\frac{M_{2+2/D}}{M_2} \right)^{D/2}. \quad [57]$$

Then Equation (56b) becomes

$$S_{\text{eff}}(q) = C C_p (q R_{g,z})^{-D}; \quad q R_g \gg 1. \quad [58]$$

Given a size distribution, the polydispersity factor C_p can be calculated. It is well established that an aggregating system develops a self-preserving, scaling distribution (Friedlander and Wang 1966; Wang and Friedlander 1967; van Dongen and Ernst 1985) given by (see Appendix A)

$$n(N) = A x^{-\tau} e^{-\alpha x}, \quad [59]$$

where x is the relative size

$$x = N/s \quad [60]$$

and s is a mean size. Notice size in this context is the aggregation number, N . The exponent τ is a measure of the width of the distribution with large τ implying a broad distribution. This scaling form is valid when $x > 1$, the small x form being different. Since scattering strongly weights the large end, i.e., $x > 1$, of the distribution, the small x has little effect on the properties of scattering from an ensemble of aggregates and hence can be ignored. Some details of the distribution are described in Appendix A.

Other forms for the size distribution of aggregates exist, but caution must be exercised in their use. For example, the intuitive log-normal distributions are frequently used in the literature. However, we have shown (Sorensen et al. 1992b) that these distributions yield erroneous values for distribution moments higher than the second when compared to the exact scaling distribution. For the second moment and lower, the distributions agree well. Since scattering involves higher moments, such as $M_{2+2/D} \simeq M_3$ for $D \simeq 2$, it is erroneous to use the log-normal distribution for light scattering analysis.

In Appendix B we derive a general expression for the i th moment of the scaling distribution, Equations (A6) and (A8). With this, we find the polydispersity factor to be

$$C_p = \frac{1}{2-\tau} \left[\frac{\Gamma(3-\tau+2/D)}{\Gamma(3-\tau)} \right]^{D/2}, \quad [61]$$

where $\Gamma(x)$ is the gamma function. In Figure 13 we graph C_p as a function of the width parameter τ for a variety of fractal dimensions D . We find C_p in general to be significantly greater than unity, thus our warning not to use single cluster structure factors for analysis of scattering experiments involving a polydisperse ensemble of aggregates is quite appropriate. In particular, for DLCA in the continuum regime it is expected and well verified that $\tau = 0$ and $D = 1.75$ to 1.8. Then from Equation (61) or

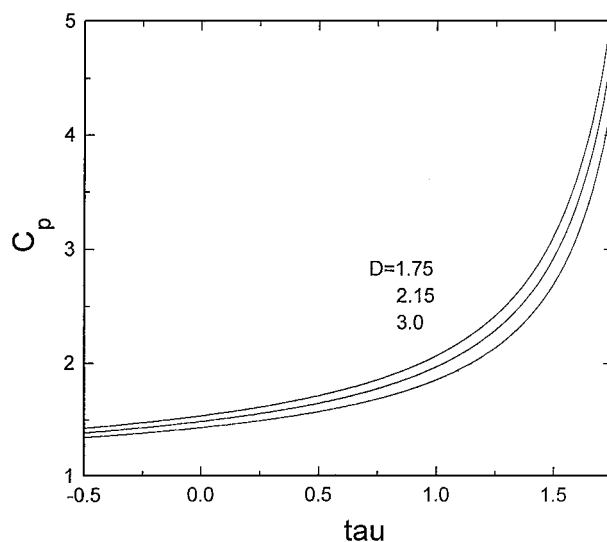


Figure 13. The polydispersity factor C_p , Equation (61), which describes the level of the power law regime of the structure factor of a polydisperse ensemble of fractal aggregates, Equation (58), as a function of the polydispersity exponent τ for various fractal dimensions.

Figure 13 we find $C_p = 1.53$. As the Knudsen number of the aggregates increases above 0, the continuum regime is left and τ becomes negative (Wang and Sorensen 2000) and then swings back to positive values in the free molecular limit (Mulholland et al. 1988; Oh and Sorensen 1997). Hence C_p would vary with the kinetic regime. The significance of C_p is that its measurement allows for a determination of the polydispersity exponent τ . We have applied Equation (61) for measuring the size distribution exponent with success (Sorensen and Wang 1999), and we describe this in the Optical Particle Sizing section below.

SCATTERING OF LIGHT

The study of electromagnetic scattering from aggregates has a long history. For our purposes aggregates can be classified into two categories: 1) geometric aggregates in which the spherical monomers are arranged into geometric patterns such as linear chains, zig-zag chains, planes, spheres, etc., and 2) fractal aggregates. We will not consider other situations such as particles within particles or dispheres.

The essential question that must be understood for scattering from any body of finite size parameter, $ka > 0$, is how much does that body interact with itself during scattering? For an aggregate, this question becomes how much does the scattering from the other monomers of the aggregate influence the total field at a given monomer? For a single sphere the question is the same, we need only to make the sphere an aggregate by dividing the sphere into a number of domains analogous to the monomers of the aggregate. If the interaction is negligible, the field at the monomer is just the incident field and the first order result of independent scattering, the RDG theory given above (Table 1)

results. These intracluster interactions may be called multiple scattering, a term used to mean that the field at a given monomer is due to the incident field plus the fields scattered by all the other monomers in the aggregate. Calculation of the fields due to the other monomers is an iterative process. One first calculates the field at a given monomer due to all the other monomers, assuming the fields they see are just in incident fields. This yields a corrected incident field for that monomer. This is repeated for all the monomers in the system to complete the first iteration. The process can then be repeated with the corrected incident fields for as many iterations as deemed necessary. Usually the fields are assumed uniform across the monomer, thus the monomers act as dipoles. Hence multiple scattering can also be called “coupled dipole scattering.”

GEOMETRIC AGGREGATE LIGHT SCATTERING

Geometric aggregates have a longer history because the fractal concept applied to aggregates is relatively new. Ku and Shim (1992) did a nice job of reviewing this subject up to 1992 and have also made detailed comparisons of three prominent electromagnetic approaches to this problem. The oldest approach is that of Jones (1979), which is based on an original formulation derived from Maxwell’s equations by Saxon (1974). The Jones approach, when corrected (Ku 1991), considered multiple scattering to second order in reciprocal distance between monomers. They also considered the coupled dipole method of Purcell and Pennypacker (1973) (PP), which views each monomer as a dipole (hence a Rayleigh scatterer) and includes multiple scattering to third order. Finally, they considered the volume integral equation formulation (VIEF) of Iskander et al. (1989) (ICP), which is very similar to the coupled dipole approach in that multiple scattering is included to third order, but in addition a self-interaction term, where the field in the monomer sphere induces an interaction with itself, is included. All three approaches assumed uniform fields across the monomer particles (the Rayleigh approximation). The refractive indices used were $m = 1.71 + 0.0i$, $2.98 + 0.56i$, and $1.7 + 0.7i$, the last of which represents soot formed in a flame.

The results of the intercomparisons of these three methods and comparisons with the exact Mie results available for spherical particles favored the ICP approach slightly over PP and greatly over Jones. For dense, spherical aggregates the failure of the Jones solution was ascribed to insufficient handling of multiple scattering. ICP and PP began to fail for angular scattering patterns near $kR \sim 5$, where R is the cluster sphere radius. This work explicitly demonstrates the importance of multiple scattering as the size parameter for a sphere takes it out of the Rayleigh regime.

A variety of geometric aggregates were also studied. Linear chains, zig-zag chains, side-by-side chains, rectangles, etc. Again ICP was a bit better than PP due to the inclusion of the self term in ICP and both were much better than the Jones solution hence, once again, accentuating the importance of multiple scattering.

Lou and Charalampopoulos (1994) utilized Saxon’s (1974) integral equation to obtain a general form for the scattering from an assembly of Rayleigh particles. They concluded that the verdict against the Jones solution is not so negative as concluded by Ku and Shim. They also agreed with Ku and Shim that the self term is important. Comparisons were made with a soot-like $m = 1.7 + 0.7i$ for straight chains and dense aggregates.

For our purposes here, important qualities that also come out of Ku and Shim’s comprehensive study is that the absorption and the near forward angle scattering cross sections for the “chain-like” arrays (i.e., linear arrays, zig-zag and double linear arrays) are proportional to N and N^2 , respectively. This is the simple RDG result predicted from scaling and expected if no multiple scattering occurs. Thus these functionalities endure despite the presence of multiple scattering. Finite size, $D < 2$, aggregates with soot-like refractive indices all show between 10 to 60% (the latter is an extreme case) enhancements in both scattering and absorption when multiple scattering is included. Another important result is that the depolarization ratio $\rho_v = I_{VH}/I_{VV}$ (see below) is nonzero and increases with N . Since $\rho_v = 0$ in the single scattering limit, ρ_v is a direct indicator of multiple scattering. However, as we shall see below, ρ_v increasing with N is not found for fractal aggregates, the increase being symptomatic of geometric aggregates.

Fractal Aggregate Light Scattering

Theoretical Studies. The onset and importance of multiple scattering for fractal aggregates has been studied extensively, mostly in the context of testing how well the simple RDG theory works under various conditions and lesser so in regard to depolarized light scattering. Studies of the optics of fractal aggregates date back to Berry and Percival (1986), who made the Rayleigh approximation for the monomers ($ka \ll 1$) and considered arbitrary fractal dimension D . The aggregates were assumed to have an exponential cutoff, hence their ultimate result for scattering was the exponential structure factor, Table 2. Multiple scattering was studied by assuming all the monomers experienced the same multiply scattered field from its neighbors, a mean field approximation. Formulas for scattering and absorption with multiple scattering were not derived, but its importance relative to single scattering was studied. For $D < 2$ it was concluded that multiple scattering contributes a small constant amount relative to single scattering. For $D > 2$, however, multiple scattering can become significant and grow relative to single scattering as N increases. The onset of its significance was set at $N \gtrsim (ka)^{-D/(D-2)}$. Nelson (1989a) continued the work of Berry and Percival with further investigation of multiple scattering. She found that indeed when $D < 2$ the multiple scattering relative contribution tends to a constant. For $D > 2$, however, the total scattering cross section first rises like $N^{2-2/D}$, due to single scattering, but then crosses over as $N \rightarrow \infty$ to a $N^{2/D}$ dependence as multiple scattering dominates. The absorption cross section crosses over from N to $N^{4/D-1}$ dependencies. The

scattering result is intuitively pleasing since it is the same as the geometric limit for spheres where $\sigma_{sca} \sim R^2 \sim N^{2/3}$. However, also expected is $\sigma_{abs} \sim N^{2/3}$, which is inconsistent with $N^{4/D-1}$ at $D = 3$. Also, despite these changes the power law q^{-D} dependency remained as multiple scattering increased.

This impediment at large N for fractal aggregates with $D > 2$ of scattering and absorption by multiple scattering has interesting implications. The same amount of material dispersed in $D < 2$ aggregates rather than compressed into compact, sphere-like clusters with $D > 2$ will be much more effective at scattering and absorption. This has important consequences for nuclear winter (Colbeck and Harrison 1986; Nelson 1989b) or meteor impact scenarios as well as current day concerns regarding energy balance in the atmosphere. The effect of mass dispersion is well illustrated for the case of absorption by the work of Hage and Greenberg (1990), who considered a cube made of either 1000, 3375, or 8000 smaller cubes all with a size parameter $ka = 0.19$. These smaller cubes were either packed into a larger cube with complete efficiency, hence a porosity $p = 0$, or they were uniformly dispersed into large cubes parameterized by $p > 0$. Note that p is related to the volume fraction f of the small cubes in the larger cubes by $f = 1 - p$. The smaller cubes were spread uniformly over the volume of the large cube and hence the “aggregates” were not fractals but rather, to use their term, “fluffy aggregates.” The absorption was calculated using both the VIEF method and the Maxwell-Garnet effective medium theory (1904) in combination with Mie theory. Both methods agreed well.

The results are shown in Figure 14. Note how as the porosity increases the absorption cross section increases for the same amount of material. Furthermore, at $p = 1$, i.e., the dispersed (very fluffy) case, Figure 14 shows $\sigma_{abs}/N \simeq 280/1000 = 0.28$, $900/3375 = 0.27$, and $2150/8000 = 0.27$, thus $\sigma_{abs} \sim N$ in

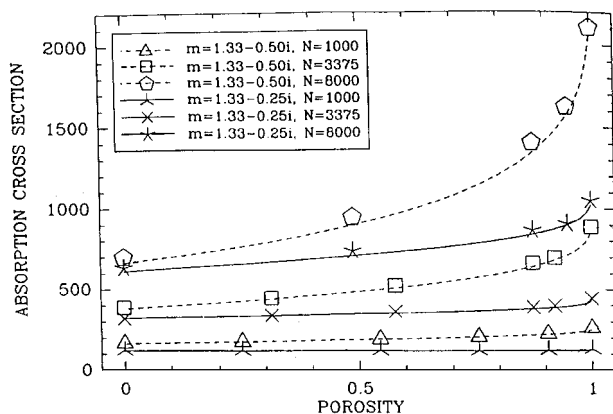


Figure 14. Absorption cross section for a cube composed of N smaller cubes with size parameter $ka = 0.19$. When the porosity is 0, all the small cubes are touching to form a compact large cube. As the porosity increases toward 1, the smaller cubes are separated and placed randomly on a larger cubic lattice occupying a fraction $1 - p$ of the sites.

all cases. Also at $p = 1$, σ_{abs}/N is directly proportional to the imaginary part of m (each σ_{abs} approximately doubles for a given N as the imaginary part of m doubles). At the other extreme, $p = 0$, the completely dense case, $\sigma_{abs} \sim N^{2/3}$ for $m = 1.33 + 0.5i$ ($\sigma_{abs}/N^{2/3} \simeq 170/1000^{2/3} = 1.7$, $380/3375^{2/3} = 1.7$, $700/8000^{2/3} = 1.7$) and approximately so for $m = 1.33 + 0.25i$. This $N^{2/3}$ dependency implies only the surface of the dense aggregate is absorbing light. The discrepancy for $m = 1.33 + 0.25i$ can be explained by the fact that with a smaller imaginary part for m , the wave penetrates deeper into the cube and is not constrained to the surface. Hence the absorption will have a dependency between the surface $N^{2/3}$ and volume N dependency.

Singham and Bohren (1993) used the coupled dipole method to study multiple scattering in both DLCA, $D \simeq 1.8$, and DLA, $D \simeq 2.5$, aggregates. Their aggregates had as many as $N = 1000$ monomers with a soot-like refractive index of $m = 1.75 + 0.5i$ and monomer size parameters as large as $ka = 0.628$. In general, they found for the differential scattering cross section that inclusion of the dipolar interactions (multiple scattering) had essentially no effect when $ka = 0.157$ and only a small effect (ca. 10% from reading their graphs) when $ka = 0.314$ for the $D \simeq 2.5$, DLA aggregates. Moreover, the effect was to decrease the cross section.

The impediment is also, at first thought perhaps, counterintuitive. Why should multiple scattering yield less scattering? The answer is that it is waves that are scattering and they can interfere. Multiple scattering in essence removes the field from the interior of the aggregate leaving only the surface material active at scattering and absorption. Realize that this is different than assumption 3 of our scaling approach above. There we assume each scatterer experiences the same field, whether inside the system or not. But the interior scatterer’s scattered waves destructively interfere in the far field at all nonzero scattering angles as a consequence of the Ewald-Oseen extinction theorem. In contrast, when the system has $D > 2$, multiple scattering abolishes the field at the interior scatterers; there is no field to scatter.

An alternative approach to the integral formulation is that based on the principal of superposition developed by Brunning and Lo (1971), who achieved the first successful formulation of electromagnetic wave scattering from more than one sphere. In this method the scattered field of the aggregate is the superposition of the fields from individual monomers, which are expressed as vector spherical harmonics with origins at each sphere. Then clever use is made of addition theorems in which harmonics expanded about one origin can be expanded about another so that the fields from all the monomers can be combined to yield the field from the aggregate. This yields an exact result incorporating internal multiple scattering. It also includes higher order multipoles from the sphere, whereas the volume integral formulation considers the spheres as electric dipoles only.

This superposition method has been applied to biospheres (Brunning and Lo 1971; Fuller 1991, 1994; Mishchenko and Mackowski 1994; Mackowski 1994), clusters of spheres

(Gerardy and Ausloos 1982; Mackowski 1994; Fuller 1995a; Mackowski 1995), planar arrays (Quinten and Kreibig 1993), and spheres with inclusions (Fuller 1995b). The method is still progressing and the reader is referred to a new book edited by Mishchenko, Hovenier, and Travis (2000), and in particular the article by Fuller and Mackowski (2000) in that book.

Results that can be used here for aggregate studies have been given by Mackowski (1994 and 1995). For two touching spheres it was noted that even for a very small size parameter of $ka = 0.01$, both absorption and scattering were 5 to 10% bigger than that predicted by RDG. For straight chains, this grew both as a function the number of monomers and $|m - 1|$ to be as large as 40% enhancements over RDG. Fractal aggregates with $D = 1.9$ also show increased absorption and extinction cross sections of about 5–20% over the RDG prediction.

Mackowski (1995) has also used an electrostatics analysis to calculate absorption and scattering from fractal aggregates with $D = 1.9$ and variable N . The restriction to this analysis is that the aggregate size must be less than the optical wavelength. Under this condition there is no length scale, so the size parameter of the monomer is arbitrary. For a soot-like refractive index in the visible region of $m = 2 + 1i$, scattering and absorption are 10 and 25% larger than the RDG limit. For midinfrared wavelengths, however, where $m \simeq 3 + 2i$, the absorption cross section is a factor of two or more greater than the RDG result.

Fractal dimension $D = 2$ appears to be an important boundary above which the effects of internal multiple scattering become increasingly important with size. In fact, the $D = 2$ boundary is important in other physical aspects as well (Oh and Sorensen 1997b; Cai and Sorensen 1994; Teixeira 1986). The simplest basis for this is that when $D < 2$, projection of the three-dimensional aggregate onto a two-dimensional plane can be achieved with very little monomer-monomer occultation. When $D > 2$, however, one can't possibly compress this greater dimensionality onto the smaller dimensional $d = 2$ plane. We say when $D < 2$ the cluster is transparent, whereas for $D > 2$ it is opaque. The results for scattering and absorption discussed above appear to be affected by this.

The importance of $D = 2$ to the optics can be made a bit more quantitative by considering the aggregate as a dispersion of one optical material, the monomers, in another, the vacuum, and then applying the Maxwell-Garnet effective medium theory. This theory is good for low and uniform density dispersions, the second condition is not satisfied by fractal aggregates. Under this caveat, we proceed. The Maxwell-Garnet theory predicts that the effective index of refraction is related to the refractive index of the dispersed phase and its volume fraction f by

$$\left(\frac{m^2 - 1}{m^2 + 2}\right)_{\text{eff}} = f \left(\frac{m^2 - 1}{m^2 + 2}\right). \quad [62]$$

We simplify this to

$$(m - 1)_{\text{eff}} \propto f(m - 1), \quad [63]$$

an approximation quite good when $m \rightarrow 1$ and not too bad otherwise.

For a fractal aggregate the volume fraction of monomers can be approximated as

$$f = \frac{Na^3}{R_g^3}. \quad [64]$$

More accurate expressions for f could be concocted, but given the other approximations, they are not warranted. Equation (64) does have the correct functionality. Finally, we use the fundamental scaling relationship for fractal aggregates, Equation (1). Combining this with Equations (63) and (64) yields ($k_o = 1$)

$$(m - 1)_{\text{eff}} \propto (R_g/a)^{D-3}(m - 1). \quad [65]$$

We now argue in analogy to the RDG theory for spherical particles which requires that the phase difference between a wave that travels through the particle and one that travels the same distance alongside the particle be small. This is the phase shift parameter ρ and the condition requires $\rho = 2ka|m - 1| < 1$. This phase-shift parameter for an aggregate becomes, with Equation (65),

$$2kR_g|m - 1|_{\text{eff}} = 2k|m - 1|a^{3-D}R_g^{D-2}. \quad [66]$$

For a given optical wave number k and monomer of size a and refractive index m , Equation (66) shows that for $D < 2$ the phase shift parameter gets *smaller* with increasing aggregate size. Thus the condition to be much less than one can be ultimately satisfied and, if our analysis is sound, the RDG theory should hold. On the other hand, for $D > 2$ increasing R_g increases the cluster phase shift parameter, taking it further away from the regime in which the RDG theory can be successful. At this time, Equation (66) must be viewed with some caution because of the misuse of the Maxwell-Garnet theory. Future work to test Equation (66) would be valuable.

In a similar vein, Khlebtsov (1993) used the principle of the anomalous diffraction approximation of van de Hulst (1957) to calculate the absorption and scattering cross sections for fractal aggregates at large N . Anomalous diffraction implies a regime where the size parameter kR_g can increase without bound, but the phase shift parameter is fixed well below unity. This is the essence of the argument that led to Equation (66) above. Khlebtsov uses Maxwell-Garnet theory to find the effective refractive index of the aggregate as a function of the radial position in the aggregate, rather than the cruder average over the whole aggregate used above. He finds asymptotic results consistent with RDG for $D < 2$ in that both the absorption and scattering cross sections go as N as $N \rightarrow \infty$. For $D > 2$ he finds a crossover in the scattering functionalities from $N^{2-2/D}$ and N , respectively, to both obeying $N^{2/D}$ as $N \rightarrow \infty$. This latter result is consistent with geometric optics, i.e., a shadow.

Mulholland et al. (1994) included the magnetic dipole term along with the electric dipole in their coupled dipole (multiple

scattering) study of DLCA ($D \simeq 1.9$) aggregates with $N = 2$ to 165. For soot-like aggregates (i.e., a complex refractive index of $m = 1.7 + 0.7i$) they found that this coupled electric and magnetic dipole (CEMD) calculation led to enhanced scattering and absorption (several percent) over RDG for primary particles with size parameters $ka \lesssim 0.25$, but this crossed over to smaller cross sections at larger ka . For silica aggregates (with a real refractive index of $m = 1.55$) the scattering cross section showed no cross over, rather it increased relative to the Rayleigh cross section monotonically with monomer size parameter by as much as 20% by $ka = 1.0$. The cross section enhancement was interpreted as due to the enhanced fields, relative to the incident field, at each monomer due to the multiple scattering, whereas the reduction in cross section for larger ka was interpreted as due to monomer shielding. Inclusion of the magnetic dipole extended the range of the coupled dipole method (i.e., versus using only electric dipole coupling) from $ka \simeq 0.5$ to $\simeq 1.0$ for soot-like aggregates and spheres.

In a subsequent paper, Mulholland and Mountain (1999) used the CEMD calculation for a broader range of N , viz. up to 1390, and included orientational averaging of the clusters, a feature lacking in the earlier work. They found that the absorption cross sections were about 10 and 20% larger than predicted by RDG for clusters with monomer size parameters of $ka = 0.05$ and 0.21, respectively, with $3 \leq N \leq 1000$. For clusters with monomer size parameter $ka = 0.6$, however, the absorption cross section fell monotonically with N from values 20% larger than RDG to 30% smaller by the time $N \simeq 1000$. The specific extinction was 21 to 36% larger than the RDG (i.e., no multiple scattering) prediction for N in the 100 to 1000 range and $ka = 0.15$ to 0.30.

Frey et al. (1988) also used coupled electric dipoles to study the effects of multiple scattering for soot-like fractal aggregate scattering. Their study varied D through the values 1.0, 1.5, 1.9, and 3.0 and $N \leq 512$. For $D = 1.5$ and 1.9, the $\theta = 0$ scattering increased by 20% as the monomer size parameter ka increased from 0.1 to 0.5.

In summary, it appears that for DLCA ($D \simeq 1.8$) aggregates multiple scattering can affect the scattering and absorption cross sections by 10 to 20%. For small ka there is an enhancement which can cross over to a reduction if the refractive index has a significant imaginary part, as does soot. Fractal dimension > 2 can also see an eventual diminution of cross section as size increases.

It is worthwhile to remind ourselves that Mie theory for light scattering by a sphere shows an analogous diminishment relative to RDG and Rayleigh theory as the sphere size increases. This is illustrated in Figure 15. For small size, scattering is proportional to volume squared or radius to the 6th power. Included in Figure 15 is the Rayleigh scattering limit for the total cross section, Equation (34), which has this functionality. Notice how it overpredicts the scattering relative to Mie theory. In the limit of large size (more precisely, when the phase shift parameter $\rho = 2kR|m - 1|$ is much greater than 1) the

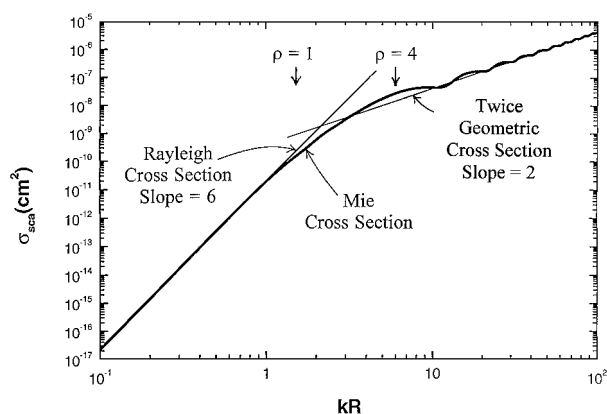


Figure 15. Total Mie scattering cross section for incident polarized light with $\lambda = 500$ nm for a spherical particle with a refractive index of $m = 1.33$ (e.g., water) versus size parameter kR calculated using the BHMIE algorithm of Bohren and Huffman (1983) (thick line). Also drawn are lines representing the Rayleigh scattering cross section calculated using Equation (34) and the geometric plus diffraction cross section, $2\pi R^2$, for the large kR limit. Values of the phase shift parameter $\rho = 2kR|m - 1|$ are also given at various points.

scattering crosses over to the geometric limit which has two parts: the geometric cross section or shadow of magnitude πR^2 , and diffraction around the geometric edge also of magnitude πR^2 (Kerker 1969; Bohren and Huffman 1983). These total to $2\pi R^2$ and this functionality is included in Figure 15. In unpublished work we have shown that the R^2 functionality in the $\rho = 2kR|m - 1| > 1$ limit can also be explained as due to a combination of two things: first, the light localizes near the surface of the particle when $\rho \gtrsim 4$ due to its electromagnetic nature. The surface is proportional to R^2 , hence the scattered wave amplitude is proportional to R^2 . In the forward direction the in-phase scattering constructively adds these waves to yield an intensity proportional to R^4 . Combined with this is the fact that this forward-scattering lobe narrows with increasing R according to $q \sim R^{-1}$. Therefore the solid angle of this forward lobe narrows with R^{-2} . These two functionalities yield the R^2 dependency seen in Figure 15, predicted by Mie scattering and by the usual geometric argument given above. The important concepts to obtain from our argument is the importance of the field localization at the surface, and a concomitant lack of illumination in the interior, of the sphere. Notice how this is similar to the concept of monomer shielding if we divide the sphere into a system of monomers. Also notice that two approaches to the problem of scattering could be taken: first, a multiple scattering argument for a system of scatterers representing the sphere, or second, the classical electromagnetic approach. This author suspects that both approaches yield the equivalent result, viz. exclusion of the field from the interior of the sphere with a concomitant negative deviation from RDG theory at large ρ . It would be valuable to quantitatively make this comparison for

spheres. For fractals with a real refractive index and $D < 2$, we can speculate based on this and Equation (66) that a significant diminishment of scattering relative to RDG will never occur because ρ decreases with increasing aggregate size. However, if the refractive index has an imaginary part, then absorption, not multiple scattering, can shield the interior from the incident field and consequently diminish the scattered intensity as seen by Mulholland and Mountain.

In a series of papers, Farias et al. (1995, 1996a, 1996b) have directly addressed the validity of the RDG theory compared to the VIEF formalism, as expressed by Iskander et al. (1989), for fractal aggregates. In their first two papers, the computer simulated aggregates were soot-like with $D = 1.7$ to 1.8 , $m = 1.57 + 0.57i$, $N = 16$ to 256 , and $ka = 0.1$ to 0.4 . Both orientation and ensemble averaging were employed. The agreement for both scattering and absorption between VIEF and RDG was 10% or better. The second paper included both aggregate and monomer polydispersity and the agreement remained very good. This work firmly establishes the RDG approximation for fractal soot.

Most recently, Farias et al. (1996b) generalized their comparison of VIEF and RDG to a wide variety of aggregates with a wide range of refractive indices, $|m - 1| = 0.1$ to 2.0 , aggregate sizes, $N = 16$ to 256 , monomer sizes, $ka = 0.01$ to 1.0 , and fractal dimensions, $D = 1.0$ to 3.0 . Figure 16 is a recreation of their results for the scattering cross sections for $D \simeq 1.8$ aggregates. Added to the figure is the curve representing a constant phase shift parameter for the aggregate

$$2kR_g|m - 1| = 3. \quad [67]$$

To calculate R_g we used ka and Equation (1) with $k_o = 1.3$. Values other than 3 would also yield hyperbolic curves either closer or further from the origin. There is nothing special about 3 except that it is near unity and yields a curve that does a nice job separating the regions of where RDG theory is adequate or not. Region I extends in a peninsula beyond the boundary of Equation (67), but as Farias et al. (1996b) point out, this is due to cancellation of compensating, larger errors.

It is worthwhile to note both enhancements and diminutions of the cross sections relative to the RDG cross section as indicated by the + and - signs, respectively, in Figure 16. This is in qualitative agreement with the conclusions of previous results discussed above, but now resolved in $|m - 1|$ versus ka space.

The effect of fractal dimension was also studied. Farias et al. concluded the deviation from RDG was not a strong function of D . This conclusion, however, may be in error, because a and N were held fixed while D was varied. As D increases, R_g will decrease and the important phase shift parameter, Equation (67), will decrease as well. Since a decrease in the phase shift parameter should improve the deviation, the relative constancy of the deviation implies increasing D for a fixed size would increase the deviation.

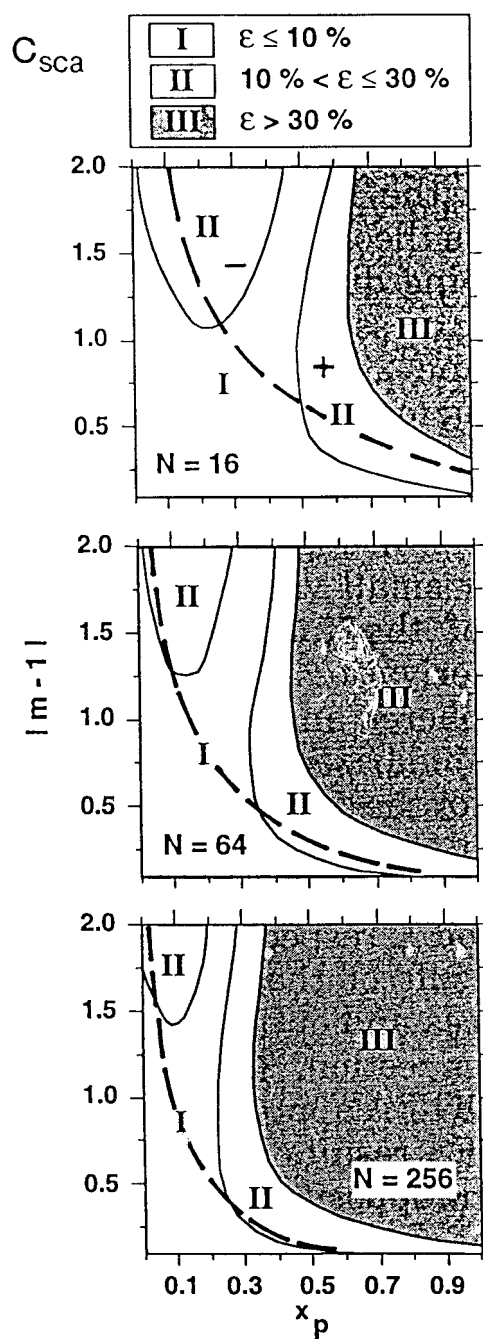


Figure 16. Deviation contour plot of the RDG theory from the more exact VIEF calculation for the scattering cross section as presented by Farias et al. (1996b) for a $D \simeq 1.8$ fractal aggregate composed of N monomers with various refractive indices m and size parameters $x_p = ka$. Also drawn are dashed lines of constant phase shift parameter for the aggregate $\rho = 2kR_g|m - 1| = 3$, Equation (67). Regions I, II, and III represent errors of $\leq 10\%$, 10% to 30% , and $\geq 30\%$, respectively. The plus sign indicates the RDG predicts a larger scattering cross section than VIEF, negative is smaller. Note that the ordinate axis does not include 0.

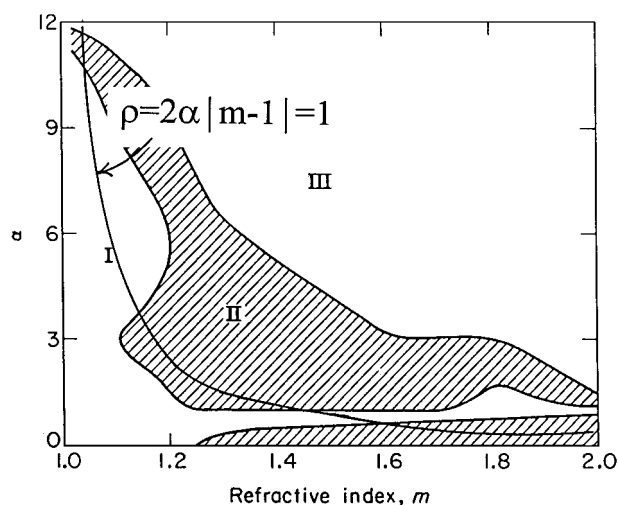


Figure 17. Deviation contour plot of the RDG theory from the Mie theory for the total scattering cross section of a spherical particle with various refractive indices m and size parameters ka . These results were taken from Kerker (1969). Also drawn is a line of constant phase shift parameter for the sphere, $\rho = 2kR|m - 1| = 1$. Regions I, II, and III represent errors of $\leq 10\%$, 10 to 100%, and $\geq 100\%$, respectively. Note the peninsula of small error along the m -axis similar to Figure 16.

Our final conclusion is that the aggregate phase shift parameter is a key quantity in predicting the validity of the RDG theory. Whether this phase shift parameter should include Maxwell-Garnet averaging of the refractive index as expressed by Equation (66), or more simply the monomer refractive index as in Equation (67), is an interesting speculation but remains to be substantiated. For fractal aggregates with $D \simeq 1.8$, the RDG is quite good (10% error or better) as long as the phase shift parameter, Equation (67), is < 1 . We expect that as D increases the RDG accuracy declines at constant aggregate phase shift parameter. At $D = 3$, we obtain a dense sphere. Kerker et al. (1963) have compared the RDG result for the sphere to exact Mie calculations and we reproduce these results in Figure 17 along with the phase shift parameter condition, Equation (67). As seen previously in Figure 16, Figure 17 shows that Equation (67) does qualitatively demarcate the range of validity of the RDG, $D = 3$ theory, however, not as successfully at large m and ka . (We remark that for a sphere $R_g = \sqrt{3/5}R$, but the qualitative comparison here does not warrant this detail.) The facility of the phase shift parameter for nonfractal shapes, such as the geometric shapes of Ku and Shim, is not known. Future work in this regard and as a function of D for fractal aggregates would be interesting, although one must question the utility.

Experimental Studies. An experimental test of the RDG theory for fractal aggregates seems simple enough. One need only scatter and absorb light from a system, determine size and morphological parameters, and compare these to samples collected from the system. Unfortunately, however, both the optical

and the sampling methods have uncertainties beyond that of the validity of the RDG theory. Moreover, the optical and sampling methods measure different moments of the distribution of aggregates that exists in any real system. Add to this the uncertainty of how the sampling method perturbs the system, and one can see the comparison is far from straightforward. Despite these worries, we must try, and a few groups have done just that.

Soot in flames, an aerosol, is the only venue in which scattering and absorption as described by RDG theory have been comprehensively compared to sampling with microscopic observation. Soot offers an advantage in that it has a complex refractive index with a significant imaginary part. Thus one can make use of the different functionalities of scattering and absorption on cluster size, N^2 and N , respectively, as given in Equations (28) and (29). We will describe below how this allows a combination of structure factor, calibrated scattering, and absorption measurements to give complete optical determination of the size and morphology of an aggregate through measurement of R_g , D , N , and a . Soot in a flame is also hot, hence it can be collected quickly by thermophoresis (Dobbins and Megaridis 1987), which does not appear to have a size bias for submicrometer soot.

Whereas the complex refractive index of soot is an advantage, it is also a disadvantage in that it is poorly known. Many soot refractive index measurements exist in the literature, and at present it is the opinion of this author that there is little reason to choose one measurement as the best (see Table 4 below). This soot uncertainty leads to uncertainties in N and a determined from light scattering measurements of about a factor of 2.

Another source of uncertainty for any optical versus sampling comparison lies in the proportionality constant k_o in Equation (1). The importance of this constant for light scattering measurements was realized early in our work (Sorensen et al. 1992b). In that work we estimated that $k_o = (5/3)^{D/2}$ based on the $N = 1$ limit of Equation (1). For $D = 1.8$ this yields $k_o = 1.58$. Wu and Friedlander (1993) surveyed a variety of simulation and experimental results to conclude that k_o was in the range 1.05 to 1.59. Mountain and Mulholland (1988) simulated DLCA aggregates and found $k_o = 1.55$ when $D = 1.9$. In contrast, Sampson et al. (1987) studied stereo TEM images of soot to find $k_o \simeq 3.4$ with $D \simeq 1.44$. Using the data of Sampson et al. (1987), Puri et al. (1993) found $k_o \simeq 3.5$ with $D \simeq 1.40$. We remark that these values of D are much smaller than expected based on current findings that $D \simeq 1.7$ to 1.8, consistent with a DLCA mechanism. In fitting N versus R_g data, k_o and D are anticorrelated. If we reanalyze the Puri et al. data and force $D = 1.75$, a force which is not inconsistent with the data, we find $k_o = 1.3$. Since then, two groups have made careful attempts to determine k_o : our group at Kansas State and efforts lead by Köylü at Michigan and Yale. In our work we have collected soot from premixed methane flames (Cai et al. 1993) and with TEM analysis found Equation (1) to hold with $k_o = 1.23 \pm 0.07$ and $D = 1.74 \pm 0.04$ and from acetylene diffusion flames (Sorensen and Fekke 1996) to find $k_o = 1.66 \pm 0.4$

and $D = 1.84 \pm 0.11$. Our numerical simulations of DLCA have yielded $k_o = 1.19 \pm 0.1$ and $D = 1.82 \pm 0.04$ (Sorensen and Roberts 1997) and $k_o = 1.30 \pm 0.07$ with $D = 1.80 \pm 0.03$ (Oh and Sorensen 1997b). Köylü et al. (1995) have extensively sampled a number of flames to find (on average) $k_o = 2.7$ with $D = 1.65$ and performed computer simulations to find $k_o = 2.4$ with $D = 1.75$. Their simulations, however, were performed "with the additional restriction that the aggregates should have" k_o in the area near 2.4. Köylü and Faeth (1994a, 1994b) using fractal aggregate light scattering techniques find $k_o = 2.3$ with $D = 1.8$. Similar results were found by Köylü et al. (1995), who also summarized the past work on k_o . In their optical work, Köylü et al. use a soot refractive index of $m = 1.57 \pm 0.56i$. This yields a large value of E/F . Other possible soot refractive index values yield E/F as much as a factor of two larger (see Table 4 below). By Equation (110) below, use of these other refractive index values would cause the optically determined k_o values of Köylü et al. to be smaller by a factor of 2. The jury is still out on this discrepancy, so the uncertainty remains.

Observation of sampled soot with TEM involves visualization of a two-dimensional projected image of the three-dimensional cluster. Thus one must know how to reconstitute the true three-dimensional parameters such as R_g , D , and N from the two-dimensional image. This problem seems to be largely solved with modest uncertainty through efforts of a number of groups (Köylü et al. 1995; Oh and Sorensen 1997).

Finally, one must contend with the polydispersity of the soot. Light scattering and absorption measures moments of the distribution. These are discussed extensively below in the Optical Particle Sizing section. These moments can be of fairly high order, such as $R_g^2 \propto M_{2+2/D}/M_2 \simeq M_3/M_2$. Then to make an accurate comparison to direct TEM observation of sampled soot requires good statistics at the large size end of the distribution. This end, however, is inherently poorly populated, hence good statistics are hard to achieve.

In our work (Cai et al. 1993) we performed optical structure factor measurements in combination with absolute scattering/extinction measurements via methods described below on a premixed methane/oxygen flame. We found R_g and D determined from the optical and sampling methods to compare well, within 5%. Aggregation number N and monomer size were strongly dependent on k_o and the soot refractive index for the optical measurements and on the statistics of the size distribution in the case of N for the sampling measurements. These led to uncertainties of about a factor of 2 and the comparisons fell within this range. We concluded that there was no egregious error in the RDG theory and that sampling and optics were consistent.

Köylü and Faeth (1994a, 1994b) using laminar and turbulent flames had similar results. R_g and D agreed typically within 5% between the two methods, although an acetylene diffusion flame systematically yielded R_g from sampling about 50% larger than the optical method. TEM measurements of N and a were used, along with soot refractive indices, k_o , and sample statistics, to calculate the scattering which compared well with the data.

It is edifying that the two experimental methods, optical and sampling, agreed within their uncertainties, which are large for a and N . That R_g and D agree well is not a stringent test of RDG since the theoretical studies discussed above and to be discussed below in regard to depolarization indicate that the $I(q)$ versus q behavior, i.e., the structure factor, is not significantly affected by deviations from RDG. The more exacting test lies in measurements of N and a , which is related to the absolute (as opposed to the relative) nature of $I(q)$ versus q scattering and absorption cross sections. As a light scatterer and as one who has labored with sampling measurements, my money is on the light scattering technique with the RDG theory. Once k_o and refractive index are well known, which they eventually will be with our diligent efforts, light scattering with its ability for an unbiased sampling of the entire polydisperse distribution of clusters will prove to be far more accurate and easier to interpret than sampling. For now we retreat to the theoretical work described earlier that has substantiated RDG to 10%.

Depolarized Scattering

Single scattering of vertically polarized light into a horizontal scattering plane, the usual laser light scattering experimental set up, will yield vertically polarized scattered light. Any multiple scattering will incur some depolarization of the scattered light, which for the set up above means that some horizontally polarized scattered light will occur. Hence the presence of depolarization is an indicator of multiple scattering. The relative amount of depolarization may be quantified by the depolarization ratio

$$\rho_v = \frac{I_{VH}}{I_{VV}}, \quad [68]$$

where I_{VH} designates the intensity of the light with a horizontal polarization scattered from a vertically polarized beam and I_{VV} is for both incident and scattered light vertically polarized. In the single scattering limit $\rho_v = 0$.

In an experiment, multiple scattering can occur either between two different clusters, intercluster scattering (e.g., Sorensen et al. 1976, 1978), or within one cluster, intracuster scattering. The former is typically an experimental pain, the latter, however, is useful to indicate the end of the RDG approximation and possibly for investigating the internal structure and anisotropy of the aggregate.

In our laboratory we studied depolarized scattering from laminar, premixed, sooting flames of methane, ethylene, and propane (Lu and Sorensen 1994). These flames were well characterized with I_{VV} , which was dominated by single scattering to yield in situ measurements of R_g , N , $D (= 1.79 \pm 0.1)$, and $a (= 15 \pm 3 \text{ nm})$. I_{VH} was measured at small angles to achieve the Rayleigh regime ($qR_g < 1$) and the resulting depolarization ratio is plotted in Figure 18. There it is shown that the depolarization ratio is at most a percent and is well described by

$$\rho_v \sim N^{-0.6} \quad [69]$$

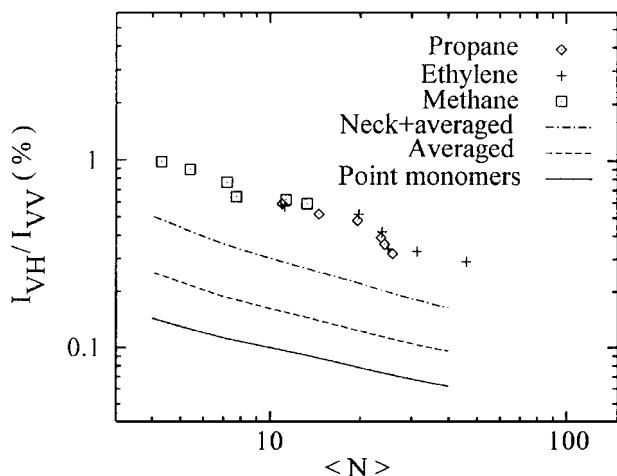


Figure 18. Comparison of the flame data for the depolarization ratio versus average number of aggregates per cluster and calculation. The soot clusters are fractals with $D \simeq 1.75$. Fits are shown for a dipole-induced-dipole multiple scattering algorithm assuming a soot refractive index of $m = 1.6 + 0.6i$. The solid line is for no field averaging and no necking, the dashed line is for field averaging over the monomer and no necking, and the dot-dashed line is for both field averaging and necking.

with good flame to flame consistency. Since for $qR_g < 1$, $I_{VV} \sim N^2$, Equation (69) implies $I_{VH} \sim N^{1.4}$ in the aggregate Rayleigh regime (i.e., $qR_g < 1$).

Two analyses were used to explain the result. First, a scaling argument was presented for double scattering, an argument which we extend here. To lowest order the scattering of light is governed by the electric dipole tensor (Jackson 1962; Sorensen et al. 1976). The electric field at \vec{r}_2 due to an oscillating dipole \vec{p} at \vec{r}_1 is given by

$$\vec{E}(\vec{r}_2) = k^2 \vec{T}(\vec{r}_{21}) \cdot \vec{p}(\vec{r}_1), \quad [70]$$

where $k = 2\pi/\lambda$ and the electric dipole tensor is given by

$$\vec{T}(\vec{r}_{12}) = \frac{e^{ikr_{21}}}{r_{21}} \left[\left(1 + \frac{i}{kr_{12}} - \frac{1}{k^2 r_{21}^2} \right) \vec{I} - \left(1 + \frac{3i}{kr_{21}} - \frac{3}{k^2 r_{21}^2} \right) \hat{r}_{21} \hat{r}_{21} \right], \quad [71]$$

where $r_{12} = |\vec{r}_2 - \vec{r}_1|$. In scattering an oscillation dipole \vec{p} is induced by an applied field

$$\vec{p}(\vec{r}_1) = \vec{\alpha} \cdot \vec{E}(\vec{r}_1), \quad [72]$$

where $\vec{\alpha}$ is the polarizability tensor.

The electric dipole tensor has terms involving powers of kr_{12} . The first term, $(kr_{12})^0 = 1$, dominates the other two terms when $kr_{12} \gg 1$. This term is called the far field term and is the most common situation because scattering usually involves detection at a point much farther away from the scatterer than the wavelength. The other extreme is when $(kr_{12})^{-2}$ dominates for

$kr_{12} < 1$. This term is called the near field term. We shall call the $(kr_{12})^{-1}$ term the intermediate term. Note that while it can contribute to the tensor when $kr_{12} \sim 1$ it can never dominate.

We now consider single and double scattering scaling with k , monomer size a , and monomers per aggregate N . For single scattering the scattered field is

$$E_{SS} \sim k^2 T_{FF} \alpha E_o. \quad [73]$$

The leading term in the electric dipole tensor is the far field term, $T_{FF} \sim e^{ikr_{12}}/r_D$, where r_D is the distance to the detector. For small monomers in the Rayleigh regime $\alpha \sim a^3$. For a modest amount of multiple scattering, single scattering is by far the major contributor to I_{VV} , so $I_{VV} \sim E_{SS}^2$. Moreover, in the aggregate Rayleigh regime, $qR_g < 1$, the N monomers will add their scattered fields in phase. With all this, we find

$$I_{VV} \sim N^2 k^4 a^6, \quad [74]$$

as expected from Equations (26), (27), and (36a).

Double scattering provides an interesting twist on the usual scattering arguments in that the internal scattering event can involve terms of the dipole tensor other than the usual far field term. In the small cluster limit, $kr_{12} < 1$ for all pairs of monomers, and then the near field term dominates. The sequence of double scattering is an internal event followed by an event that takes the photon out of the aggregate, a far field event. Thus

$$E_{DS} \sim k^2 T_{NF} \alpha \cdot k^2 T_{FF} \alpha \cdot E_o, \quad [75]$$

where T_{NF} is the near field term of the electric dipole tensor. From Equation (71), $T_{NF} \sim \langle r_{12}^{-3} \rangle k^{-2}$, where $\langle r_{12}^{-3} \rangle$ indicates an average all pairs of monomers within a cluster. Since r_{12} is a center-to-center monomer distance, it scales with the monomer size, $\langle r_{12}^{-3} \rangle \sim a^{-3}$. This average can also be determined by integration with the density autocorrelation function $g(\vec{u})$ which describes, given a particle at \vec{r} , the probability of another particle at $\vec{r} + \vec{u}$. Then

$$\langle r_{12}^{-3} \rangle = \int u^{-3} g(\vec{u}) d\vec{u}. \quad [76]$$

This and the fundamental scaling relation (Equation (1), $R \sim aN^{1/D}$) yields

$$\langle r_{12}^{-3} \rangle \sim a^{-3} N^{-3/D}. \quad [77]$$

The last ingredient for double scattering is that, since it involves two scattering events within the N monomer aggregate, it is proportional to $N(N-1) \sim N^2$. Then, with all this, Equation (75) becomes

$$E_{DS} \sim N^2 \cdot k^2 k^{-2} a^{-3} N^{-3/D} a^3 \cdot k^2 a^3 \cdot E_o \sim N^{2-3/D} k^2 a^3 E_o. \quad [78]$$

Again for modest multiple scattering, double scattering dominates I_{VH} so $I_{VH} \sim E_{DS}^2$ to yield

$$I_{VH} \sim N^{4-6/D} k^4 a^6 I_o. \quad [79]$$

Combining this with Equation (74), the depolarization ratio is expected to be

$$\rho_v \sim N^{2-6/D}. \quad [80]$$

We stress that Equation (80) has no wavelength or monomer size dependence.

Equation (80) can be compared to experiment. For $D = 1.8$ Equation (80) predicts $\rho_v \sim N^{-1.3}$, which quantitatively disagrees with the experimental $N^{-0.6}$ measured dependency but does, at least, explain the decrease of ρ_v with increasing N . Equation (80) does describe well the lack of wavelength dependence that was measured in our experiment. However, this measurement was confined to the small range of $\lambda = 459$ to 514.5 nm (available with an Ar^+ laser).

Equation (80) depends on the near field term of the electric dipole tensor being dominate. This requires $kr_{12} < 1$ for all pairs of monomers. Since $\lambda \simeq 500$ nm, this implies $r_{12} < 80$ nm, which requires a fairly small cluster; by Equation (1) $N < 25$. Some of our clusters were this big or larger, see Figure 19. Therefore we make similar scaling arguments for the other two terms in the electric dipole tensor to find the following dependencies for ρ_v when measured in the aggregate's Rayleigh regime (i.e., $qR_g < 1$), where $I_{VV} \sim k^4 a^6 N^2$:

$$\rho_v \sim N^{2-6/D}, \quad \text{near field} \quad [81a]$$

$$\sim k^2 a^2 N^{2-4/D}, \quad \text{intermediate term} \quad [81b]$$

$$\sim k^4 a^4 N^{2-2/D}, \quad \text{far field.} \quad [81c]$$

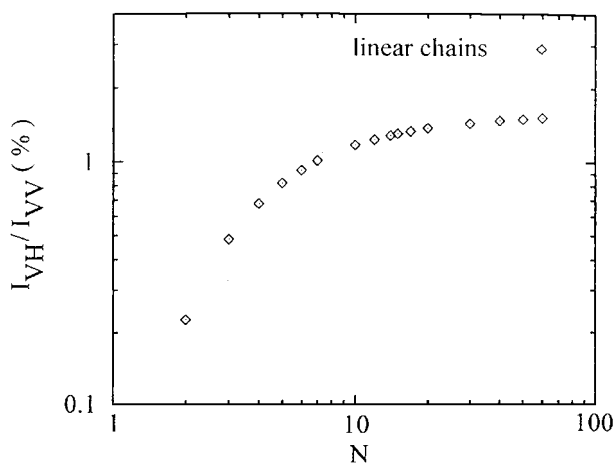


Figure 19. The depolarization ratio versus number of monomers per aggregate for linear chains calculated with the same algorithm as used in Figure 18. $m = 1.6 + 0.6i$ and $ka = 0.2$.

The results in Equations (81) apply for $qR_g < 1$, but the arguments for I_{VH} are independent of q (hence θ). Thus we expect I_{VH} to be isotropic. This is physically reasonable since for any incident and scattered direction an infinite and fairly random number of intermediate scattering directions (i.e., those between the first and second scattering events) can occur. This is substantiated by Lindsay et al. (1987), who calculated the depolarized scattering for $D = 1.77$ gold fractal aggregates and found it to be isotropic.

As the aggregate size increases, the functionality of ρ_v will shift from Equation (81a) to Equation (81c). For $D = 1.8$ this shift will cause the exponent of N to range from -1.3 through -0.2 to 0.9 . For aggregates of intermediate size with $kr_{12} \sim 1$, all three terms above will be active and some average dependency will occur. Then it is reasonable that the experimentally observed $\rho_v \sim N^{-0.6}$ dependency lies between Equations (81a) and (81b) when $D \simeq 1.8$.

We conclude that the scaling arguments are useful for visualizing how the complex formulas of Equation (71) contribute to the functionalities of the scattered fields. Scaling is invoked to uncover simplicity in apparent complexity, which we have done, but the need to find an average behavior among Equations (81) vitiates scaling's quantitative ability. Thus we resort to a numerical calculation.

The numerical calculation of Lu and Sorensen (1994) involved a set of DLCA clusters created with an off-lattice simulation. These clusters had a fractal dimension of $D = 1.75 \pm 0.10$. The scattered field from these aggregates was calculated with iteration to yield a self-consistent, electric dipole-induced-dipole result. We gave these aggregates a soot index of refraction of $m = 1.6 \pm 0.6i$, a monomer size parameter of $ka = 0.2$ (at $\lambda = 488$ nm, $a = 15.5$ nm), and used $N = 3$ to 98 with orientational averaging.

We found large cluster-to-cluster variation with values of ρ_v ranging by a factor of 5. The average values for an ensemble of aggregates, however, when plotted versus N showed $\rho_v \sim N^{-x}$ with $x = 0.6 \pm 0.1$ in excellent agreement with the experiment. However, the magnitude of the calculated ρ_v was about a factor of 8 too small.

Attempts to obtain quantitative agreement to the magnitude of ρ_v required a number of strategies. Improvements were gained by considering the $a = 15.5$ nm monomers as extended objects. This is usually unnecessary for such small ($a \ll \lambda$) particles, but the near field term has a rapid r^{-3} dependency so that the field scattered from a nearby monomer changes significantly over the volume of the receiving monomer. This field averaging correction increased ρ_v by a factor of about 2, as shown in Figure 18. We also attempted to simulate the real soot aggregate by including "necking," i.e., nonpoint contacts, between monomers in our calculation. This also caused a factor of about 2 increase in ρ_v , also shown in Figure 18. Despite these efforts, the calculated ρ_v values are still too small. In unpublished work, we found a quantitative fit could be obtained by varying the refractive index. The fit did not yield a unique value for the refractive

index but did yield a unique mass specific extinction. When the two corrections above were included, the best fit extinction was $8.1 \pm 1 \text{ m}^2/\text{g}$, which corresponds to $m = 1.5 \pm 1.0i$, among other values.

We applied our self-consistent electric dipole-induced-dipole calculation to a linear chain of soot monomers to find ρ_v increasing monotonically with N as shown in Figure 19. This is very different than the monotonically decreasing functionality of depolarization seen in small fractal aggregates. This serves to stress the great difference between random fractal aggregates and various contrived “geometric” aggregates, such as linear chains, in scattering nature. Any worker purporting to study random aggregates formed in nature with such geometric aggregates should beware.

Chen et al. (1987) and Keyes et al. (1987) (Seeley et al. 1988) considered second-order multiple light scattering from a general context of higher-order correlations within the aggregate, correlations more subtle than and not described by the fractal dimension of the aggregate. Their work involved diffusion limited aggregates (DLA), i.e., aggregates formed via single particles diffusing to a (relatively) fixed aggregate (Witten and Sander 1981; see also Family and Landau 1984; Viscek 1992) and bond percolation aggregates (BPC). These models give $D \simeq 2.5$ and, while found in other aspects of nature, do not seem to occur in aggregating aerosols and colloids where cluster-cluster aggregation is the rule. They found that the second-order scattering should scale as $I_{DS} \sim N^x$, and a renormalization group analysis found $x = 4 - 6/D$, entirely consistent with our Equation (81a). Both groups used only the “long wavelength limit” of the electric dipole tensor, i.e., the near field term. Simulations found $x \simeq 1.1$ for DLA and 1.6 for BPC, the latter in agreement with $x = 4 - 6/D$ when $D = 2.5$. Both groups concluded that this demonstrated second-order light scattering’s ability to distinguish two families of clusters with essentially the same fractal dimension.

We concur with this conclusion and offer the following explanation. Pearson and Anderson (1993) have shown that the structure factors of DLA and BPC differ, the DLA being much less uniform in $S(q)$ versus q than BPC. In recent work (Oh and Sorensen 1998) we have shown that whereas DLCA clusters are essentially homogeneous in q -space with a fractal dimension of $D = 1.8$, the DLA aggregate shows DLCA structure with $D = 1.8$ over length scales on the order of $10a$. With this, near field scaling arguments for I_{DS} or ρ_v from DLA would imply use of a fractal dimension smaller than the overall $D = 2.5$, perhaps as small as the local structure $D = 1.8$. The value $x = 1.1 = 4 - 6/D$ implies $D = 2.07$, which is consistent with this argument.

Other work on depolarization is largely consistent with the story above. Frey et al. (1988) considered intra-aggregate multiple scattering for fractal aggregates with Rayleigh monomers with size parameters of $ka \leq 0.5$. The electric dipole tensor used included only the far field and intermediate term (i.e., second order in $(kr)^{-1}$). The monomers were soot-like with $m = 1.6 + 0.8i$. Clusters had fractal dimensions of $D = 1,$

1.5, 1.9, and 3.0 and monomer numbers of 16 to 512. The calculated depolarization ratios were small, on the order of 10^{-4} . The depolarization decreased with N , characteristic of fractal aggregates. Our analysis of their data plotted in their Figures 4 and 5 yields $\rho_v \sim N^{-0.7}$ for $D = 1.5$ and 1.9. This is in good agreement with our data. Comparison to Equations (81) would imply a contribution due to the near field term (81a), which was not included in their calculation; a puzzle I can’t explain. Despite this, this study qualitatively supports our picture here that ρ decreases with N when $q \rightarrow 0$.

Mulholland and coworkers (1994, 1999) also considered depolarization in their CEMD calculations. However, they defined depolarization, differently than here, as

$$\rho_H = \frac{I_{HH}}{I_{VV}}, \quad [82]$$

i.e., the incident beam is horizontally polarized as well as detection of horizontal polarization. The advantage of this definition of depolarization is that it is a sensitive, monotonic function of particle size for single spheres with size parameter, ka , less than about 2.5 (Kerker 1969). This fact has been used in the past for size measurements (Kerker 1950, 1969). Mulholland et al. reasoned that if the RDG theory for fractal aggregates is accurate, then the assumption that forms the basis for RDG theory, viz. that there is no intra-aggregate multiple scattering, is true as well. With no multiple scattering, the sole source of depolarization would be the individual monomers. This would then allow for a measurement of monomer size in the aggregate. Unfortunately, these hopes proved unsupported by their CEMD calculations. A comparison of a ρ_H for a single sphere and an aggregate of $N = 17$ spheres showed that the depolarization for the aggregate is more than an order of magnitude larger than for the sphere. Thus multiple scattering within the aggregate overwhelms the depolarization due to the individual monomers.

This multiple scattering can be described by the scaling description of Equations (81) because the leading contribution to I_{HH} at a 90° scattering angle is double scattering. The near field term should dominate when $ka \lesssim 1$. For $N = 17$, Equation (1) with $k_o = 1.3$ implies this will happen when $ka \lesssim 0.24$. Figure 20 shows that for $ka \lesssim 0.24$ ρ_H is only a weak function of monomer size, less so for smaller ka , in agreement with the prediction of Equation (81a). For $ka > 0.24$, Figure 20 shows that the dependency crosses over to $\rho_H \sim a^2$. This agrees with Equation (81b) and the concept that for larger clusters the intermediate field term must become important. Mulholland and Mountain also looked at the N dependencies of ρ_H . For small monomers with $ka = 0.05$, hence small clusters, they found $\rho_H \sim N^{-0.55}$. Equation (81a) for near field multiple scattering predicts $\rho_H \sim N^{-1.3}$ when $D = 1.8$ but also when scattering is constrained to an angle small enough that $qR_g < 1$, hence $I_{vv} \sim N^2$. Since Mulholland and Mountain used $\theta = 90^\circ$, much of their data is outside of this regime, so that $I_{vv} \sim N$. Then scaling Equation (81a) would predict $N^{-0.3}$. These two

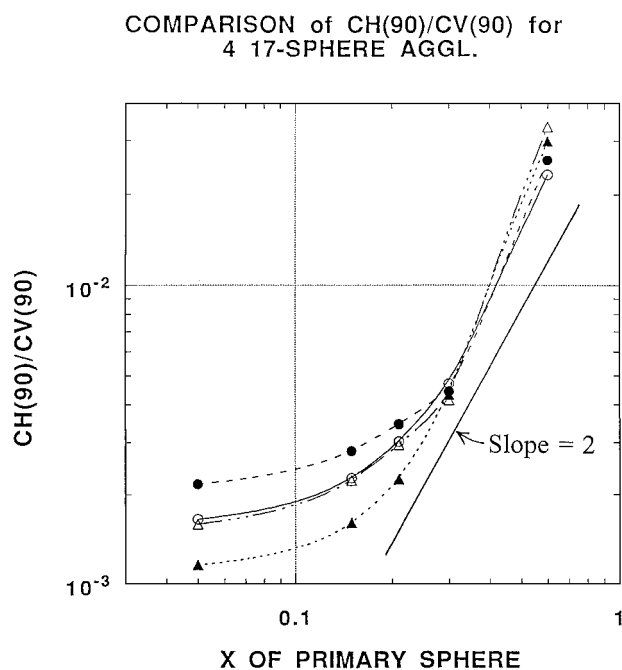


Figure 20. Depolarization ratio $\rho_H = I_{HH}/I_{VV} = CH(90)/CV(90)$ at $\theta = 90^\circ$ for four soot-like aggregates of $N = 17$ spheres generated by a DLCA algorithm (hence $D \sim 1.8$). The monomeric spheres have $m = 1.7 + 0.7i$ and size parameter $x = ka$. Calculation was performed using the coupled electric and magnetic dipole algorithm by Mulholland and Mountain (1999).

extremes are consistent, within the admittedly wide range, with the computed data. The trend remains favorable for bigger ka as the exponent x of $\rho_H \sim N^x$ increases with increasing cluster size. This is expected via the scaling argument as the internal scattering progressively uses more of the intermediate and far field terms, hence develop dependencies similar to Equations (81b) and (81c), as the cluster size grows.

The discussion and results above show that intra-aggregate multiple scattering exists for typical clusters; it can be simply understood with scaling arguments, and it is the dominant mechanism for depolarization. So if it exists, is RDG void? Figure 21 shows our attempt to answer this. The same iterative dipole-induced-dipole program that successfully calculated ρ due to multiple scattering shown in Figure 18 was used to calculate the total light scattered as a function of q for the same aggregates. Comparison to the strictly single scattering, hence RDG, case shows the same shape, hence same structure factor, with a uniform enhancement in scattering of $\sim 10\%$. This small deviation is consistent with the numerous studies discussed above. We surmise for soot-like particles with $D \simeq 1.75$ that multiple scattering is significant for depolarization, but it is minor for the overall scattering of light.

For future work on depolarization I advocate use of ρ_v , Equation (68) over ρ_H , Equation (82). Measurement of ρ_H yields

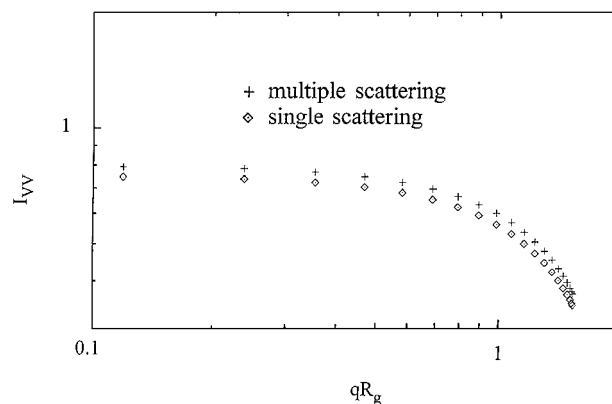


Figure 21. Total vv scattering from a soot-like aggregate of 50 monomers with $m = 1.6 + 0.6i$ and $ka = 0.2$ with and without multiple scattering between the monomers. This was calculated with the same dipole-induced-dipole algorithm used in Figure 18.

experimental and interpretational difficulties: i) most lasers are vertically polarized so polarization rotation is necessary for ρ_H . ii) Detection of I_{HH} must be exactly at $\theta = 90^\circ$, otherwise single scattering contributes. Any finite collection angle compromises this requirement. iii) $\theta = 90^\circ$ is ill defined relative to the important parameter qR_g . The scattering regime, hence nature of the scattering, is determined by whether $qR_g < 1$ or > 1 . $\theta = 90^\circ$ may be in either depending upon R_g (and λ but less so since its variation range is limited by lasers and detectors). The simplest regime to work in is $qR_g < 1$, the aggregate Rayleigh regime.

OPTICAL PARTICLE SIZING

One of the major motivations for understanding how aggregates scatter and absorb light is so that this knowledge can be used for in situ light scattering and absorption measurements of particle size, morphology, and number density. Light scattering is noninvasive, remote, and, even without these favorable attributes, as good as or better than any other more direct method. Indeed, why should real space be any better than reciprocal space?

The Optical Structure Factor

Scattered intensity versus angle is the most fundamental measurement for sizing. Angle is, of course, the experimental parameter, but it is the functionality with q that we strongly advocate because it leads us to understand the scattered intensity and quantify our analysis. We will call measurement of I versus q an optical structure factor measurement. From the optical structure factor one can in principle determine the aggregate R_g and D , the polydispersity of the aggregate size distribution, and the monomer size a if short wavelengths or large a is available. All this is obtainable without the need to know the refractive index of the particle or aggregate. These facts are outlined schematically

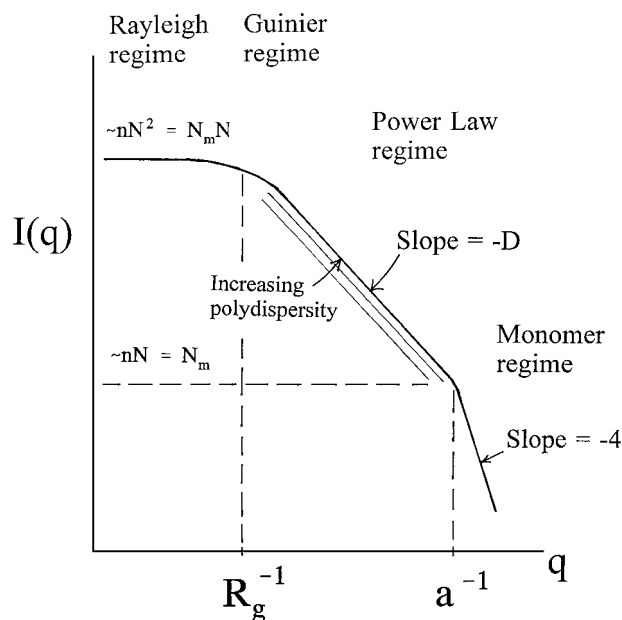


Figure 22. Schematic representation of the scattered light intensity $I(q)$ versus $q = 4\pi\lambda^{-1} \sin \theta/2$, where θ is the scattering angle, from an ensemble of fractal aggregates of dimension D with N monomers per aggregate on a log-log plot. In the ensemble n is the number density of clusters and N_m is the total number of monomers, $nN = N_m$.

in Figure 22. Many examples of optical structure factor measurements on particulate systems exist in the literature (Schaefer et al. 1984; Martin et al. 1986; Hurd and Flower 1988; Zhang et al. 1988; Gangopadhyay et al. 1991; Bonczyk and Hall 1991, 1992; Dobbins and Megarides 1991; Sorensen et al. 1992b; Köylü and Faeth 1994a, 1994b; Köylü 1998; Sorensen et al. 1998; Xing et al. 1999).

An example from some of our early work (Gangopadhyay et al. 1991) is given in Figure 23 for a soot aerosol in a premixed methane/oxygen flame. Increasing height above burner h means later in the aggregation process. Inspection of Figure 23 shows that with increasing height, the bend in the optical structure factor, i.e., where the slope of I versus q goes from 0 to negative, progresses to smaller q . A cardinal rule is that a change in slope implies a length scale. In this case the length scale is the overall aggregate size, and since $R \sim q^{-1}$, this is a direct observation, albeit qualitative, of the aggregate size increasing with time. Notice the essentially isotropic scattering at $h = 8$ nm to indicate very small particles. Figure 24 presents a more recent example of scattering from a titania aerosol. Note the scale in q is an order of magnitude smaller than in Figure 23, hence the clusters of titania are an order of magnitude larger. In Figure 24 a significant power law regime is seen with a slope implying $D \simeq 1.7$. Notice also other general features. The $I(q=0)$ limit (the Rayleigh regime) increases with either height above burner or run time. This is the Tyndall effect (see below) that as a system coarsens as it scatters more light. On the other hand, the power law regime

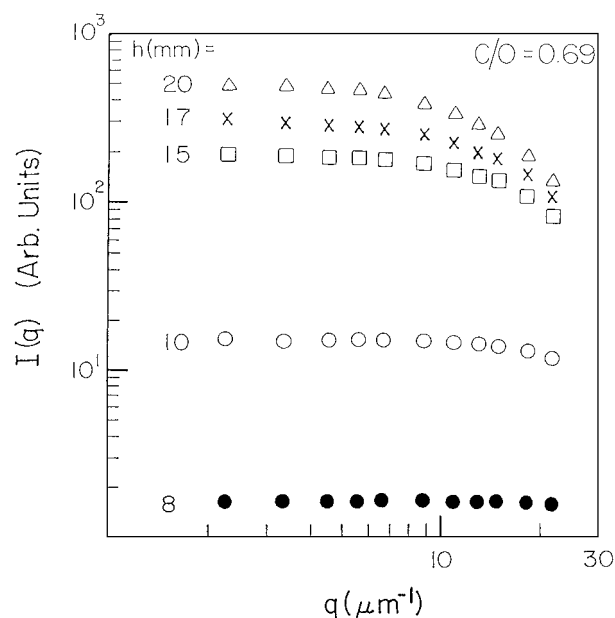


Figure 23. Scattered light intensity $I(q)$ as a function of the scattering wave vector q for 5 different heights above burner h for a premixed methane/oxygen flame.

in Figure 24 is approaching an intensity constant with time as described above.

Quantitative analysis of the optical structure factor proceeds in two steps (Gangopadhyay et al. 1991; Sorensen et al. 1992b). First, the Guinier regime is analyzed to yield the aggregate radius of gyration. The Guinier equation, Equation (48), may be

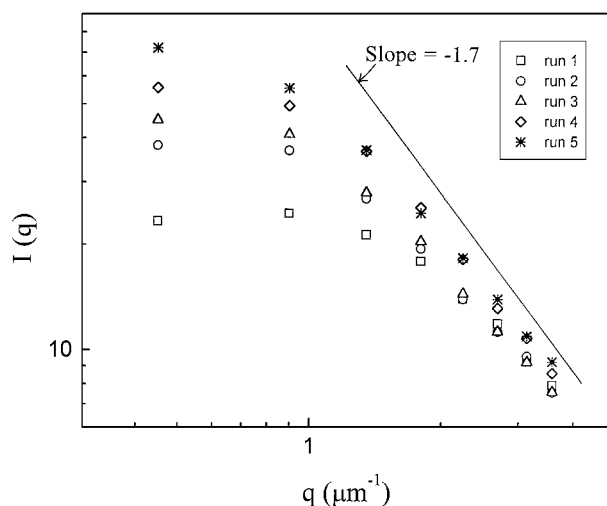


Figure 24. Scattered light intensity $I(q)$ as a function of the scattering wave vector q for 5 different times (runs) of an aggregating titania aerosol.

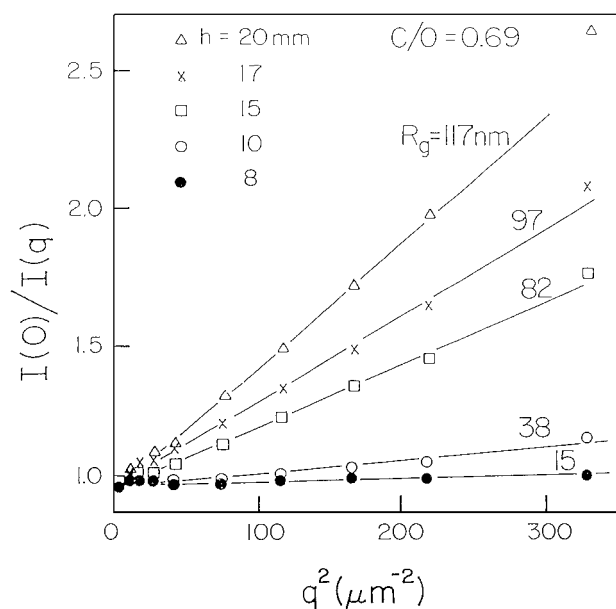


Figure 25. Flame soot aerosol data of Figure 23 plotted for a Guinier analysis, Equation (83).

expressed as

$$I(0)/I(q) \simeq 1 + \frac{1}{3} R_g^2 q^2. \quad [83]$$

This implies that a graph of $I(0)/I(q)$ versus q^2 should be linear with a slope of $R_g^2/3$. Such a plot has a venerable history since the axes and the result are the same as for the Zimm plot of biophysics (Zimm 1948; Tanford 1961; Kerker 1969). The data of Figures 23 and 24 are so plotted in Figures 25 and 26, respectively. Figure 25 is a proper Guinier analysis in that, for

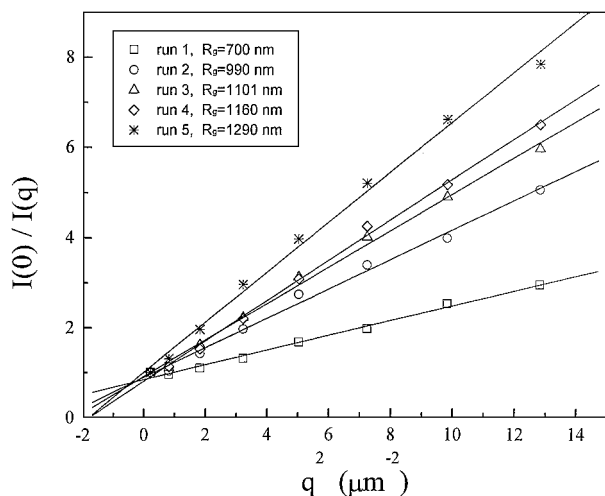


Figure 26. Titania aerosol data of Figure 24 plotted for a Guinier analysis, Equation (83). Note that the bulk of the data extend beyond the Guinier regime.

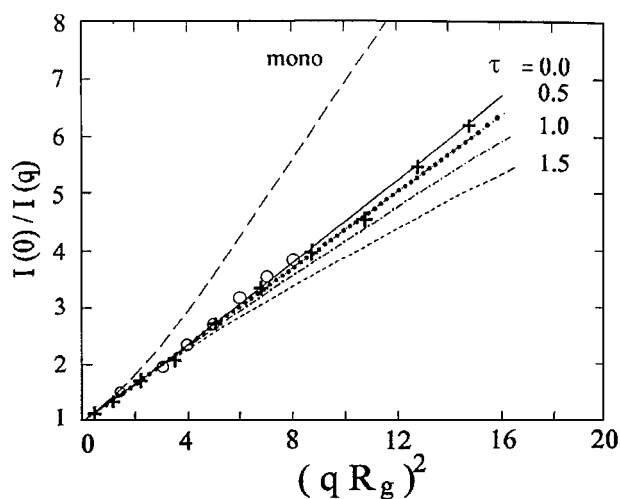


Figure 27. Inverse normalized scattered intensity versus $(q R_g)^2$. Lines are calculated for a Gaussian structure factor with $D = 1.75$ convoluted with a size distribution: monodisperse; $\tau = 0.0, 0.5, 1.0,$ and 1.5 are for the scaling distribution, Equation (A5). Data are from a soot aerosol in a premixed methane/oxygen flame.

the most part, for the data used $q R_g < 1$, which is equivalent to $I(0)/I(q) < 4/3$. Figure 26 is not so proper since data well beyond the Guinier regime are used in the Guinier analysis. We have shown that this is acceptable for analysis of fractal aggregate systems with polydispersity determined by the aggregation kinetics. We describe this below in reference to Figure 27.

Equation (83) yields the aggregate radius of gyration for a system of monodisperse aggregates. Nearly any real particle system will have a polydisperse distribution of aggregate sizes, hence Equation (83) must be modified to read

$$I(0)/I(q) \simeq 1 + \frac{1}{3} R_{g,meas}^2 q^2, \quad [84]$$

where $R_{g,meas}$ is the Guinier measured radius of gyration. This represents an average over the distribution weighted by the light scattering cross section. $R_{g,meas}$ is sufficient for describing the “average” radius of gyration of an ensemble of aggregates.

A more detailed approach is necessary if we are to describe what “average” means and relate the measurement to other measurements of the aggregate size. We can determine how $R_{g,meas}$ is related to the radius of gyration of the mean-sized aggregate from the effective structure factor for the entire ensemble, Equation (53). We use the fact that $I(0)/I(q) = S_{eff}(0)/S_{eff}(q)$, then substitute the Guinier expansion for $S[q R_g(N)]$, Equation (48), into Equation (53) to find

$$I(0)/I(q) = 1 - (q^2/3) \int N^2 R_g^2(N) n(N) dN / \int N^2 n(N) dN, \quad [85]$$

$$= 1 - (q^2/3) R_{g,z}^2. \quad [86]$$

Equations (85) and (86) define the so-called z -average value of the radius of gyration, a term which applies whenever the size distribution is weighted by the square of the mass. Next we substitute $R_g^2 = a^2 k_o^{-2/D} N^{2/D}$, which follows from Equation (1), into Equation (85) to obtain

$$I(0)/I(q) = 1 - \frac{1}{3} q^2 a^2 k_o^{-2/D} \frac{M_2 + 2/D}{M_2}. \quad [87]$$

Equations (84), (86), and (87) imply

$$R_{g,meas}^2 = R_{g,z}^2 = a^2 k_o^{-2/D} \frac{M_2 + 2/D}{M_2}. \quad [88]$$

Equation (88) shows that $R_{g,meas}$ is strongly influenced by the large end of the distribution because it depends on high order moments, viz. $\sim M_3/M_2$ when $D \sim 2$.

What is the mean size $\langle N \rangle$? There are, in fact, an infinite number of ways to define mean size, as described in Appendix B, Equation (B3). Light scattering in the Rayleigh regime of the aggregate where $I \propto N^2$ “chooses” a convenient definition as the ratio of the second and first moments of the distribution. We will write this as $s_2 = M_2/M_1$. It then follows from Equation (1) that the radius of gyration of this mean size is

$$R_{g,2} = a k_o^{-1/D} s_2^{1/D}. \quad [89]$$

Equations (88) and (89) can be combined with $s_2 = M_2/M_1$ to obtain

$$R_{g,2}^2 = R_{g,z}^2 \left(\frac{M_2}{M_1} \right)^{2/D} \frac{M_2}{M_2 + 2/D}. \quad [90]$$

This equation gives the radius of gyration of the mean size defined by M_2/M_1 in terms of the radius of gyration measured from the Guinier analysis.

We now have both $R_{g,z}$ and $R_{g,2}$ expressed in terms of moments of the distribution. If we know the distribution, we can directly relate the two. We will assume again that the distribution is the self-preserving, scaling distribution. Then we can apply Equation (B7) to change Equation (90) to

$$R_{g,2}^2 = R_{g,z}^2 \frac{m_2^{1+2/D}}{m_2 + 2/D}. \quad [91]$$

The expression for m_i for the scaling distributions is given in Equation (B8).

Precisely speaking, this Guinier analysis should be limited to $qR_g \leq 1$, which corresponds to $I(0)/I(q) \leq 4/3$. Often, however, the data are not plentiful and precise enough within these bounds to yield an accurate R_g . Indeed, the data of Figure 26 extend well beyond these limits. We have found (Cai et al. 1995) both through experience with real data and numerical calculations to create simulated data with the complete structure factors of Table 1 that $I(0)/I(q)$ versus q^2 remains linear well beyond these limits and data up to about $I(0)/I(q) \sim 2$ can be trusted to

yield accurate R_g values. Moreover, divergence from linearity beyond this empirical limit are related to D , β , and τ . If D and β are known, this allows for a measurement of the polydispersity exponent τ . Figure 27 gives an example of this behavior. Such a measurement appears viable, but this procedure has yet to be stringently tested with data.

The power law regime yields the fractal dimension D by its slope. Of course one would like to have a good decade of linearity to get a good measure of this slope, but this is rarely the case, e.g., Figure 23. Moreover, the true power law character doesn't really show until $qR_g \lesssim 5$. Hence one must beware when data in this regime are limited.

A well-endowed power law regime has another advantage besides easy extraction of an accurate fractal dimension, and that is a measure of the polydispersity using Equations (58) and (61). In a recent study (Sorensen and Wang 1999) we measured the structure factors of both a titania aerosol aggregating via DLCA kinetics and a polystyrene colloid aggregating via RLCA kinetics. Fractal dimensions of 1.7 and 2.15 were found for these two systems, respectively, in agreement with previous work (Jullien and Botet 1987; Lin et al. 1990b). To illustrate the different coefficients in the power law regime, we plot in Figure 28 $(qR_{g,z})^D S(qR_{g,z})$ versus $qR_{g,z}$. By Equations (56) such a log-log plot will initially rise with a slope of D , then level off for $qR_{g,z} > 1$ to the value CC_p . From our considerations of the single cluster structure factor above we expect $C = 1.0$, thus the level in Figure 28 is C_p , with values dramatically different for the two systems. Our complete analysis of several sols found $\tau = 0.24 \pm 0.23$ for the DLCA aerosol

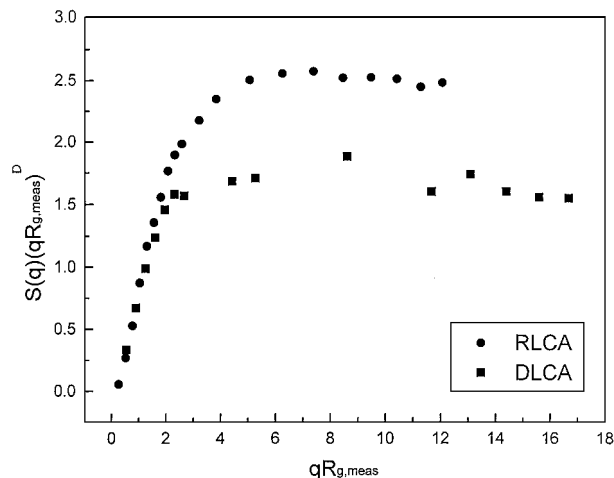


Figure 28. Scattered light structure factor $S(q)$ multiplied by $(qR_{g,meas})^D$ versus $(qR_{g,meas})$. $R_{g,meas}$ ($= R_{g,z}$) is the radius of gyration measured with the Guinier analysis and D is the fractal dimension. Data for two systems are shown: an aerosol aggregating via DLCA with $D = 1.75$ and a colloid aggregating via RLCA with $D = 2.15$. The constant level at large $qR_{g,meas}$ is, by Equation (58), $CC_p = C_p$ since $C = 1$. From C_p and Equation (61) or Figure 13, the polydispersity can be measured.

and $\tau = 1.5 \pm 0.2$ for the RLCA colloid, values consistent with previous work (van Dongen and Ernst 1985; Weitz et al. 1985; Brown and Ball 1985; Lin et al. 1990b). Thus the level of the power law regime provides a convenient and straightforward measure of the aggregate polydispersity.

In summary, the optical structure factor is a very able method capable of yielding R_g , D , and the polydispersity τ . The particle refractive index need not be known. If data beyond $qR_g \simeq 5$ are not available, the D measurement can only be considered qualitative. In fitting optical structure factor data one should use one of the structure factors for which $C = 1$ (see Table 2 and Figure 12). The fit should also include the size distribution of the aggregates (i.e., the polydispersity). One procedure is to use the integral of Equation (53) and fit the effective structure factor to the data. This is laborious and opaque. We have found that an excellent procedure is to determine R_g with the Guinier analysis using small q data and then D with a log-log plot (or fit) using large q data. Then the polydispersity can be determined via C_p and the analysis depicted in Figure 28.

Absolute Scattering and Extinction

Scattering, calibrated to make an absolute measurement, and extinction can yield the aggregate (or particle) volume equivalent sphere radius R_v and volume fraction f_v of material and cluster number density n in the sol if the refractive index is imaginary through methods pioneered by D'Alessio (D'Alessio et al. 1975; D'Alessio 1981) for soot in flames. Combination of the optical structure factor measurement with scattering/extinction measurements allows for a remarkably complete characterization of aerosols or colloids of particles with a complex index of refraction such as soot (Sorensen et al. 1992b; Köylü 1998). The methods yield R_g , D , and τ via the optical structure factor; R_v and n via scattering/extinction; and N and a when combined. In the following we will describe this method in the context of carbonaceous soot, a system to which the scattering/extinction method has been widely applied, but in principle it will work whenever the particle refractive index has an imaginary part. We start by considering scattering and extinction.

The classical scattering/extinction method (D'Alessio et al. 1975; D'Alessio 1981) relies upon the different functionalities of the scattering and extinction on the aggregate size. It was originally developed under the assumptions of spherical particles in the Rayleigh regime, both of which are limitations for aerosols such as flame soot. The RDG theory for aggregates, however, releases the method from these limitations.

Scattering and extinction are determined by the cross sections and the number density of the aggregates n . Let I_s be the light scattered intensity at a detector which subtends a given solid angle relative to the scattering volume a given distance away when the incident intensity is I_o . Then (Sorensen 1997)

$$I_s = c_o I_o n \frac{d\sigma^{agg}}{d\Omega}, \quad [92]$$

where c_o is a constant accounting for the unknown solid angle,

distance, etc.; it can be determined with calibration. Now with Equation (28) above we have

$$I_s = c_o I_o n N^2 \frac{d\sigma^m}{d\Omega} S(q), \quad [93]$$

combining with Equation (26) yields

$$I_s = c_o I_o n N^2 k^4 a^6 F(m) S(q). \quad [94]$$

These equations result from use of single aggregate formulas and hence apply to ensembles of single-sized aggregates, i.e., monodisperse systems. Generalization to the polydisperse case involves integration over the size distribution. In such an integration the terms nN (to be obtained below) and nN^2 become the moments of the size distribution M_1 and M_2 , respectively, as defined by Equation (B4). Absolute scattering measurements are best performed in either the Rayleigh ($qR_g < 1$) or power law ($qR_g > 1$) limiting regimes so that the functionalities on aggregation number N are simple. Failure to recognize this can cause error. Equations (36a) and (36c) provide these limits for the structure factor. Combining these with Equation (94), we obtain for the Rayleigh regime

$$I_s = I_o c_o n N^2 k^4 a^6 F(m) \quad (\text{monodisperse}) \quad [95a]$$

$$= I_o c_o M_2 k^4 a^6 F(m) \quad (\text{polydisperse}). \quad [95b]$$

For the power law regime we use Equations (1), (36c), and (94) to find

$$I_s = c_o I_o n N k^4 a^6 k_o C(aq)^{-D} \quad (\text{monodisperse}) \quad [96a]$$

$$= c_o I_o M_1 k^4 a^6 k_o C(aq)^{-D} \quad (\text{polydisperse}). \quad [96b]$$

Equations (95b) and (96b) are the polydisperse forms of (95a) and (96a). The value of c_o can be determined by scattering from gases and liquids of known Rayleigh ratio or standard colloid solutions, such as commercially available monodisperse polystyrene microspheres. In Table 3 we compile Rayleigh ratios for some common substances. Note that the units of a Rayleigh ratio are steradian⁻¹ cm⁻¹ and so are equivalent to a differential cross section (steradian⁻¹ cm²) times a number density (cm⁻³).

The extinction measurement is performed by comparing the incident light before and the transmitted light after it passes through a length ℓ of the system

$$I_T = I_o \exp(-\tau_{ext}\ell). \quad [97]$$

The extinction turbidity τ_{ext} is related to both the absorption and total scattering cross section and the soot cluster number density n by

$$\tau_{ext} = n(\sigma_{abs}^{agg} + \sigma_{sca}^{agg}). \quad [98]$$

Table 3

Rayleigh ratios are differential scattering cross sections multiplied by number densities, hence their units are cm^{-1} steradian $^{-1}$. They may be used for calibration of scattering from an unknown if the calibrating fluid and the unknown have the same scattering volume length, collection solid angle and incident power. Since incident intensity is power per unit area, the cross-sectional area of the scattering volume is not relevant so long as it is not too wide to be totally observed by the detector. The Rayleigh ratios below are for $T = 25^\circ\text{C}$ and $p = 1$ atm. They are for incident light polarized perpendicular to the scattering plane (i.e., vertical polarization, usually) and no polarizer on the detector. The units below are 10^{-6} cm^{-1} steradian $^{-1}$. The literature review for this table includes Rudder and Bach (1968), Kerker (1969), D'Alessio (1981), and Olivier et al. (1992). The uncertainty is ca. $\pm 5\%$. Gas Rayleigh ratios vary as λ^{-4} . Liquid Rayleigh ratios are more complex and our examination shows a rough $\lambda^{-4.66}$ variation

Material	$\lambda = 514.5$ nm	$\lambda = 488$ nm
H ₂	0.0038	0.0047
Ar	0.0154	0.019
O ₂	0.0148	0.0183
N ₂	0.0173	0.0214
CO ₂	0.034	0.042
CH ₄	0.0386	0.0477
Xe	0.0943	0.117
C ₂ H ₄	0.102	0.126
C ₂ H ₆	0.113	0.140
CCl ₄	13	17
C ₆ H ₆	29	37
C ₆ H ₅ CH ₃	32	41
CS ₂	33	170

From Equations (29) and (33), Equation (98) becomes

$$\tau_{ext} = n(N\sigma_{abs}^m + N^2\sigma_{sca}^m G(kR_g)). \quad [99]$$

With Equations (30) and (34) we obtain

$$\tau_{ext} = n \left[4\pi Nka^3 E(m) + \frac{8}{3}\pi N^2 k^4 a^6 F(m)G(kR_g) \right]. \quad [100]$$

We will first consider the extinction in the so-called Rayleigh limit where $\sigma_{abs} \gg \sigma_{sca}$. Then turbidity is the first term in Equation (100):

$$\tau_{ext} \simeq nN 4\pi ka^3 E \quad (\text{monodisperse}) \quad [101a]$$

$$\simeq M_1 4\pi ka^3 E \quad (\text{polydisperse}). \quad [101b]$$

The first moment M_1 is the total number of monomers per unit volume, $4\pi a^3/3$ is the volume of a monomer, so

$$f_v = nN \frac{4\pi a^3}{3} = \frac{\tau_{ext}}{3kE} \quad (\text{monodisperse}), \quad [102a]$$

$$f_v = M_1 \frac{4\pi a^3}{3} = \frac{\tau_{ext}}{3kE} \quad (\text{polydisperse}) \quad [102b]$$

is the aerosol or colloid volume fraction.

Comparison of Equations (95a) and (101a) for the monodisperse case shows that a ratio of these equations eliminates the unknown n and leaves Na^3 the volume equivalent "scattering/extinction" radius R_v . If τ_{ext} in Equation (101a) is first squared and then ratioed by Equation (95a), the factors of $(Na^3)^2$ cancel and the unknown cluster number density remains. Thus from the measured τ_{ext} and I_s , the aggregate volume equivalent sphere radius R_v and number density can be obtained.

The same procedure for the polydisperse case, Equations (95b) and (101b), yields

$$n_2 = \frac{M_1}{s_2} = \left(\frac{k}{4\pi} \right)^2 \frac{F}{E^2} \frac{\tau_{ext}^2}{I_s/I_o c_o} \quad [103]$$

and

$$R_v^3 = a^3 \frac{M_2}{M_1} = \frac{4\pi}{k^3} \frac{E}{F} \frac{I_s/I_o c_o}{\tau_{ext}}. \quad [104]$$

The monodisperse calculation is simple, but unrealistic; the polydisperse calculation is more complex, but realistic. Thus, regrettably, we must use the polydisperse calculation, but we shall keep the monodisperse calculation whenever heuristically useful. In that regard the volume equivalent sphere is written as $R_v^3 = a^3 N$ in the monodisperse case and $R_v^3 = a^3 M_2/M_1$ in the polydisperse case. This latter formula is completely reasonable because the ratio of any two consecutive moments of the size distribution is a mean size, i.e., $s_p = M_p/M_{p-1}$, see Appendix B. Certainly the units are correct and that is all one needs. Thus we in essence have the average number of monomers per aggregate $\langle N \rangle = s_2 = M_2/M_1$. The average number of aggregates per unit volume of aerosol is the total number of monomers per volume, M_1 , divided by a mean size, which in general is $n_p = M_1/s_p$. Equation (103) allows $n_2 = M_1/s_2$ to be determined.

An important lesson from these polydispersity considerations is that light scattering, in particular light scattering making use of the Rayleigh regime, selects the mean size s_2 from all the possibilities s_p .

In Figure 29 both R_g , determined via the optical structure factor, and R_v , determined via scattering extinction, Equation (104), are plotted for a flame soot aerosol as a function of height above burner. This figure demonstrates the ramified nature of the aggregate, since R_g becomes significantly greater than the volume equivalent R_v .

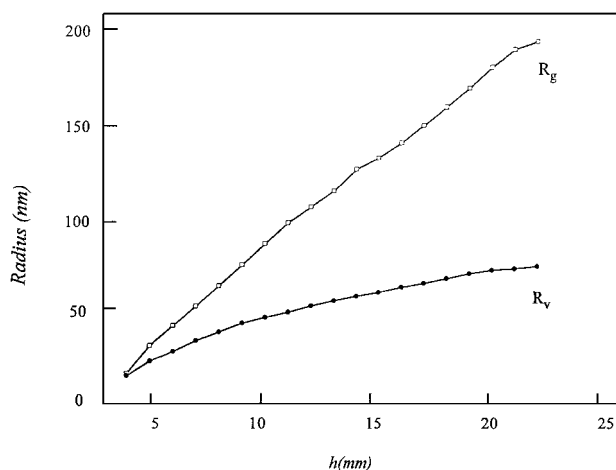


Figure 29. Aggregate radius of gyration R_g determined via the optical structure factor and volume equivalent sphere radius R_v determined via the scattering/extinction analysis for a soot aerosol in a premixed ethylene/oxygen flame as a function of height above burner.

Scattering and extinction methods applied to sizing of soot particles in flames have a long and venerable history. Early work, for lack of a theory for scattering and absorption by aggregates, used electromagnetic theory for spherical or ellipsoidal particles either in the Rayleigh approximation or with the full Mie theory. With our understanding of aggregate scattering and absorption, we now see that these early scattering/extinction methods are successful in measuring the soot volume fraction and the volume equivalent radius.

Combined Optical Structure Factor and Scattering/Extinction Measurements—Complete Characterization of the System

We now take stock of what we have and, consequently, what we can get from combined optical structure factor and scattering/extinction measurements. The optical structure factor yields R_g , D , and τ . With R_g and D , one can calculate G . If the complex index of refraction is known (see below), calibrated measurement of I_s and τ_{ext} yields the mean number of aggregates per volume n_2 and the aggregate volume equivalent radius R_v .

Selecting and gathering these quantities further in their monodisperse form we have $R_v^3 = a^3 N$, R_g , D , and from Equation (1) we have $N = k_o(R_g/a)^D$. The two equations in this ensemble have two unknowns, a and N , which can be solved for given the other measured values. This is the principle of the combined optical method that allows for complete aggregate characterization.

We proceed with the polydisperse case. We have $R_v^3 = a^3 s_2$ and from Equation (88) $R_{g,z}^2 = a^2 k_o^{-2/D} M_{2+2/D}/M_2$. This moment ratio must be evaluated in terms of s_2 . From Equation (B6)

we find

$$R_{g,z}^2 = a^2 k_o^{-2/D} s_2^{2/D} \frac{m_{2+2/D}}{m_2}. \quad [105]$$

Solving the two equations, two unknowns situation yields

$$\langle N \rangle = s_2 = \left[R_{g,z} R_v^{-1} \left(\frac{m_2}{m_{2+2/D}} \right)^{1/2} k_o^{1/D} \right]^{\frac{3D}{3-D}}, \quad [106]$$

$$a = \left[R_{g,z}^D R_v^{-3} \left(\frac{m_2}{m_{2+2/D}} \right)^{D/2} k_o \right]^{\frac{1}{D-3}}. \quad [107]$$

The values of m_i for the scaling distribution are given in Equation (B8).

The combined optical structure factor, scattering/extinction method represents a very powerful optical diagnostic for complete characterization of soot particles in flames. This method was tested in our laboratory by comparing it to TEM analysis (Cai et al. 1993). As described above, the method was successful, but ultimately limited by the uncertainty in the refractive index of the soot. This has become through the years the Achilles heel of all optical diagnostics for soot aerosols involving scattering/extinction. Fortunately the optical structure factor is immune to this problem, hence R_g and D measurements are relatively secure. Below (Table 4) we describe the current knowledge of the soot refractive index. Although these soot refractive index uncertainties can cause large uncertainties in R_v , a , and $\langle N \rangle = s_2$, these are uncertainties in accuracy, not precision. Thus measurements looking for changes or trends are not affected by the uncertainty in m .

Examples of these measurements are shown in Figures 30 and 31, which show a and $\langle N \rangle = s_2$, respectively, for a premixed ethylene/air flame. In particular, the graph of monomer size a versus height above burner shows how the precision of the measurement can indicate when surface growth ends, indicated by when a stops increasing.

Equations (103) and (104) were derived under the assumption of $\sigma_{abs} \gg \sigma_{sca}$, hence $\tau_{ext} \simeq n\sigma_{abs}$. We now consider the exact case when

$$\tau_{ext} = n(\sigma_{abs}^{agg} + \sigma_{sca}^{agg}). \quad [98]$$

Fortunately, the modifications are straightforward and one finds

$$n_2 = \frac{M_1^2}{M_2} = \left(\frac{k}{4\pi} \right)^2 \frac{F}{E^2} \frac{(\tau_{ext} - 4\pi G I_s/I_o c_o)^2}{I_s/I_o c_o} \quad [108]$$

and

$$R_v^3 = a^3 \frac{M_2}{M_1} = \frac{4\pi E}{k^3 F} \frac{I_s/I_o c_o}{(\tau_{ext} - 4\pi G I_s/I_o c_o)}. \quad [109]$$

These equations replace Equations (103) and (104). Note that the assumption, $\sigma_{abs} \gg \sigma_{sca}$, is equivalent to $G = 0$. As before, the value of R_v can be used in Equations (106) and (107) to

Table 4
Soot refractive indices

Reference	λ (nm)	Refractive index	E	F	Comments
Dalzell and Sarofim (1969)	Visible	$1.57 + 0.56i$	0.260	0.218	Standard value
Roessler and Faxvog (1980)	515	$1.75 + 0.5i$	0.200	0.242	Mean of review
Pluchino et al. (1980)	488	$1.7 + 0.7i$	0.285	0.305	$8 \mu\text{m}$ carbon sphere
Lee and Tien (1981)	633	$1.9 \pm 0.1 + (0.55 \pm 0.1)i$	0.19	0.30	Soot
Sloane (1983)	633	$1.7 + 0.8i$	0.32	0.352	Soot
Mullins and Williams (1987)	633	$1.85 + 0.4i$	0.149	0.245	Soot
Chang and Charalampopoulos (1990)	540	$1.77 + 0.63i$	0.244	0.291	Soot
Stagg and Charalampopoulos (1993)	633	$1.53 + 0.38i$	0.184	0.147	Soot
Köylü and Faeth (1996)	515	$1.54 + 0.48i$	0.229	0.180	Soot
Mulholland and Choi (1998)	—	$1.55 + 0.8i$	0.366	0.332	Soot specific mass extinction

yield $s_2 = \langle N \rangle$ and a . Figures 30 and 31 show results both uncorrected ($G = 0$) and corrected ($G \neq 0$) for scattering effect on extinction.

Köylü and Faeth (1996) have ratioed absolute scattering in the power law regime, Equations (96), and extinction, Equations (101), to obtain a formula independent of the state of aggregation

$$\frac{I_s}{\tau_{ext}} = \frac{c_o}{4\pi} (ka)^3 \left[\frac{F(m)}{E(m)} k_o \right] (aq)^{-D}. \quad [110]$$

They obtained Equation (110) under the assumption that $C = 1$, an assumption which has been validated above. This formula is useful for in situ measurement of either the monomer size a , the coefficient k_o , or the ratio $F(m)/E(m)$, depending on which two of these one already has from independent mea-

surements. Köylü and Faeth applied Equation (110) to a measurement of $F(m)/E(m)$. Then with values of $E(m)$ obtained from a consensus of the literature (Dalzell and Sarofim 1969; Lee and Tien 1981; Charalampopoulos and Chang 1988) determined the soot refractive index to be $m = 1.54 + 0.48i$ for turbulent diffusion flames of acetylene, propylene, ethylene, and propane in air. This value was based on TEM measurements of the monomer size a and previous measurements of k_o to be 2.44 (their $k_f = 8.5 \pm 0.5$ where $k_o = k_f/2^D$). Their specific value is $F(m)/E(m) = 0.78 \pm 0.09$, which is in agreement with the same ratio measured by Dalzell and Sarofim and Charalampopoulos and Chang. On the other hand, if we use $k_o = 1.30$, as found in much of our work, then their work implies $F(m)/E(m) = 1.46 \pm 0.17$, which is in good agreement with the Lee and Tien value of 1.58.

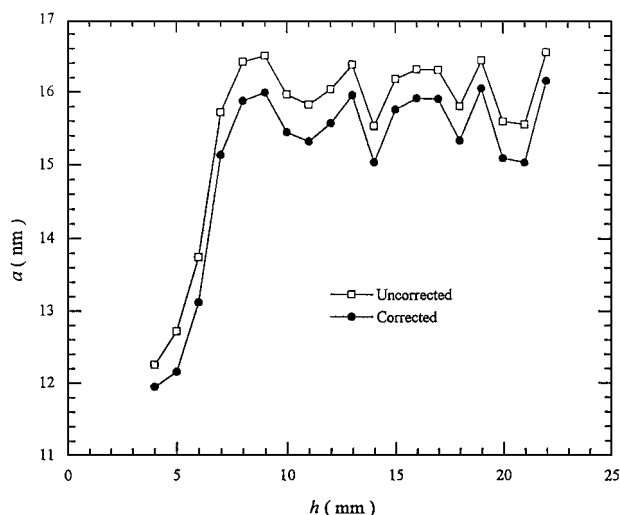


Figure 30. Monomer radius a versus height above burner h for soot fractal aggregates in an ethylene/oxygen premixed flame. Uncorrected assumes no scattering contribution to the extinction and uses Equations (107) and (104). Corrected corrects for the contribution of scattering to extinction and uses Equations (107) and (109).

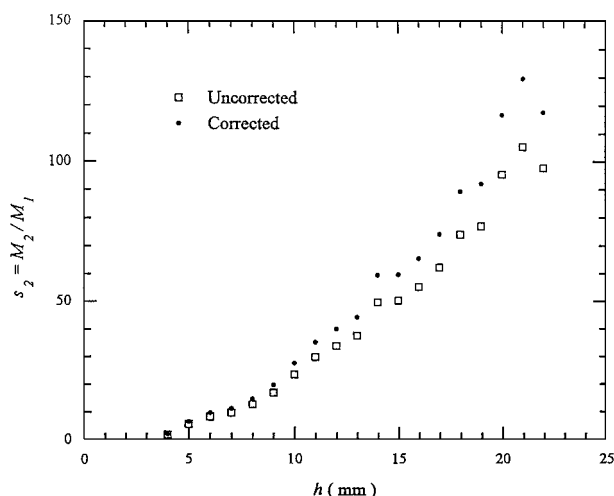


Figure 31. Mean aggregate size $s_2 = M_2/M_1 = \langle N \rangle$ versus height above burner h for soot fractal aggregates in an ethylene/oxygen premixed flame. Uncorrected assumes no scattering contribution to the extinction and uses Equations (106) and (104). Corrected corrects for the contribution of scattering to extinction and uses Equations (106) and (109).

In subsequent work Köylü (1998) used Equation (110) to measure monomer particle size a given the knowledge of m and k_o derived above. In principle this is a nice way to make monomer size measurements, but one must be careful not to make a circular argument and instead derive the input variables from completely independent measurements.

The Albedo

How large is the correction for $G \neq 0$? A useful way to consider this question is to study the albedo, which is the ratio of scattering to total extinction (Kerker 1969):

$$\omega = \sigma_{sca}/\sigma_{ext} = \sigma_{sca}/(\sigma_{sca} + \sigma_{abs}). \quad [111]$$

For a particle or aggregate with a real refractive index (no imaginary part), $\sigma_{abs} = 0$ hence $\omega = 1$. With Equation (111), the extinction turbidity of Equation (98) can be modified to

$$\tau_{ext} = n \sigma_{abs}^{agg} (1 - \omega_{agg})^{-1}. \quad [112]$$

For systems with a complex refractive index consider first a Rayleigh scattering sphere. Equation (111) with Equations (30) and (34) gives

$$\omega_{ray} = \left(1 + \frac{3}{2}(ka)^{-3}E/F\right)^{-1}. \quad [113]$$

In the Rayleigh regime, $ka < 1$ so the second term in (113) dominates, hence

$$\omega_{ray} \simeq \frac{2}{3}(ka)^3 F/E. \quad [114]$$

This cubic dependency with size must level off as ka approaches 1, but then the Rayleigh equations are no longer valid. As an example, let $ka = 0.2$, typical of a soot monomer (if $\lambda = 488$ nm, $a = 15.5$ nm), and let $2/3(E/F) = 1$ (see Table 4), then $\omega = 8 \times 10^{-3}$. This small value justifies Equation (114) for $ka < 1$.

For an aggregate use of Equations (29), (30), (33), and (34) in Equation (111) yields

$$\omega_{agg} = \left(1 + \frac{3}{2}E/F(ka)^{-3}(NG(kR_g))^{-1}\right)^{-1}, \quad [115]$$

where $G(kr_g)$ is given by Equation (35). This albedo is plotted for soot in Figure 32. The calculations were performed for $\lambda = 500$ nm. With Equation (1), one can see that Equation (115) contains the factor $3(E/F)/2k_o$, which we set equal to 1 in our calculation. This is a typical value combination for soot fractal aggregates; for example, if $k_o = 1.3$, as we have contended, then this would require $E/F = 0.87$, typical of soot (see Table 4 below). Figure 32 shows that initially $\omega_{agg} \sim R_g^D$, but this quickly saturates for $R_g \gtrsim 100$ nm. Recall Equation (114), where for a sphere $\omega_{Rag} \sim a^3$. For a typical monomer size of $a = 20$ nm, ω_{agg} saturates at 0.2.

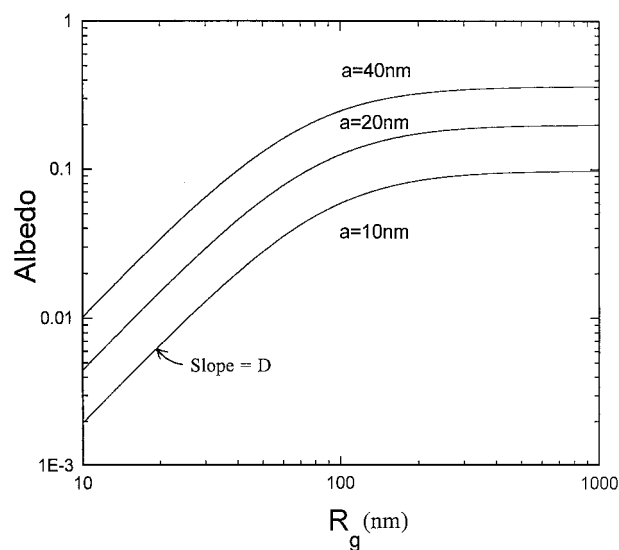


Figure 32. The albedo, the ratio of scattering to extinction, versus radius of gyration for a soot-like fractal aggregate calculated using Equation (115) with $D = 1.75$, $(E/F)/k_o = 2/3$, and $\lambda = 500$ nm. Results for 3 different monomer sizes a are shown.

We now deal with the accuracy of Equation (115), which essentially tests the accuracy of $G(kR_g)$ as well. Mulholland and Choi (1998) gave experimental values for the albedo of soot produced by laminar and turbulent acetylene and ethane flames. Monomer sizes for these flames were reported as $a = 24$ and 34 nm, respectively. Albedo values in the range of 0.19 to 0.25 were found, consistent with the calculated values at large R_g in Figure 32. This figure is for $\lambda = 500$ nm, and Mulholland and Choi used $\lambda = 632.8$ nm. Calculation of ω with Equation (115) with $\lambda = 632.8$ nm in the asymptotic range $R_g > 200$ nm with $m = 1.55 + 0.8i$, a value proposed by Mulholland and Choi, and $k_o = 1.3$, yields $\omega = 0.14$ and 0.20 , somewhat smaller, but given all the input parameters with their uncertainties, still consistent with the experimental values.

Mulholland and Mountain (1999) have applied their coupled electric and magnetic dipole calculation to simulated DLCA aggregates ($D \simeq 1.8$), as described above, to calculation of the albedo as well. Their particles had $m = 1.7 + 0.7i$, which leads to $E/F = 0.93$. They used three different monomer size parameters, $x_p = ka = 0.05, 0.21, \text{ and } 0.60$. We assume their fractal aggregates have $D = 1.8$ and $k_o = 1.3$, and then calculated ω_{agg} from Equation (115). This calculation is compared to their computer data in Figure 33 quite successfully. These nice comparisons buy up our confidence in Equation (115), the corrections to calculation of R_v and n_2 to be described immediately below, and our confidence in the form of G , Equation (35).

To use the albedo to correct the scattering/extinction measurements follow a similar procedure that led to Equations (103) and (104), viz. combine Equations (95b), (112), and (29) and (30)

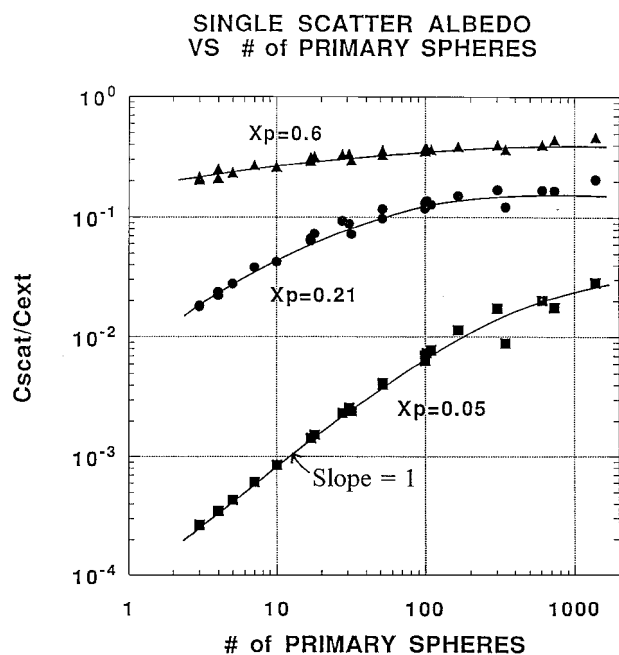


Figure 33. The albedo, the ratio of scattering to extinction, versus number of primary spheres (monomers) in soot-like fractal aggregates with $D \simeq 1.8$. Data points were calculated by Mulholland and Mountain (1999) for $m = 1.7 + 0.7i$, lines were calculated with Equation (115). Three different primary particle size parameters, $x_p = ka$, are shown.

to obtain

$$n_2 = \left(\frac{k}{4\pi}\right)^2 F/E^2 \frac{\tau_{ext}^2}{I_s/I_o C_o} (1 - \omega)^2, \quad [116]$$

and

$$R_v^3 = \frac{4\pi}{k^3} \frac{E}{F} \frac{I_s/I_o C_o}{\tau_{ext}} (1 - \omega)^{-1}. \quad [117]$$

These are straightforward modifications of Equations (103) and (104). One can now estimate errors incurred by not accounting for scattering contributing to the extinction. From Figure 30 for $a = 20$ nm, we find $\omega \simeq 0.2$ for $R_g \gtrsim 100$ nm. Thus, by Equation (116) n_2 would need a $\sim 40\%$ downward correction if Equation (103) was used instead of Equation (108), and by Equation (117) R_v would need a $\sim 7\%$ upward correction if Equation (104) was used instead of the more correct version, Equation (109). Propagation of these errors into $s_2 = \langle N \rangle$ and a via Equations (106) and (107) is straightforward.

The Refractive Index of Soot

Throughout this history perhaps the greatest uncertainty has come from a poorly known, complex index of refraction for soot. Does it depend on fuel type, burner conditions, soot age, etc? What is its dispersion with λ ? These important questions are largely unanswered because the uncertainty in any measurement

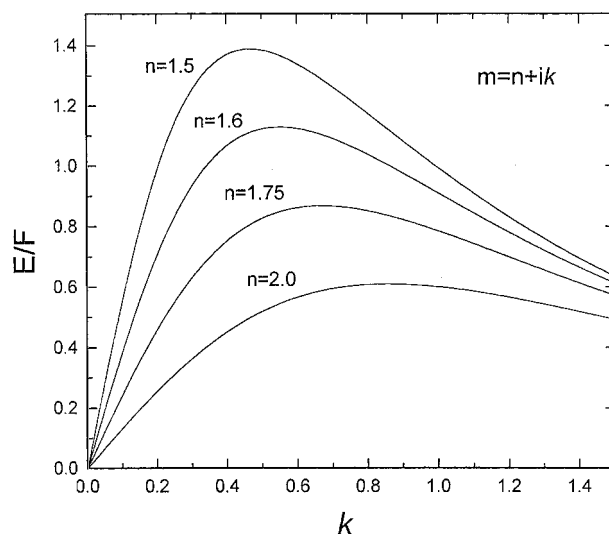


Figure 34. The ratio $E(m)/F(m)$, Equations (31) and (27), as a function of the real and imaginary parts of the refractive index m .

of the refractive index of soot is probably greater than changes due to these functionalities.

In Table 4 a variety of soot refractive indices $m = n + ik$ available in the literature are given. Scattering and absorption involve the functions $E(m)$ and $F(m)$, Equations (27) and (31), and the interpretation of scattering and absorption data involves E/F and F/E^2 . Figures 34 and 35 plot these as a function of the imaginary part k for various real parts n . We see variations in E/F of as much as a factor of 2 and in F/E^2 of as much as a factor of 3. These uncertainties propagate into the parameters we desire to measure, such as n_2 , R_v , $\langle N \rangle$, and a via Equations (108) and

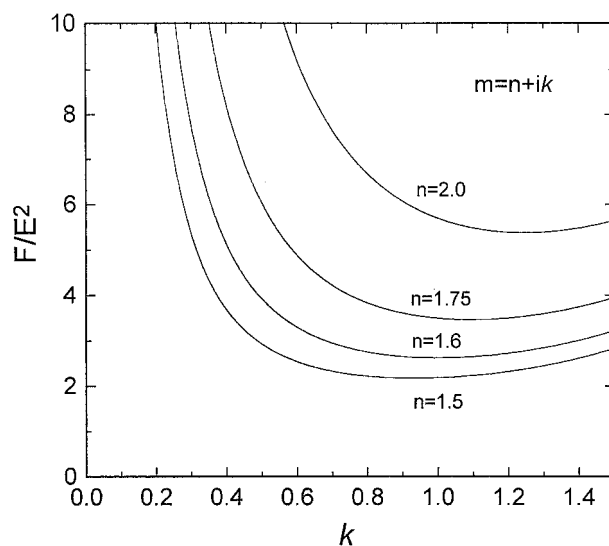


Figure 35. The ratio $F(m)/E(m)^2$, Equations (27) and (32), as a function of the real and imaginary parts of the refractive index m .

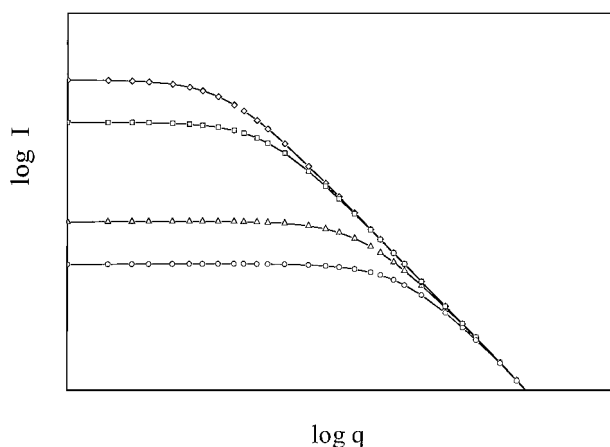


Figure 36. Schematic of the Tyndall effect for fractal aggregates. The scattered intensity increases in a narrowing Rayleigh regime as the system coarsens through aggregation. The power law regime is invariant with aggregation. Sequence of time is circles, triangles, squares, and diamonds (earliest to latest).

(109), and f_v via Equation (102). For example, not knowing E/F to better than a factor of 2 implies R_v is uncertain by $\sim 26\%$. Of course, some authors have their favorite m and such uncertainties don't exist for them. Less cynically, the precision in the measurements is considerably better than this uncertainty, and precision allows for detection of changes, which can be very valuable.

The Tyndall Effect

Before we leave the subject of sizing, we describe the evolution of the scattered intensity in an aggregating system. We make the reasonable assumption that the total number of monomers per unit volume in the system is a conserved quantity during aggregation. This will hold if there are no sources, such as nucleation or surface growth (the latter keeps the monomer number density constant but increases the monomer size, hence scattering cross section) or sinks, such as settling, or wall losses. We also require no expansion or contraction of the system to maintain constant volume. Then we use for the Rayleigh regime Equations (92), (26), (21), and (36a) and for the power law regime Equations (92), (26), (27), and (36b) to represent the scattering in the Rayleigh and power law regimes as

$$I \propto nN^2 \sigma_{sca}^m, \quad qR_g < 1, \quad [118a]$$

$$I \propto nN^2 \sigma_{sca}^m (qR_g)^{-D}, \quad qR_g > 1. \quad [118b]$$

The monomer concentration is the product of the cluster concentration and the number of monomers per cluster, $n_m = nN$. Moreover, Equation (1) implies $R_g^{-D} = a^{-D} k_o N^{-1}$. Then Equations (118) become

$$I \propto n_m N \sigma_{sca}^m, \quad qR_g < 1, \quad [119a]$$

$$I \propto n_m k_o \sigma_{sca}^m (qa)^{-D}, \quad qR_g > 1. \quad [119b]$$

Since n_m is a constant, we see that as aggregation proceeds, N increases and the scattering in the aggregate Rayleigh regime increases in direct proportion to N . On the other hand, the scattering in the power law regime remains a constant. This is an expression of the Tyndall effect, the increase in scattering as a system aggregates, but here we see that the increase is confined to the Rayleigh regime. Figure 36 displays this schematically, and Figure 24 gives an example from an aggregating aerosol.

CONCLUSION

If left with the allowance of only one final and brief remark, I would say “ q .” It is q , the scattering wave vector, that is physically motivated with an inverse that describes the length scale probed by the scattering experiment. Conceptualization of the scattering as a function of q allows for facile interpretation of the scattering function. This is in strong contrast to the scattering angle θ , which, although experimentally convenient, gives no physical insight for the scattering process. Plot the scattering data versus q .

If allowed a second remark, I would say “logarithmic.” This is, by and large, a geometric universe not an arithmetic one, and therefore we should space our detectors and plot our data accordingly.

Beyond these comments, I will let the work above speak for itself.

REFERENCES

- Abramowitz, M., and Stegun, I. A., editors. (1965). *Handbook of Mathematical Functions*, Dover, New York.
- Berry, M. V., and Percival, I. C. (1986). Optics of Fractal Clusters Such as Smoke, *Optica Acta* 33:577–591.
- Bohren, C. E., and Huffman, D. R. (1983). *Absorption and Scattering of Light by Small Particles*, Wiley, New York.
- Bonczyk, P. A., and Hall, R. J. (1991). Fractal Properties of Soot Agglomerates, *Langmuir* 7:1274–1280.
- Bonczyk, P. A., and Hall, R. J. (1992). Measurement of the Fractal Dimension of Soot Using UV Laser Radiation, *Langmuir* 8:1666–1670.
- Born, M., and Wolf, E. (1975). *Principles of Optics*, Pergamon, Oxford.
- Brown, W. D., and Ball, R. C. (1985). Computer Simulation of Chemically Limited Aggregation, *J. Phys. A* 18:L517–L521.
- Brunning, J. H., and Lo, Y. T. (1971). Multiple Scattering of EM Waves of Spheres. Part I. Multipole Expansion and Ray-Optical Solutions, *IEEE Trans. Antennas Propag.* AP-19:378–390.
- Cai, J., and Sorensen, C. M. (1994). Diffusion of Fractal Aggregates in the Free Molecular Regime, *Phys. Rev. E* 50:3397–3400.
- Cai, J., Lu, N., and Sorensen, C. M. (1993). Comparison of Size and Morphology of Soot Aggregates as Determined by Light Scattering and Electron Microscope Analysis, *Langmuir* 9:2861–2068.
- Cai, J., Lu, N., and Sorensen, C. M. (1995a). Analysis of Fractal Cluster Morphology Parameters: Structural Coefficient and Density Autocorrelation Function Cutoff, *J. Colloid Interface Sci.* 171:470–473.
- Cai, J., Lu, N., and Sorensen, C. M. (1995b). Fractal Cluster Size Distribution Measurement Using Static Light Scattering, *J. Colloid Interface Sci.* 174:456–460.
- Chang, H., and Charalampopoulos, T. T. (1990). Determination of the Wavelength Dependence of Refractive Indices of Flame Soot, *Proc. R. Soc. Lond. A* 430:557–591.

- Charalampopoulos, T. T. (1992). Morphology and Dynamics of Agglomerated Particulates in Combustion Systems Using Light Scattering Techniques, *Prog. Energy Combust. Sci.* 18:13–45.
- Charalampopoulos, T. T., and Chang, H. (1988). In Situ Optical Properties of Soot Particles in the Wavelength Range from 340 nm to 600 nm, *Combust. Sci. Tech.* 59:401–421.
- Chen, Z.-Y., Weakliem, P., Gelbart, W. M., and Meakin, P. (1987). Second-Order Light Scattering and Local Anisotropy of Diffusion-Limited Aggregates and Bond-Percolation Clusters, *Phys. Rev. Lett.* 58:1996–1999.
- Colbeck, I., and Harrison, R. M. (1986). The Atmospheric Effects of Nuclear War—A Review, *Atmos. Environ.* 20:1673–1681.
- D'Alessio, A. (1981). *Laser Light Scattering and Fluorescence Diagnostics of Rich Flames, Particulate Carbon*, edited by D. C. Siegla and G. W. Smith. Plenum, New York, pp. 207–259.
- D'Alessio, A., DiLorenzo, A., Sarofim, A. F., Beretta, F., Masi, S., and Venitozzi, C. (1975). Soot Formation in Methane-Oxygen Flames. In *Fifteenth Symposium (International) on Combustion*. Combustion Institute, Pittsburgh, PA, pp. 1427–1438.
- Dalzell, W. H., and Sarofim, A. F. (1969). Optical Constants of Soot and their Application to Heat-Flux Calculations, *J. Heat Transfer* 91:100–104.
- Dobbins, R. A., and Megaridis, C. M. (1987). Morphology of Flame-Generated Soot as Determined by Thermophoretic Sampling, *Langmuir* 3:254–259.
- Dobbins, R. A., and Megaridis, C. M. (1991). Absorption and Scattering of Light by Polydisperse Aggregates, *Appl. Optics* 30:4747–4754.
- Family, F., and Landau, D. P., editors. (1984). *Kinetics of Aggregation and Gelation*, North-Holland, Amsterdam.
- Farias, T. L., Carvalho, M. G., Köylü, U. O., and Faeth, G. M. (1995). Computational Evaluation of Approximate Rayleigh-Debye-Gans/Fractal-Aggregate Theory for the Absorption and Scattering Properties of Soot, *J. Heat Transfer* 117:152–159.
- Farias, T. L., Koylu, U. O., and Carvalho, M. G. (1996a). Effect of Polydispersity of Aggregates and Primary Particles on Radiative Properties of Simulated Soot, *J. Quant. Spectrosc. Radiat. Transfer* 55:357–371.
- Farias, T. L., Koylu, U. O., and Carvalho, M. G. (1996b). Range of Validity of the Rayleigh-Debye-Gans Theory for Optics of Fractal Aggregates, *Appl. Optics* 35:6560–6567.
- Fisher, M. E., and Burford, R. J. (1967). Theory of Critical-Point Scattering and Correlations I. The Ising Model, *Phys. Rev. A* 156:583–622.
- Forrest, S. R., and Witten, Jr., T. A. (1979). Long-Range Correlations in Smoke-Particle Aggregates, *J. Phys. A* 12:L109–L117.
- Freltoft, T., Kjems, J. K., and Sinha, S. K. (1986). Power-Law Correlations and Finite-Size Effects in Silica Particle Aggregates Studied by Small-Angle Neutron Scattering, *Phys. Rev. B* 33:269–272.
- Frey, J., Pivdic, J. J., Botet, R., and Jullien, R. (1988). Light Scattering by Fractal Aggregates: A Numerical Investigation, *J. Phys. France* 49:1969–1976.
- Friedlander, S. K. (1977). *Smoke, Dust, and Haze*, Wiley-Interscience, New York.
- Friedlander, S. K., and Wang, C. S. (1966). The Self-Preserving Particle Size Distribution for Coagulation by Brownian Motion, *J. Colloid Interface Sci.* 22:126–132.
- Fuller, K. A. (1991). Optical Resonances and Two-Sphere Systems, *Appl. Optics* 33:4716–4731.
- Fuller, K. A. (1994). Scattering and Absorption Cross Sections of Compounded Spheres. I. Theory for External Aggregation, *J. Opt. Soc. Am. A* 11:3251–3260.
- Fuller, K. A. (1995a). Scattering and Absorption Cross Sections of Compounded Spheres. II. Calculations for External Aggregation, *J. Opt. Soc. Am. A* 12:881–892.
- Fuller, K. A. (1995b). Scattering and Absorption Cross Sections of Compounded Spheres. III. Spheres Containing Arbitrarily Located Spherical Inhomogeneities, *J. Opt. Soc. Am. A* 12:893–904.
- Fuller, K. A., and Mackowski, D. W. (2000). Electromagnetic Scattering by Compounded Spherical Particles, In *Light Scattering by Nonspherical Particles*, edited by M. I. Mishchenko, J. W. Hovenier, and L. D. Travis. Academic Press, New York.
- Gangopadhyay, S., Elminyawi, I., and Sorensen, C. M. (1991). Optical Structure Factor Measurements of Soot Particles in a Premixed Flame, *Appl. Optics* 30:4859–4864.
- Gerardy, J. M., and Ausloos, M. (1980). Absorption Spectrum of Clusters of Spheres from the General Solution of Maxwell's Equations: The Long Wavelength Limit, *Phys. Rev. B* 22:4950–4959.
- Guinier, A. (1939). La Diffraction Des Rayons X Aux Trespetits Angles: Application a L'etude de Phenomes Ultramicroscopiques, *Ann. Phys.* 12:161–237.
- Guinier, A., Fournet, G., Walker, C. B., and Yudowitch, K. L. (1955). *Small Angle Scattering of X-Rays*, Wiley, New York.
- Hage, J. I., and Greenberg, J. M. (1990). A Model for the Optical Properties of Porous Grains, *Ap. J.* 361:251–259.
- Hasmy, A., Foret, M., Pelous, J., and Jullien, R. (1993). Small-Angle Neutron-Scattering Investigations of Short-Range Correlations in Fractal Aerogels: Simulations and Experiments, *Phys. Rev. B* 48:9345–9353.
- Hausdorff, F. (1919). Dimension und Aübers Mass, *Math Ann.* 79:157–179.
- Haw, M. D., Sievwright, M., Poon, W. C. K., and Pusey, P. N. (1995). Structure and Characteristic Length Scales in Cluster-Cluster Aggregation Simulation, *Physica A* 217:231–260.
- Hecht, E. (1998). *Optics*, Addison-Wesley, Reading, MA.
- Hurd, A. J., and Flower, W. L. (1988). In Situ Growth and Structure of Fractal Silica Aggregates in a Flame, *J. Colloid Interface Sci.* 123:178–192.
- Iskander, M. F., Chen, H. Y., and Penner, J. E. (1989). Optical Scattering and Absorption by Branched Chains of Aerosols, *Appl. Optics* 28:3083–3091.
- Jackson, J. D. (1962). *Classical Electrodynamics*, Wiley, New York.
- Jones, A. R. (1979). Electromagnetic Wave Scattering by Assemblies of Particles in the Rayleigh Approximation, *Proc. R. Soc. Lond. A* 366:111–127.
- Jullien, R. (1992). From Guinier to Fractals, *J. Phys. I France* 2:759–770.
- Jullien, R., and Botet, R. (1987). *Aggregation and Fractal Aggregates*, World Scientific, Singapore.
- Kazakov, A., and Frenklach, M. (1998). Dynamic Modeling of Soot Particle Coagulation and Aggregation; Implementation with the Method of Moments and Application to High-Pressure Laminar Premixed Flames, *Combust. Flame* 114:484–501.
- Kerker, M. (1950). The Use of White Light on Determining Particle Radius by the Polarization Ratio of the Scattered Light, *J. Colloid Interface Sci.* 5:165–167.
- Kerker, M. (1969). *The Scattering of Light and Other Electromagnetic Radiation*, Academic, New York.
- Kerker, M., Farone, W. A., and Matijevic, E. (1963). Applicability of Rayleigh-Gans Scattering to Spherical Particles, *J. Opt. Soc. Am.* 53:758–759.
- Keyes, T., Seeley, G., Weakliem, P., and Ohtsuki, T. (1987). Collision-Induced Light Scattering from Growing Clusters, *J. Chem. Soc. Faraday Trans.* 83:1859–1866.
- Khlebtsov, N. G. (1993). Optics of Fractal Clusters in the Anomalous Diffraction Approximation, *J. Mod. Opt.* 40:2221–2235.
- Kolb, M., Botet, R., and Jullien, R. (1983). Scaling of Kinetically Growing Clusters, *Phys. Rev. Lett.* 51:1123–1126.
- Köylü, U. O. (1997). Quantitative Analysis of In Situ Optical Diagnostics for Inferring Particle/Aggregate Parameters in Flames: Implications for Soot Surface Growth and Total Emissivity, *Combust Flame* 109:488–500.
- Köylü, U. O., and Faeth, G. M. (1992). Structure of Overfire Soot in Buoyant Turbulent Diffusion Flames at Long Residence Times, *Combust. Flame* 89:140–156.
- Köylü, U. O., and Faeth, G. M. (1994a). Optical Properties of Overfire Soot in Buoyant Turbulent Diffusion Flames at Long Residence Times, *J. Heat Transfer* 116:152–159.
- Köylü, U. O., and Faeth, G. M. (1994b). Optical Properties of Soot in Buoyant Laminar Diffusion Flames, *J. Heat Transfer* 116:971–979.
- Köylü, U. O., and Faeth, G. M. (1996). Spectral Extinction Coefficients of Soot Aggregates from Turbulent Diffusion Flames, *J. Heat Transfer* 118:415–421.

- Köylü, U. O., Faeth, G. M., Farias, T. L., and Carvalho, M. G. (1995). Fractal and Projected Structure Properties of Soot Aggregates, *Combust. Flame* 100: 621–633.
- Köylü, U. O., Xing, Y., and Rosner, D. E. (1995). Fractal Morphology Analysis of Combustion-Generated Aggregates Using Angular Light Scattering and Electron Microscope Images, *Langmuir* 11:4848–4854.
- Ku, J. C. (1991). Correction for the Extinction Efficiency Factors Given in the Jones Solution for Electromagnetic Scattering by Agglomerates of Small Spheres, *J. Phys. D.* 24:71–75.
- Ku, J. C., and Shim, K.-H. (1992). A Comparison of Solutions for Light Scattering and Absorption by Agglomerated or Arbitrarily-Shaped Particles, *J. Quant. Spectrosc. Radiat. Transfer* 47:201–220.
- Lee, S. C., and Tien, C. L. (1981). *Eighteen Symposium (International) on Combustion*, The Combustion Institute, Pittsburgh, p. 1159.
- Lin, M. Y., Klein, R., Lindsay, H. M., Weitz, D. A., Ball, R. C., and Meakin, P. (1990a). The Structure of Fractal Colloidal Aggregates of Finite Extent, *J. Colloid Interface Sci.* 137:263–280.
- Lin, M. Y., Lindsay, H. M., Weitz, D. A., Ball, R. C., Klein, R., and Meakin, P. (1990b). Universal Reaction-Limited Colloid Aggregation, *Phys. Rev. A* 41:2005–2020.
- Lindsay, H. M., Lin, M. Y., Weitz, D. A., Sheng, P., Chen, Z., Klein, R., and Meakin, P. (1987). Properties of Fractal Colloid Aggregates, *Faraday Discuss. Chem. Soc.* 83:153–165.
- Lou, W., and Charalampopoulos, T. T. (1994). On the Electromagnetic Scattering and Absorption of Agglomerated Small Spherical Particles, *J. Phys. D* 27:2258–2270.
- Lu, N., and Sorensen, C. M. (1994). Depolarized Light Scattering from Fractal Soot Aggregates, *Phys. Rev. E* 50:3109–3115.
- Mackowski, D. W. (1994). Calculation of Total Cross Sections of Multi-Sphere Clusters, *J. Opt. Soc. Am. A* 11:2851–2861.
- Mackowski, D. W. (1995). Electrostatic Analysis of Radiative Absorption by Sphere Clusters in the Rayleigh Limit: Application to Soot Clusters, *Appl. Optics* 34:3535–3545.
- Mandelbrot, B. B. (1977). *Fractals: Form, Chance and Dimension*, W. H. Freeman, San Francisco, CA.
- Mandelbrot, B. B. (1982). *Fractal Geometry of Nature*, W. H. Freeman, San Francisco, CA.
- Martin, J. E., and Hurd, A. J. (1987). Scattering from Fractals, *J. Appl. Cryst.* 20:61–78.
- Martin, J. E., Schaefer, D. W., and Hurd, A. J. (1986). Fractal Geometry of Vapor-Phase Aggregates, *Phys. Rev. A* 33:3540–3543.
- Maxwell-Garnett, J. C. (1904). Colours in Metal Glasses and Metal Films, *Phil. Trans. R. Soc. London A* 203:385–420.
- Meakin, P. (1983). Formation of Fractal Clusters and Networks by Irreversible Diffusion-Limited Aggregation, *Phys. Rev. Lett.* 51:1119–1122.
- Meakin, P. (1984). Effects of Cluster Trajectories on Cluster-Cluster Aggregation: A Comparison of Linear and Brownian Trajectories in Two- and Three-Dimensional Simulations, *Phys. Rev. A* 29:997–999.
- Meakin, P. (1988). Fractal Aggregates, *Adv. Coll. Interface Sci.* 28:249–331.
- Mishchenko, M. I., Hovenier, J. W., and Travis, L. D., editors. (2000). *Light Scattering by Nonspherical Particles*, Academic, New York.
- Mishchenko, M. I., and Mackowski, D. W. (1994). Light Scattering by Randomly Oriented Biopheres, *Opt. Lett.* 19:1604–1606.
- Mockler, R. C., and O'Sullivan (1978). Multiple Scattering of Light from a System of Brownian Particles, *Phys. Rev. A* 17:2030–2035.
- Mountain, R. D., and Mulholland, G. W. (1988). Light Scattering from Simulated Smoke Agglomerates, *Langmuir* 4:1321–1326.
- Mulholland, G. W., Bohren, C. F., and Fuller, K. A. (1994). Light Scattering by Agglomerates: Coupled Electric and Magnetic Dipole Method, *Langmuir* 10:2533–2546.
- Mulholland, G. W., and Choi, M. Y. (1998). *Measurement of the Mass Specific Extinction Coefficient for Acetylene and Ethene Smoke using the Large Agglomerate Optics Facility*, Twenty-Seventh Symposium (International) on Combustion/The Combustion Institute, pp. 1515–1522.
- Mulholland, G. W., and Mountain, R. D. (1999). Coupled Dipole Calculation of Extinction Coefficient and Polarization Ratio for Smoke Agglomerates, *Combust. Flame* 119:56–68.
- Mulholland, G. W., Sampson, R. J., Mountain, R. D., and Ernst, M. H. (1988). Cluster Size Distribution for Free Molecular Agglomeration, *Energy Fuels* 2:481–486.
- Mullins, J., and Williams, A. (1987). The Optical Properties of Soot: A Comparison between Experimental and Theoretical Values, *Fuel* 66:277–284.
- Nelson, J. (1989a). Test of Mean Field Theory for the Optics of Fractal Clusters, *J. Mod. Opt.* 36:1031–1057.
- Nelson, J. (1989b). Fractality of Sooty Smoke: Implications for the Severity of Nuclear Winter, *Nature* 339:611–613.
- Nelson, J. A., Crookes, R. J., and Simons, S. (1990). On Obtaining the Fractal Dimension of a 3D Cluster from its Projection on a Plane—Application to Smoke Agglomerates, *J. Phys. D* 23:465–468.
- Nicolai, T., Durand, D., and Gimel, J.-C. (1994). Static Structure Factor of Dilute Solutions of Polydisperse Fractal Aggregates, *Phys. Rev. B* 50:16357–16363.
- Oh, C., and Sorensen, C. M. (1997a). Light Scattering Study of Fractal Cluster Aggregation Near the Free Molecular Regime, *J. Aerosol Sci.* 28:937–957.
- Oh, C., and Sorensen, C. M. (1997b). The Effect of Monomer Overlap on the Morphology of Fractal Aggregates, *J. Colloid Interface Sci.* 193:17–25.
- Oh, C., and Sorensen, C. M. (1998). Structure Factor of Diffusion Limited Aggregation Clusters: Local Structure and Non-Self-Similarity, *Phys. Rev. E* 57:784–790.
- Oh, C., and Sorensen, C. M. (1999). Scaling Approach for the Structure Factor of a Generalized System of Scatterers, *J. Nanopart. Res.* 1:369–377.
- Olivier, B. J., Sorensen, C. M., and Taylor, T. W. (1992). Scaling Dynamics of Aerosol Coagulation, *Phys. Rev. A* 45:5614–5623.
- Pearson, A., and Anderson, G. W. (1993). Long-Range Pair Correlation and its Role in Small-Angle Scattering from Fractal Clusters, *Phys. Rev. B* 48:5865–5885.
- Pluchino, A. B., Goldberg, S. S., Dowling, J. M., and Randall, C. M. (1980). Refractive-Index Measurements of Single Mirror Sited Carbon Particles, *Appl. Optics* 19:3370–3372.
- Porod, G. (1951). Die Röntgonkleinwinkelstreuung von Dichtgepackten Kolloiden Systemen, *Kolloid Z.* 124:83–114.
- Purcell, E. M., and Pennypacker, C. R. (1973). Scattering and Absorption of Light by Nonspherical Dielectric Grains, *The Astrophysical Journal* 186:705–714.
- Puri, R., Richardson, T. F., Santoro, R. J., and Dobbins, R. A. (1993). Aerosol Dynamic Processes of Soot Aggregates in a Laminar Ethene Diffusion Flame, *Combust. Flame* 92:320–333.
- Quinten, M., and Kreibig, U. (1993). Absorption and Elastic Scattering of Light by Particle Aggregates, *Appl. Optics* 32:6173–6182.
- Roessler, D. M., and Faxvog, F. R. (1980). Optical Properties of Agglomerated Acetylene Smoke Particles at 0.5145 μm and 10.6 μm Wavelength, *J. Opt. Soc. Am.* 70:230–235.
- Rudder, R. R., and Bach, D. R. (1968). Rayleigh Scattering of Ruby-Laser Light by Neutral Gases, *J. Opt. Soc. Am.* 58:1260–1266.
- Sampson, R. J., Mulholland, G. W., and Gentry, J. W. (1987). Structural Analysis of Soot Agglomerates, *Langmuir* 3:272–281.
- Saxon, D. S. (1974). Lectures on the Scattering of Light. In *The UCLA International Conference on Radiation and Remote Probing of the Atmosphere*, edited by J. G. Kuriyan. University California Press, Los Angeles, CA, pp. 227–259.
- Schaefer, D. W., Martin, J. E., Wiltzius, P., and Cannell, D. S. (1984). Fractal Geometry of Colloidal Aggregates, *Phys. Rev. Lett.* 52:2371–2374.
- Seeley, G., Keyes, T., and Ohtsuki, T. (1988). Higher-Order Fractal Geometry; Application to Multiple Light Scattering, *Phys. Rev. Lett.* 60:290–293.

- Singham, S. B., and Bohren, C. F. (1993). Scattering of Unpolarized and Polarized Light by Particle Aggregates of Different Size and Fractal Dimension, *Langmuir* 9:1431–1435.
- Sloane, C. G. (1983). Optical Properties of Aerosols—Comparison of Measurement with Model Calculations, *Atmos. Environ.* 17:409–416.
- Sorensen, C. M. (1997). Scattering and Absorption of Light By Particles and Aggregates. In *Handbook of Surface and Colloid Chemistry*, edited by K. S. Birdi. CRC Press, Boca Raton, pp. 533–558.
- Sorensen, C. M., Cai, J., and Lu, N. (1992a). Test of Static Structure Factors for Describing Light Scattering from Fractal Soot Aggregates, *Langmuir* 8:2064–2069.
- Sorensen, C. M., Cai, J., and Lu, N. (1992b). Light-Scattering Measurements of Monomer Size, Monomers Per Aggregate, and Fractal Dimension for Soot Aggregates in Flames, *Appl. Optics* 31:6547–6557.
- Sorensen, C. M., and Feke, G. D. (1996). The Morphology of Macroscopic Soot, *Aerosol Sci. Technol.* 25:328–337.
- Sorensen, C. M., Mockler, R. C., and O'Sullivan, W. J. (1976). Depolarized Correlation Function of Light Double Scattered from a System of Brownian Particles, *Phys. Rev. A* 14:1520–1532.
- Sorensen, C. M., Oh, C., Schmidt, P. W., and Rieker, T. P. (1998). Scaling Description of the Structure Factor of Fractal Soot Composites, *Phys. Rev. E* 58:4666–4672.
- Sorensen, C. M., and Roberts, G. C. (1997). The Prefactor of Fractal Aggregates, *J. Colloid Interface Sci.* 186:447–452.
- Sorensen, C. M., and Wang, G. M. (1999). Size Distribution Effect on the Power Law Regime of the Structure Factor of Fractal Aggregates, *Phys. Rev. E* 60:7143–7148.
- Stagg, B. J., and Charalampopoulos, T. T. (1993). Refractive Indices of Pyrolytic Graphite, Amorphous Carbon, and Flame Soot in the Temperature Range 25° to 600°C, *Combust. Flame* 94:381–384.
- Tanford, C. (1961). *Physical Chemistry of Macromolecules*, Wiley, New York.
- Teixeira, J. (1986). Experimental Methods for Studying Fractal Aggregates. In *On Growth and Form, Fractal and Non-Fractal Patterns in Physics*, edited by H. E. Stanley and N. Ostrowski. Nijhoff, Dordrecht, pp. 145–165.
- van de Hulst, H. C. (1957). *Light Scattering by Small Particles*, Wiley, New York.
- van Dongen, P. G. J., and Ernst, M. H. (1985). Dynamic Scaling in Kinetics of Clustering, *Phys. Rev. Lett.* 54:1396–1399.
- Viscek, T. (1992). *Fractal Growth Phenomena*, World Scientific, San Francisco, CA.
- Wang, C. S., and Friedlander, S. K. (1967). The Self-Preserving Particle Size Distribution for Coagulation by Brownian Motion, *J. Colloid Interface Sci.* 24:170–179.
- Weitz, D. A., and Oliveria, M. (1984). Fractal Structures Formed by Kinetic Aggregation of Aqueous Gold Colloids, *Phys. Rev. Lett.* 52:1433–1436.
- Weitz, D. A., Huang, J. S., Lin, M. Y., and Sung, J. (1985). Limits of Fractal Dimension for Irreversible Kinetic Aggregation of Gold Colloids, *Phys. Rev. Lett.* 54:1416–1419.
- Witten, Jr., T. A., and Sander, L. M. (1981). Diffusion-Limited Aggregation, A Kinetic Critical Phenomena, *Phys. Rev. Lett.* 47:1400–1403.
- Wu, M. K., and Friedlander, S. K. (1993). Note on the Powerlaw Equation for Fractal-Like Aerosol Agglomerates, *J. Colloid Interface Sci.* 159:246–247.
- Xing, Y., Koylu, U. O., and Rosner, D. E. (1999). In Situ Light-Scattering Measurements of Morphologically Evolving Flame-Synthesized Oxide Nanoaggregates, *Appl. Optics* 38:2686–2697.
- Zhang, H. X., Sorensen, C. M., Ramer, E. R., Olivier, B. J., and Merklin, J. F. (1988). In Situ Optical Structure Factor Measurements of an Aggregating Soot Aerosol, *Langmuir* 4:867–871.
- Zimm, B. H. (1948). Apparatus and Methods for Measurement and Interpretation of the Angular Variation of Light-Scattering, Preliminary Results on Polystyrene Solutions, *J. Chem. Phys.* 16:1099–1116.

APPENDIX A

We will prove that

$$R_g^2 = \frac{1}{2} \int u^2 g(\vec{u}) d\vec{u}. \quad [A1]$$

To do so retrace the steps of Equations (35) to (34) to (33), i.e., write

$$\int u^2 g(\vec{u}) d\vec{u} = \iint u^2 n(\vec{r}) n(\vec{r} + \vec{u}) d\vec{r} d\vec{u}. \quad [A2]$$

Let $\vec{u} = \vec{r}' - \vec{r}$ to obtain

$$\iint (\vec{r} - \vec{r}')^2 n(\vec{r}) n(\vec{r}') d\vec{r} d\vec{r}'. \quad [A3]$$

Now use the center of mass of the aggregate

$$\vec{r}_{cm} = \int \vec{r} n(\vec{r}) d\vec{r} \quad [A4]$$

in

$$\begin{aligned} (\vec{r} - \vec{r}')^2 &= [(\vec{r} - \vec{r}_{cm}) - (\vec{r}' - \vec{r}_{cm})]^2 \\ &= (\vec{r} - \vec{r}_{cm})^2 + (\vec{r}' - \vec{r}_{cm})^2 \\ &\quad - 2(\vec{r} - \vec{r}_{cm})(\vec{r}' - \vec{r}_{cm}). \end{aligned} \quad [A5]$$

Substitute (A5) into (A3). The third term is 0. The first two terms are equal and may be added to obtain

$$\int u^2 g(\vec{u}) d\vec{u} = 2 \iint (\vec{r} - \vec{r}_{cm})^2 n(\vec{r}) n(\vec{r}') d\vec{r} d\vec{r}'. \quad [A6]$$

The density is normalized so

$$\int u^2 g(\vec{u}) d\vec{u} = 2 \int (\vec{r} - \vec{r}_{cm})^2 n(\vec{r}) d\vec{r}. \quad [A7]$$

The integral on the RHS of Equation (A7) is, by definition, the radius of gyration; hence Equation (A1) is proved. If the aggregate is isotropic, then $g(\vec{u}) = g(u)$. R_g represents a root mean square radius.

APPENDIX B

The large size limit of the scaling distribution is

$$n(N) = M_1 s_p^{-2} \phi(x), \quad [B1]$$

with normalized size

$$x = N/s_p, \quad [B2]$$

mean size

$$s_p(t) = M_p/M_{p-1}, \quad [B3]$$

and moments

$$M_i = \int_0^\infty N^i n(N) dN. \quad [B4]$$

The reduced size distribution or scaling function is

$$\phi(x) = Ax^{-\tau}e^{-\alpha x}, \tag{B5}$$

where τ is the kernel homogeneity (Class II kernels, see van Dongen and Ernst (1985)) and A and α are constants determined below.

Substitute Equations (B1) and (B2) into equation (B4) to find

$$M_i = M_1 s_p^{i-1} m_i, \tag{B6}$$

where m is the i th moment of the scaling function

$$m_i = \int x^i \phi(x) dx. \tag{B7}$$

Substitute Equation (B5) into Equation (B7) to find

$$m_i = A\alpha^{\tau-i-1} \Gamma(i+1-\tau), \tag{B8}$$

where $\Gamma(x)$ is the Gamma function.

The choice of the mean size s_p is arbitrary and hence can be made in accord with experimental convenience. Once a value of p is chosen for s_p , the value of α in Equation (B5) is determined as follows. Substitute Equation (B6) into Equation (B3) to find

$$m_p = m_{p-1} \tag{B9}$$

when the mean size is defined as s_p . Use Equation (B8) in Equation (B9) to find

$$\alpha = p - \tau. \tag{B10}$$

The constant A is found from the normalization condition for the size distribution to the total mass (or volume or number of monomers) M_1 . For $i = 1$, Equation (B6) yields

$$m_1 = 1. \tag{B11}$$

From this and Equation (B8) one obtains

$$A = \alpha^{2-\tau} / \Gamma(2-\tau). \tag{B12}$$

Next we find a relationship between the various mean sizes. Consider the ratio s_{i+1}/s_i . From Equations (B3) and (B6), this equals $m_{i+1}m_{i-1}m_1^{-2}$. Then Equation (B8) yields $(i+1-\tau)/(i-\tau)$, which leads to

$$s_n = s_1 \frac{n-\tau}{1-\tau}. \tag{B13}$$

In summary, the scaling distribution is given by Equations (B1), (B2), and (B5). The constants α and A in Equation (B5) are determined by the choice of which mean size to use in Equation (B1), i.e., what value of p , and normalization to the total mass, and are given by Equations (B10) and (B12), respectively. We conclude with two simple cases, both of which have $\tau = 0$.

If $p = 1$,

$$\alpha = 1, \quad A = 1, \quad s_n = ns_1.$$

If $p = 2$,

$$\alpha = 2, \quad A = 4, \quad s_n = ns_1.$$